American Mineralogist, Volume 106, pages 730–761, 2021

An evolutionary system of mineralogy, Part IV: Planetesimal differentiation and impact mineralization (4566 to 4560 Ma)

Shaunna M. Morrison[1,†] and Robert M. Hazen[1,*]

[1]Earth and Planets Laboratory, Carnegie Institution for Science, 5251 Broad Branch Road NW, Washington, D.C. 20015, U.S.A.

Abstract

The fourth installment of the evolutionary system of mineralogy considers two stages of planetesimal mineralogy that occurred early in the history of the solar nebula, commencing by 4.566 Ga and lasting for at least 5 million years: (1) primary igneous minerals derived from planetesimal melting and differentiation into core, mantle, and basaltic components and (2) impact mineralization resulting in shock-induced deformation, brecciation, melting, and high-pressure phase transformations.

We tabulate 90 igneous differentiated asteroidal minerals, including the earliest known occurrences of minerals with Ba, Cl, Cu, F, and V as essential elements, as well as the first appearances of numerous phosphates, quartz, zircon, and amphibole group minerals. We also record 40 minerals formed through high-pressure impact alteration, commencing with the period of asteroid accretion and differentiation. These stages of mineral evolution thus mark the first time that high pressures, both static and dynamic, played a significant role in mineral paragenesis.

Keywords: Classification, mineral evolution, planetesimals, non-chondrite meteorites, iron meteorites, stony-iron meteorites, achondrites, differentiation, shock minerals

Introduction

The evolutionary system of mineralogy amplifies the well-established International Mineralogical Association (IMA) classification system, which is based on mineral species that display unique combinations of idealized chemical composition and crystal structure (e.g., Burke 2006; Mills et al. 2009; Schertl et al. 2018). We expand on IMA protocols by incorporating time and parageneses as central aspects of mineral classification. The emphasis is thus on the historical sequence of physical, chemical, and ultimately biological processes that led to the observed diversity and distribution of minerals on Earth, as well as on other planets and moons (Hazen et al. 2008; Hazen 2019). Previous contributions in this series considered stellar minerals that predate our solar nebula, prior to 4.567 Ga (Part I; Hazen and Morrison 2020); primary interstellar and nebular condensates commencing ~4.567 Ga (Part II; Morrison and Hazen 2020); and the primary mineralogy of chondrules from ~4.567 to ~4.563 Ga (Part III; Hazen et al. 2021).

In this contribution, we consider the primary mineralogy of planetesimals and their shattered asteroidal remnants, as preserved in diverse suites of non-chondritic meteorites (Mittlefehldt et al. 1998; Krot et al. 2014; Mittlefehldt 2014). All of these meteorites reflect large-scale igneous processing within more than 100 presumed parental asteroidal objects (Keil et al. 1994; Grady and Wright 2006), which ranged from tens to hundreds of kilometers in diameter, coupled in many cases with evidence for transformative impact events. Each non-chondritic meteorite thus tells a story of the time when gravity and high pressures first began to play central roles in mineral evolution.

Asteroids are thought to have formed within the first few million years of the solar nebula and thus experienced thermal processing, and in larger bodies melting and differentiation, associated with heating by short-lived radionuclides, as well as melting and other forms of alteration by high-energy impact processes. Accordingly, this contribution features minerals formed in two broad paragenetic categories. First, in Part IVA, we examine the primary igneous mineralogy of differentiated asteroids, encompassing a diversity of iron, stony-iron, and achondrite meteorites. In Part IVB, we consider meteoritic shock minerals that formed through various impact processes at a range of scales and intensities.

Part IVA: Primary mineralogy of non-chondritic meteorites

The first rocks of the solar system were components of chondrite meteorites, whose minerals formed at high temperatures (>600 °C) and low pressures ($<10^{-2}$ atm) prior to 4.56 Ga. Chondrites are sedimentary accumulations of four principal components (Kerridge and Matthews 1988; Hewins et al. 1996; Brearley and Jones 1998; Scott and Krot 2014; Rubin and Ma 2017, 2021; Russell et al. 2018; Morrison and Hazen 2020; Hazen et al. 2021): (1) inclusions, including refractory calcium-aluminum inclusions and amoeboid olivine aggregates, that formed primarily through condensation from an incandescent vapor phase near the protosun; (2) chondrules, which are igneous droplets ranging from tens of micrometers to several centimeters in diameter that formed in rapid heating and cooling environments; (3) assemblages of Fe-Ni metal alloys and other opaque phases; and (4) a fine-grained matrix (to be considered in Part V of this series). In addition, chondrite meteorites often incorporate a small fraction of presolar stardust grains with a suite of refractory minerals that formed in the expanding, cooling atmospheres of earlier generations of stars (Clayton and Nittler 2004; Lodders and Amari 2005; Lugaro 2005; Davis 2011, 2014; Zinner 2014; Nittler and Ciesla 2016; Hazen and Morrison 2020).

The earliest stages of clumping in the solar nebula have been

* E-mail: rhazen@carnegiescience.edu. Orcid 0000-0003-4163-8644
† Orcid 0000-0002-1712-8057

0003-004X/21/0005–730$05.00/DOI: https://doi.org/10.2138/am-2021-7632

ascribed primarily to electrostatic forces, by which presolar dust grains and refractory inclusions coalesced into fluffy accumulations, not unlike nebular "dust bunnies." Subsequent flash heating events generated droplet-like chondrules, some of which stuck together and formed objects referred to as "pebbles," with diameters ranging from a few millimeters to a few centimeters. Current models suggest that vast numbers of pebbles collected in small volumes through interactions with nebular gas—a mechanism that leads to a collective gravitational instability and coalescence into a single body (e.g., Youdin and Goodman 2005)—perhaps enhanced by contributions from the magnetic co-attraction of ferromagnetic minerals (Hubbard 2016). Self-gravity becomes dominant in such incipient planetesimals at sizes between about 100 m and 1 km in diameter (Benz and Asphaug 1999). Numerical simulations (Johansen et al. 2007) and experimentally determined cooling rates from iron meteorite textures (Randich and Goldstein 1978; Yang and Goldstein 2005, 2006; Yang et al. 2008; Goldstein et al. 2009) suggest that the resulting solid bodies grew to sizes from tens to many hundreds of kilometers in diameter, i.e., large enough for internal heating by short-lived radioisotopes to melt Fe-Ni metal components and initiate core formation while beginning evolution of a silicate mantle (Woolum and Cassen 1999).

Thousands of such objects must have formed in the early solar system, each competing for gravitational dominance over a volume of nebular real estate. Superimposed on these melting events were large impacts, which are likely to have caused significant shock melting episodes during the first few million years of the solar nebula, as well as throughout the subsequent history of the solar system (Tonks and Melosh 1992).

The formation of myriad asteroidal bodies had profound mineralogical consequences. At the coarsest scale, melting and differentiation led to the separation of metal and silicate fractions—end-members preserved as the least-altered iron vs. achondrite meteorites. However, incomplete core/mantle separation within smaller bodies, mixed core-mantle boundary regions, and especially massive disruptions and jumblings of mineralogies through large impacts led to the complex diversity of non-chondritic meteorites, which reflect a continuum of formative processes on asteroidal bodies large and small.

Non-chondritic meteorites and their mineralogies have been reviewed by a number of authors (Mittlefehldt et al. 1998; Benedix et al. 2014; Krot et al. 2014; Mittlefehldt 2014; Rubin and Ma 2017, 2021). These objects represent fragments of diverse pre-planetary objects, ranging from <10 to >400 km in diameter (Rasmussen 1989; Yang et al. 1997a; Mittlefehldt et al. 1998). Non-chondritic meteorites are thought to have derived from chondritic precursors by melting and differentiation, as well as by impact processing. However, they differ from chondrites to varying degrees in texture, composition, and mineralogy. In contrast to chondrite meteorites, which are initially sedimentary rocks that often were modified by varying degrees of aqueous, hydrothermal, and thermal metamorphic processes (Brearley and Jones 1998; Krot et al. 2014; Russell et al. 2018), the non-chondritic meteorites initially derive from partially to completely molten material and are thus igneous rocks (Mittlefehldt et al. 1998; Benedix et al. 2014; Mittlefehldt 2014). Note, however, that continuous gradations exist in aqueous alteration, thermal metamorphism, partial melting, and shock effects so that classifications of intermediate mineralogical states are somewhat subjective.

Three broad (and overlapping) groups of non-chondritic meteorites, based on their dominant mineralogies and textures, are summarized below.

Iron meteorites

Many meteorites dominated by metallic Fe-Ni-alloys, collectively referred to as iron meteorites, represent the cores of differentiated planetesimals that have subsequently experienced catastrophic fragmentation through one or more large impacts (Benedix et al. 2014; Krot et al. 2014). Therefore, these objects display features associated with orderly fractional crystallization and cooling from a melt, as well as the subsequent disruptive effects of impact phenomena. Iron meteorites account for fewer than 100 documented falls—only about 1 in 20 occurrences (Krot et al. 2014). Nevertheless, the more than 1000 iron meteorite falls and finds represent most of the mass of meteorite collections owing to their durability, large average size, and distinctive appearance.

Iron meteorites typically incorporate 5 to 20 wt% nickel, in addition to usually minor amounts of other siderophile transition elements (notably Co, Cr, Cu, Mn, and Zn) and alkali and alkaline earth elements (Na, K, Mg, and Ca), as well as C, N, O, P, S, and Si. More than 40 mineral species containing these essential elements have been reported from iron meteorites [Mittlefehldt et al. (1998), see Table 2; Rubin and Ma (2021), see Table 1].

Fe-Ni alloys constitute >99 wt% of some iron meteorites, which prior to the 1970s were primarily divided into three types—hexahedrites, octahedrites, and ataxites (e.g., Buchwald 1975). Examples with less than ~6 wt% nickel consist almost entirely of a single alloy phase—body-centered cubic (*Im*3*m*) α-iron, universally referred to as "kamacite" in the meteoritics literature, though officially termed "iron" by the IMA. These meteorites, which may be nearly mono-mineralic, have been called "hexahedrites" in the literature owing to the cubic (i.e., hexahedral) cleavage of α-iron crystals.

More commonly, iron alloys incorporate greater than ~6 wt% Ni. These compositions initially crystallize from the melt in a single-phase region with the face-centered cubic γ-iron structure of taenite. However, below ~800 °C a miscibility gap results in the exsolution of the more Ni-rich taenite phase from kamacite, which incorporates only about 6 wt% Ni. This distinctive exsolution behavior, which is vividly revealed in the so-called Widmanstätten patterns of polished and etched meteoritic metal (Fig. 1a), follows octahedral planes of the dominant cubic α-iron phase (e.g., McSween 1999; Yang and Goldstein 2005). Consequently, these iron meteorites have traditionally been called "octahedrites." Their Ni-enriched exsolution lamellae contain several alloy phases, including taenite, tetrataenite, "martensite," and awaruite (Reuter et al. 1988; Yang et al. 1996, 1997b; Mittlefehldt et al. 1998; Benedix et al. 2014; see below). In the less common circumstances of meteorites with >15 wt% Ni, exsolution may occur at lower temperature and at a much finer scale in a group of meteorites called "ataxites."

Several schemes beyond the hexahedrite/octahedrite/ataxite division have been used to classify iron meteorites. For example, octahedrites have been subdivided into seven textural groups on the basis of the average width of exsolution features, which depend primarily on the Ni content and cooling history of the alloy

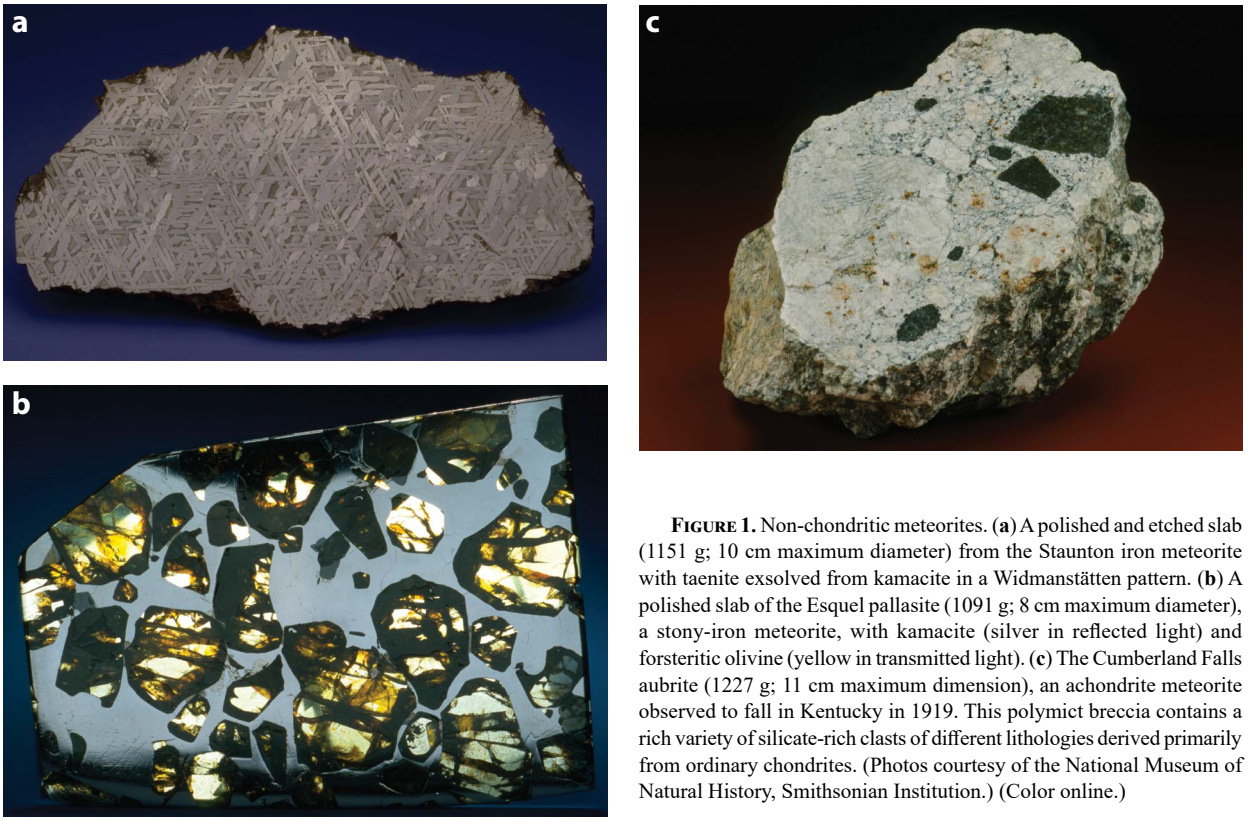

Figure 1. Non-chondritic meteorites. (**a**) A polished and etched slab (1151 g; 10 cm maximum diameter) from the Staunton iron meteorite with taenite exsolved from kamacite in a Widmanstätten pattern. (**b**) A polished slab of the Esquel pallasite (1091 g; 8 cm maximum diameter), a stony-iron meteorite, with kamacite (silver in reflected light) and forsteritic olivine (yellow in transmitted light). (**c**) The Cumberland Falls aubrite (1227 g; 11 cm maximum dimension), an achondrite meteorite observed to fall in Kentucky in 1919. This polymict breccia contains a rich variety of silicate-rich clasts of different lithologies derived primarily from ordinary chondrites. (Photos courtesy of the National Museum of Natural History, Smithsonian Institution.) (Color online.)

(Buchwald 1975; Hutchison 2004; McCoy et al. 2006; Goldstein et al. 2009; Rubin and Ma 2021). A complementary approach focuses on the development of subsequent alteration textures in hexahedrites and octahedrites, for example, mechanical twinning, fracturing, and/or phase transitions in the metal alloys by impacts (Buchwald 1975).

The modern classification of iron meteorites is based on pioneering research by John T. Wasson and colleagues at UCLA (e.g., Wasson 1967, 1970, 1971, 1974; Scott and Wasson 1975; Wasson et al. 1989, 1998), who discovered striking systematic variations in the distribution of Ni and several trace elements, notably Ga, Ge, and Ir (Wasson 1974, 1990; Willis 1980; Mittlefehldt et al. 1998), but also P, Co, Cu, As, Sb, Au, and W (e.g., Moore et al. 1969; Wasson and Choe 2009). This compositional scheme is widely employed to recognize more than a dozen different major groups of iron meteorites, each with at least five representative examples and each given a designation with a Roman numeral followed by one or more letters (e.g., IIAB or IIICD), as well as several "grouplets" with 2 to 4 members and additional unique iron meteorites (Benedix et al. 2014; Krot et al. 2014; Rubin and Ma 2021). In this scheme, the Roman numerals from I to IV are assigned based on decreasing Ge and Ga contents, while letter designations (A to G) refer to systematic differences in Ir and other trace elements that point to different parent bodies. As a consequence, iron meteorite classification schemes have led to the recognition of many discrete types of iron meteorites, each of which may represent a sample of the core from a different differentiated asteroid source (e.g., Scott 1979; Wasson 1990; Benedix et al. 2014).

Iron meteorite classification systems are not based on mineral species, per se; therefore, details of the current chemical classification system are beyond the scope of this mineralogical treatment. For additional information on iron meteorite classification see Mittlefehldt et al. (1998), Benedix et al. (2014), Rubin and Ma (2021), and references therein.

Several compositionally distinct groups of iron meteorites—the so-called "magmatic groups"—are primarily products of planetesimal differentiation and core separation and thus are essentially silicate free with a minor suite of associated phases, including graphite, carbides, schreibersite, carlsbergite, and sulfides (Benedix et al. 2014; Krot et al. 2014). These meteorites display trace element distributions that are unambiguously the consequence of fractional crystallization. Additional evidence for an origin in asteroidal cores comes from the relatively large sizes (perhaps to >10 m maximum dimension) of some iron meteorites, a feature not consistent with dispersed masses of Fe-Ni alloy, as well as the occurrence of individual kamacite crystals several meters in length—a sign of slow cooling (i.e., on the order of ~1 to 10 degrees per million years) in the differentiated interior of an asteroid at least tens of kilometers in diameter (Haack et al. 1990; McSween 1999; Goldstein et al. 2009).

Formation of a metal core and silicate mantle requires significant internal heating by sources other than long-lived radionuclides or accretional heating (Benedix et al. 2014). Hypervelocity impacts could have caused local heating to melting temperatures in some instances (Davison et al. 2010). However, the most probable heat sources for melting of asteroids >20 km in diameter were short-lived radionuclides, notably ^{26}Al (Srinivasan et al. 1999; Keil 2000) and ^{60}Fe (Shukolyukov and Lugmair 1992; Mostefaoui et

al. 2005). Nevertheless, given the 0.717 and 2.6 Ma half-lives of ^{26}Al and ^{60}Fe (Wallner et al. 2015), respectively, such heating must have been restricted to the first few million years of the solar nebula. Indeed, age determinations of iron meteorites suggest core formation within a few million years of CAI condensation, i.e., older than 4.56 Ga (Blichert-Toft et al. 2010).

By contrast, the "nonmagmatic" iron meteorite groups often have significant silicate components, as well as minor and trace element distributions that are not consistent with extensive fractional crystallization (Scott and Wasson 1975; Benedix et al. 2014). These groups are thus thought to represent metal melt pooling, shock melting, breciation, and mixing of lithologies. They commonly incorporate inclusions of other minerals, such as silicates, sulfides, graphite, carbides, and phosphates (Wasson and Kallemeyn 2002). Silicate inclusions of essentially chondritic composition are common in these nonmagmatic iron meteorites; they often feature a reduced (i.e., low-FeO content) assemblage with orthoenstatite, diopside, forsterite, albite ($An_{\sim 10-20}$), troilite, graphite, phosphates, and minor minerals (Bunch et al. 1970; Mittlefehldt et al. 1998), with varied inclusion morphologies (Bunch et al. 1970; Olsen and Jarosewich 1971; Bild and Wasson 1977; Wlotzka and Jarosewich 1977; Wasson et al. 1980; Takeda et al. 1994, 1997a; Choi et al. 1995; McCoy et al. 1996; Yugami et al. 1997; Benedix et al. 2000). Sulfide inclusions in iron meteorites are typically troilite-rich, with associated graphite and schreibersite (Buchwald 1975, 1977). Inclusions with up to 70 vol% phosphates (McCoy et al. 1993), as well as silicate inclusions with abundant phosphate minerals, are also common features of iron meteorites.

The origin of these varied inclusion-bearing iron meteorites has been ascribed to partial melting and melt migration (Kelly and Larimer 1977; McCoy et al. 1993; Yugami et al. 1997); to impact heating and segregation on a porous iron body (Wasson and Kallemeyn 2002); or to catastrophic disruption of a partially melted body, which mixed and reassembled asteroidal materials (Benedix et al. 2000). Models that invoke post-asteroidal formation mechanisms of silicate inclusions through shock events are supported by radiometric age determinations, most of which fall within the range 4.50 ± 0.03 Ga, or significantly after estimated ages of asteroid formation, but mostly well within the first 100 Ma of the solar system (Bogard et al. 1967; Niemeyer 1979a, 1979b; Stewart et al. 1996), though meteorite ages for some silicate-bearing irons are as young as 3.5 Ga (Bogard et al. 1969; Göpel et al. 1985; Olsen et al. 1994).

Mineral natural kinds in iron meteorites

A recurrent question in the evolutionary system of mineralogy, as in most classification systems, relates to the "lumping" vs. "splitting" of objects into natural kinds (Dupré 1981; Bailey 1994; Boyd 1991; Hawley and Bird 2011; Magnus 2012; Hazen 2019). Iron meteorites present a particularly relevant example. On the one hand, all iron meteorites incorporate kamacite as a major mineral—an Fe-Ni alloy with ~6 wt% Ni and a suite of dozens of minor and trace elements. All examples formed in asteroidal parent bodies in the early solar system. Furthermore, all parent bodies of iron meteorites experienced subsequent fragmentation through large impacts that produced the objects we study today. In this overview, we have chosen to lump all of these occurrences into a single natural kind: differentiated asteroidal iron, or "*DA iron*."

However, one might justifiably ask if further subdivision is warranted? For example, meteoritic iron could be split into two groups. On the one hand, "magmatic DA iron" derives from the initial melting and differentiation of an asteroidal body and is characterized by relatively unshocked kamacite with trace element distributions consistent with fractional crystallization (e.g., Benedix et al. 2014). These samples contrast with "nonmagmatic DA iron," which often display compelling textural and trace element evidence for formation via rapid impact melting (Scott 1972; Scott and Wasson 1975; Wasson et al. 1980; Wasson and Wang 1986). However, several iron meteorites display intermediate characteristics that possibly point to a combination of magmatic- and impact-related melting (Takeda et al. 1994; Benedix et al. 2000).

Evidence from Ni-, Mo-, and W-isotopic compositions suggests an additional division for iron meteorites between those that formed in planetesimals from isotope reservoirs that sample non-carbonaceous chondrite regions within Jupiter's orbit vs. planetesimals derived from carbonaceous chondrite precursors that formed beyond Jupiter's orbit (Trinquier et al. 2007, 2009; Burkhardt et al. 2011; Warren 2011; Kruijer et al. 2017). Carried to an extreme, each of the more than two dozen iron meteorite groups, grouplets, and unique examples holds a distinctive suite of compositional and textural attributes, which could be used to catalog a similar number of different natural kinds of meteoritic iron.

A recurring feature of the effort to identify natural kinds through cluster analysis is a degree of subjectivity in how coarsely to lump, or finely to split, the objects of interest. In the evolutionary system of mineralogy in general, and in this study of non-chondritic meteorites in particular, we adopt a more conservative approach. We tend to lump minerals with similar paragenetic modes, such as meteoritic kamacite, whenever possible. However, in the future, experts in meteorite mineralogy may elect to apply the ideas of multi-dimensional cluster analysis to further subdivide meteoritic iron and other meteoritic phases into several additional categories.

Stony-iron meteorites

A few percent of meteorite falls, including the mesosiderite and pallasite groups, consist of subequal mixtures of Fe-Ni alloys and silicates (Fig. 1b). These diverse "stony-iron meteorites," of which a few hundred are known, represent both transitional regions from the core-mantle boundaries of differentiated asteroids and violently shattered and mixed lithologies as a consequence of impacts.

Mesosiderites are impact breccias with 20 to 80 wt% Fe-Ni alloys and troilite, typically in millimeter-scale grains. The balance comprises igneous lithic fragments, including predominantly basalt, gabbro, and pyroxenite, with minor dunite (Mittlefehldt et al. 1998; Krot et al. 2014; Mittlefehldt 2014). Mesosiderites have experienced varying degrees of metamorphism and remelting, which leads to corresponding variations in texture. However, the origin of these complex meteorites remains enigmatic (Hewins 1983; Wasson and Rubin 1985; Scott et al. 2001; Benedix et al. 2014).

Pallasites are a suite of ~100 distinctive stony-iron meteorites, perhaps derived from as many as 10 different parent bodies, with prominent silicate crystals (most typically olivine, $Fo_{\sim 88}$) in a metal matrix (Mittlefehldt et al. 1998; Benedix et al. 2014; Fig. 1b). The mineralogy and textures of pallasites appear to be consistent with a deep mantle origin, from a cumulate zone near the core-mantle boundary [however, for alternative origin hypotheses, see

Scott (1977a, 1977b); Ulff-Møller et al. (1997); Mittlefehldt et al. (1998); Boesenberg et al. (2012); Wasson (2016)].

Note that meteorites with both metal and silicate components span the range from silicate-bearing iron meteorites with just a few silicate inclusions, to rocks that are near equal mixtures of metal and silicates, to silicate-dominant examples. Consequently, there are no sharp, unambiguous dividing criteria among iron, stony-iron, and achondrite meteorites. Nevertheless, many types of stony-iron meteorites have distinctive compositional and textural features that warrant their inclusion in a separate category.

Differentiated achondrite meteorites

Achondrite meteorites encompass a range of meteorites that lack chondrules or solar-like average compositions of chondrite meteorites. As such, they represent a range of igneous types, including melt-depleted ultramafic lithologies, mafic partial melts, and varied cumulates from felsic to ultramafic compositions that arose from crystal settling or flotation. Differentiated achondrites include the related HED meteorites (howardites, eucrites, and diogenites), the most-abundant examples, as well as less-common angrites, aubrites, and ureilites (Mittlefehldt 2014).

The HED meteorites, which are thought to derive from a single asteroidal parent body, probably 4 Vesta (McCord et al. 1970; Drake 2001; McSween et al. 2011), epitomize differentiated achondrites. Eucrites are by far the most abundant of the achondrites, with more than 600 finds and falls. When unaltered, eucrites represent either basalt or cumulate gabbro, with approximately equal amounts of calcic plagioclase and pigeonite (Takeda et al. 1997b; McSween et al. 2011; Krot et al. 2014). However, most eucrites have been altered by metamorphism and/or impacts.

The more than 200 known diogenites are igneous cumulate rocks, typically brecciated and composed of igneous rock fragments. The majority of diogenites are 85 to 100 vol% orthopyroxene, with minor olivine and chromite (McSween et al. 2011), though a few examples are olivine-dominant, ranging to dunite cumulates with up to 95 vol% forsteritic olivine (Beck et al. 2011).

Howardites are regolith breccias with mixtures of eucrites and diogenites, the consequence of impact fracturing, jumbling, and welding (McSween et al. 2011). Relative proportions of the brecciated components range continuously between the eucrite and diogenite end-members; consequently, the HED meteorites, in spite of significant differences among individual examples, represent a unified collection of differentiated igneous rocks.

Other achondrites are presumed to have originated from varied differentiated asteroidal parent bodies. Angrite meteorites are extremely alkali-depleted, silica-undersaturated (olivine-nepheline normative) basalts, dominated by fassaite, olivine, and anorthite, which occur as both extrusive volcanic and near-surface intrusive igneous rocks (Mittlefehldt and Lindstrom 1990; Clayton and Mayeda 1996; Mikouchi et al. 1996; Mittlefehldt et al. 2002; Jambon et al. 2005; Mittlefehldt 2014). The accessory mineralogy of angrites includes Fe-Ni metal, troilite, kirschsteinite (the Ca-Fe olivine), Ti-rich magnetite, hercynite, ulvöspinel, ilmenite, with rare celsian, rhönite, and baddelyite (Keil 2012; Krot et al. 2014). Angrites are thus thought to represent partial melting of primitive source material under relatively oxidizing conditions (Longhi 1999; Mittlefehldt et al. 2002).

Aubrites, also known as enstatite achondrites, are intriguing, highly reduced, orthoenstatite-dominant achondrites, with 75 to 95 vol% near end-member orthorhombic $MgSiO_3$, plus minor albite, forsterite, and diopside (Watters and Prinz 1979; Keil 2010; Mittlefehldt 2014; Fig. 1c). Aubrites also incorporate some of the same rare sulfide minerals with Ca, Cr, Mn, Na, and Ti that are found in enstatite chondrites, including alabandite (MnS), daubréelite ($FeCr_2S_4$), heidite ($FeTi_2S_4$), and oldhamite (CaS). Many aubrites are brecciated.

Ureilites, once thought to represent ultramafic cumulates, are now recognized as mantle restites formed by partial removal of basalt and metal components (Singletary and Grove 2006; Weisberg et al. 2006; Goodrich et al. 2007, 2013; Warren 2012). They are predominantly olivine with low-Ca pyroxene, though strongly depleted in a feldspathic component; ureilite mineralogy is thus consistent with >15% partial melting and melt segregation (Goodrich 1992; Goodrich et al. 2004, 2010; Mittlefehldt 2014). Evidence from short-lived radioisotopes suggest parent body formation within 1 million years of CAIs (van Kooten et al. 2017). A subset of ureilites are polymict breccias that incorporate ureilitic minerals and lithic clasts—evidence for a major disruptive event early in the parent body's history (Cohen et al. 2004; Downes et al. 2008; Herrin et al. 2010).

Several ungrouped achondrite meteorites are known in addition to the well-characterized types reviewed above. For instance, the unique felsic achondrite GRA 06128/06129 is mineralogically distinctive, with 70 to 90 vol% albitic plagioclase, with up to 25 vol% other silicates (Fe-bearing olivine, orthopyroxene, and augite), and minor chlorapatite, merrillite, troilite, pentlandite, chromite, and ilmenite (Day et al. 2009, 2012; Shearer et al. 2010). This assemblage appears to be a flotation cumulate. Also of special note is the unique achondrite NWA 11119 (Srinivasan et al. 2018), which is a silica-rich (i.e., andesitic) extrusive rock dated by ^{26}Al-^{26}Mg methods to 4564.8 ± 0.3 Ma (i.e., within ~3 Ma of CAIs), making this the oldest known silica-rich basalt. Important features include numerous millimeter-diameter vesicles representing >1 vol%, phenocrysts surrounded by quenched melt, and 30 vol% tridymite associated with an unusual mineralogical suite, including tranquillityite, zircon, fayalite, and tsangpoite.

An additional suite of "primitive achondrites," including winonaites, acapulcopites, lodranites, and perhaps brachinites, represent chondrites that have been subjected to high degrees of aqueous and thermal alteration—processes sometimes collectively referred to as "ultrametamorphism" (e.g., Krot et al. 2014; Mittlefehldt 2014). These meteorites lack chondrules, though they have not been extensively melted and thus retain some of the idiosyncratic compositional features of chondrites. The metamorphic mineralogy of primitive achondrites will be considered in Part V, along with secondary alteration mineralogy of chondrite meteorites. Note that, as with many stages of mineral evolution, there are no sharp dividing criteria between partially melted primitive achondrites and incompletely differentiated achondrites.

Systematic primary mineralogy of non-chondritic meteorites

The mineralogy of non-chondritic meteorites has been reviewed by Mittlefehldt et al. (1998) and Rubin and Ma (2017, 2021), as well as by Buchwald (1975, 1977) for iron meteorites and Ruzicka (2014) for silicate inclusions. Here we summarize

the primary igneous mineralogy of differentiated asteroidal bodies, including 90 phases formed through melt crystallization, as well as by inversion, exsolution, and other solid-state reactions on cooling, as preserved in the relatively unaltered portions of iron, stony-iron, and achondrite meteorites (Table 1). Minerals formed through impact processes are summarized in Part IVB below, whereas minerals formed by secondary aqueous alteration and thermal metamorphism will appear in Part V of this series.

Distinguishing between primary and secondary minerals, especially in the many cases of rare, sub-millimeter scale phases, is often problematic. Here we cite phases for which petrologic and mineralogic contexts strongly suggest a primary origin, defined for differentiated meteorites as the result of igneous processes or through solid-state reactions upon initial cooling. Secondary phases, by contrast, arise through subsequent aqueous, thermal, or shock processes. A significant number of other phases of less than certain origins have been deferred to Part V, for example, the enigmatic Al-bearing metal alloys from the unusual Khatyrka carbonaceous chondrite, including hollisterite (Al_3Fe), kryachkoite $(Al,Cu)_6(Fe,Cu)$, stolperite (AlCu), decagonite ($Al_{71}Ni_{24}Fe_5$), and icosahedrite ($Al_{63}Cu_{24}Fe_{13}$) (Bindi et al. 2011, 2012, 2016; Ma et al. 2017a; Rubin and Ma 2021). We also exclude the unusual carbides, andreyivanovite (FeCrP) (Zolensky et al. 2008) and florenskyite (FeTiP) (Ivanov et al. 2000) from the complex brecciated Kaidun meteorite; these minute grains may be primary but they occur embedded in secondary serpentine and their origins are uncertain. Similarly, unique minor phases from acapulcoites, including melliniite [$(Ni,Fe)_4P$; Pratesi et al. (2006)] and chopinite [$(Mg,Fe)_3\square(PO_4)_2$; Grew et al. 2010] appear in Part V.

In the following section we list 90 primary minerals formed by igneous processes in differentiated asteroidal bodies, which incorporate 24 different essential elements, 17 of which occur in multiple phases (Fig. 2). These elements include the first appearances of Ba (celsian), Cl (chlorapatite), Cu (copper), F (fluororichterite), and V (uakitite) as essential mineral-forming elements.

We employ a binomial nomenclature: in most cases the official IMA-approved species name is preceded by "DA," for "differentiated asteroidal." Thus, we list "DA iron," "DA forsterite," and so on. However, in a few instances we deviate from IMA nomenclature, as follows.

• The Fe-Ni phosphides schreibersite [$(Fe,Ni)_3P$] and nickelphosphide [$(Ni,Fe)_3P$] appear to form a continuous solid solution by identical paragenetic processes, with iron compositions predominant; therefore, we lump them together as *DA schreibersite*. Similarly, we lump barringerite [$(Fe,Ni)_2P$] and transjordanite [$(Ni,Fe)_2P$] as *DA barringerite.*

• We lump the NaCl-structured monosulfides, niningerite (MgS) and keilite (FeS), as *DA niningerite*, based on their continuous solid solution and similar mode of origin.

• Merrillite [$Ca_9NaMg(PO_4)_7$] and whitlockite [$Ca_9Mg(PO_3OH)(PO_4)_6$] form a continuous solid solution that we designate *DA merrillite*.

• Analyses of meteoritic graftonite [$Fe_3^{2+}(PO_4)_3$] and beusite [$Mn_3^{2+}(PO_4)_2$] by Steele et al. (1991) revealed a continuous range of compositions, the majority of which fall within the Fe^{2+}-rich graftonite field. Therefore, we designate all occurrences as *DA graftonite*.

• We lump all Ca-poor clinopyroxenes into *DA pigeonite*.

Native elements and alloys

Several alloys of iron and nickel, as well as minor native copper and the carbon allotrope graphite, occur as primary igneous minerals in non-chondritic meteorites. Iron-nickel alloys are the commonest of these phases, representing more than 99 vol% of some examples. These alloys occur as the IMA-approved minerals iron (also commonly known as "kamacite"), taenite, tetrataenite, and awaruite, as well as the distinctive fine-grained exsolved mixture of kamacite and taenite known as "plessite" (Goldstein and Michael 2006). Fe-Ni alloys usually hold significant amounts of other elements; high-C, -P, or -Si contents, for example, may lead to exsolution of new minerals, such as graphite, carbides, schreibersite, perryite, and/or silica glass (see below).

Iron [α-(Fe,Ni)]. The most abundant, defining phase in iron meteorites is body-centered cubic (*Im*3*m*) *DA iron*, commonly referred to as "kamacite" in the meteoritics literature (a name employed here when the term "iron" may be ambiguous) and as "ferrite" in metallurgy. Kamacite, the stable low-Ni iron alloy, typically contains up to ~6 wt% Ni, as well as minor Co (Buchwald 1977; Mittlefehldt et al. 1998; Rubin and Ma 2021). In meteorites with more than 6 wt% Ni, kamacite features exsolution of one or more Ni-enriched alloys, including taenite, tetrataenite, and awaruite. In hexahedrites with <6 total wt% Ni, kamacite may compose >99 wt% of the total meteorite mass (Henderson 1941).

Kamacite is an important phase in stony-iron meteorites, both mesosiderites and pallasites (Powell 1969; Buseck 1977; Ulff-Møller et al. 1997). It is also a minor phase in achondrites, including aubrites (Watters and Prinz 1979) and HED group meteorites (Delaney et al. 1984).

Taenite [γ-(Fe,Ni)]. The primitive cubic (*Pm*3*m*) alloy of iron and nickel, *DA taenite* (referred to as "austenite" in the metallurgical literature), typically has ~25 to 35 wt% Ni. Taenite is the solidus phase in the Fe-Ni phase diagram; however, at ~800 °C taenite transforms to a kamacite + taenite mixture. Taenite is thus typically the more Ni-rich major phase in iron and stony-iron meteorites with Widmanstätten patterns (Powell 1969; Buseck 1977; Buchwald 1977; Mittlefehldt et al. 1998). Note, however, Yang et al. (1997a, 1997b) suggests that at temperatures below ~400 °C "taenite" undergoes a solid-state reaction to a submicroscopic mixture of body-centered cubic (α_2-Fe,Ni), known as "martensite" in metallurgy, and the orthorhombic ordered phase tetrataenite. Taenite is also present in the minor metal phase of many achondrites, including aubrites, HED group meteorites, and the brachinite LEW 88763 (Delaney et al. 1984; Okada et al. 1988; Swindle et al. 1998).

Tetrataenite (FeNi). *DA tetrataenite*, a low-temperature ordered Fe-Ni alloy (tetragonal, space group *P*4/*mmm*; Clarke and Scott 1980), typically forms a layer a few micrometers thick at the kamacite-taenite boundary in iron and stony-iron meteorites with Widmanstätten patterns. As such, it is a common, if volumetrically minor, phase in many iron and stony-iron meteorites. In addition, Okada et al. (1988) described minor tetrataenite in association with kamacite and taenite from the Norton County aubrite.

Awaruite (Ni_2Fe to Ni_3Fe). The Ni-dominant alloy *DA awaruite*, with face-centered cubic structure (space group *Fm*3*m*), was reported by Yang et al. (1997a, 1997b) as forming a thin layer that separates tetrataenite from kamacite in the Widmanstätten patterns of some iron meteorites.

Copper (Cu). *DA copper* is a rare accessory phase in enstatite achondrites (aubrites), where it occurs in association with a suite of highly reduced sulfides and other phases (Keil and Fredriksson 1963; Ramdohr 1973; Watters and Prinz 1979). Native Cu is a common accessory phase in troilite nodules from the Cape York (IIIAB) iron meteorite (Kracher et al. 1977). Near end-member (~98 mol% Cu) copper occurs in the Bilanga diogenite (Domanik et al. 2004).

Graphite (C). *DA graphite* is a common accessory phase in iron meteorites, likely formed both by decomposition of cohenite and by exsolution from C-bearing metal (Mittlefehldt et al. 1998, and references therein). In some cases, graphite adopts a cube-shaped morphology (known as "cliftonite")—a form imposed by the isometric symmetry of its metallic host. Other occurrences of less well-ordered graphite in meteorites, as well as diamond and "lonsdaleite," have been ascribed to impact processes and are considered in the next section (Rubin 1997a; Rubin and Scott 1997).

Graphite is an important component of carbon-rich ureilites, which are mantle restites dominated by olivine and pigeonite. Graphite, at times in association with impact-generated chaoite and organic molecules (kerogen), is most commonly fine-grained, but also occurs as millimeter-diameter euhedral crystals and as intergrowths with metal and/or sulfide (Vdovykin 1970; Berkley and Jones 1982; Treiman and Berkley 1994).

Carbides

Cohenite (Fe_3C). *DA cohenite* is a common accessory mineral in iron meteorites (e.g., Buchwald 1975). In ureilites, cohenite occurs in association with graphite, troilite, and Fe-Ni alloy (Goodrich and Berkley 1986).

Haxonite [$(Fe,Ni)_{23}C_6$]. *DA haxonite* occurs in a variety of iron meteorites (e.g., Taylor et al. 1981), though it is significantly less common than cohenite in non-chondritic meteorites (Mittlefehldt et al. 1998).

Edscottite (Fe_5C_2). *DA edscottite* was formally described by Ma and Rubin (2019), following its reported occurrence decades earlier based on composition measurements by Scott and Agrell (1971). It occurs in slender crystal laths up to 40 μm in maximum dimension as inclusions in kamacite and in association with taenite, plessite, nickelphosphide, and cohenite in the Ni-rich Wedderburn (IAB) iron meteorite. The empirical formula found by Ma and Rubin (2019) is $[(Fe_{4.73}Ni_{0.23}Co_{0.04})C_{2.00}]$.

Silicides

Perryite [$(Ni,Fe)_8(Si,P)_3$]. *DA perryite* occurs as a minor accessory phase in the Norton County and Mt. Egerton enstatite achondrites (aubrites), in association with a suite of unusual highly reduced sulfides and other phases (Wasson and Wei 1970; Watters and Prinz 1979).

Carletonmooreite (Ni_3Si). *DA carletonmooreite* from the Norton County aubrite was approved as a new mineral based on characterization by Garvie et al. (2020). The mineral is cubic (space group $Pm\bar{3}m$) and appears to be related to suessite (Fe_3Si), an impact-generated silicide that has a different cubic space group.

Phosphides

The phosphide schreibersite (and its Ni isomorph nickelphosphide) is an important primary phase in many iron-bearing meteorites. Several other phosphides, including the barringerite-transjordanite solid solution included below, are rare in non-chondritic meteorites. However, the origins of andreyivanovite (FeCrP; Zolensky et al. 2008), florenskyite (FeTiP; Ivanov et al. 2000), and melliniite [$(Ni,Fe)_4P$; Pratesi et al. (2006)] are uncertain and will be included in Part V.

Schreibersite [$(Fe,Ni)_3P$] and nickelphosphide [$(Ni,Fe)_3P$]. *DA schreibersite* is the most important P-bearing phase in iron meteorites (Mittlefehldt et al. 1998). It occurs in most iron meteorites in several morphotypes (Buchwald 1977; Benedix et al. 2000)—as coarse masses, as skeletal inclusions, and as small euhedral crystals (the latter sometimes called "rhabdites"). Schreibersite also occurs in the reduced suite of phases in enstatite achondrites (aubrites; Watters and Prinz 1979), rarely in ureilites (Mittlefehldt et al. 1998), and as a minor phase in pallasites (Buseck 1977).

Schreibersite usually contains significant Ni, in rare instances in amounts slightly exceeding Fe in mole percent (mol%), which corresponds to the IMA-approved species nickelphosphide. For example, Ma and Rubin (2019) report a composition of $[(Ni_{1.63}Fe_{1.37}Co_{0.01})P_{0.99}]$ for a sample in association with edscottite in the Wedderburn (IAB) iron meteorite. Here we lump nickelphosphide with schreibersite, with which it forms a continuous solid solution.

Barringerite [$(Fe,Ni)_2P$] and transjordanite [$(Ni,Fe)_2P$]. *DA barringerite* from the Ollague pallasite was characterized by Buseck (1969) for a sample with composition $[(Fe_{1.11}Ni_{0.81})P]$. Britvin et al. (2020a) recently discovered Ni-dominant isomorphs with maximum Ni content $[(Fe_{0.48}Ni_{1.52})P]$ in the ungrouped Cambria iron meteorite, which they called transjordanite. Britvin and colleagues also described a range of intermediate compositions, some with Fe~Ni, such as $[(Fe_{1.18}Ni_{0.81})P]$. Given the continuous solid solution and similar paragenetic modes, we lump both species into *DA barringerite*.

Nitrides

Osbornite, carlsbergite, and uakitite [(Ti,Cr,V)N] are cubic nitrides with the NaCl structure. Solid solutions among these and other compositions may occur, but known meteoritic examples lie close to their respective end-members. Therefore, we recognize the following three natural kinds, as well as the rare iron nitride roaldite and the silicon oxy-nitride sinoite.

Osbornite (TiN). Osbornite is best known as a common accessory phase in enstatite chondrites (e.g., Hazen et al. 2020). However, *DA osbornite* also occurs in the Bishopville and Bustee enstatite achondrites (aubrites) as a rare accessory phase in association with a suite of unusual sulfides and other highly reduced phases (Bannister 1941; Watters and Prinz 1979).

Carlsbergite (CrN). *DA carlsbergite* is a common minor constituent of iron meteorites (Buchwald 1975). Published analyses of carlsbergite from the Cape York (IIIAB; Buchwald and Scott 1971) and Sikhote-Alin (IIAB; Axon et al. 1981) iron meteorites are close to the end-member composition.

Uakitite (VN). Sharygin et al. (2020) discovered the new vanadium nitride, *DA uakitite*, as euhedral (cube-shaped) to rounded crystals <5 μm maximum dimension in the Uakit (IIAB) iron meteorite. Uakitite occurs in troilite-daubréelite small inclusions (to 100 μm diameter) and large nodules (to 1 cm diameter).

TABLE 1. Primary phases in iron, stony iron, and achondrite meteorites from differentiated asteroidal (DA) parent bodies

Group and Species (formula)	Natural kind	Characteristics	References
		Native Elements and Alloys	
Iron or "kamacite" (α-Fe,Ni)	*DA iron*	The most abundant metal phase in most iron and stony-iron meteorites, typically with ~6 wt. % Ni.	1–6
Taenite (γ-Fe,Ni)	*DA taenite*	A common Fe-Ni alloy with 25 to 35 wt % Ni; exsolves from DA iron to form Widmanstätten patterns.	1,2,4,5,7
Tetrataenite (Fe,Ni)	*DA tetrataenite*	An ordered tetragonal (*P4/mmm*) phase of Fe-Ni	7,8
Awaruite (Ni_2Fe to Ni_3Fe)	*DA awaruite*	Forms thin layers that separate tetrataenite from kamacite in Widmanstätten patterns of some iron meteorites	7,9
Copper (Cu)	*DA copper*	A rare accessory phase in enstatite achondrites (aubrites)	3,10
Graphite (C)	*DA graphite*	A common accessory phase in iron meteorites	4,11,12
		Carbides	
Cohenite [$(Fe,Ni)_3C$]	*DA cohenite*	A common accessory phase in iron meteorites	1,13
Haxonite [$(Fe,Ni)_{23}C_6$]	*DA haxonite*	An accessory mineral in some iron meteorites	4,14
Edscottite (Fe_5C_2)	*DA edscottite*	A rare phase in iron meteorites	15,16
		Silicides	
Perryite [$(Ni,Fe)_8(Si,P)_3$]	*DA perryite*	A minor accessory phase in enstatite achondrites	3,17
Carletonmooreite (Ni_3Si)	*DA carletonmooreite*	A rare phase from the Norton County aubrite	18
		Phosphides	
Schreibersite [$(Fe,Ni)_3P$]	*DA schreibersite*	The most important P-bearing phase in iron meteorites	1,3,4,19
Barringerite [$(Fe,Ni)_2P$]	*DA barringerite*	A rare phase in pallasites and iron meteorites	20,21
		Nitrides	
Osbornite (TiN)	*DA osbornite*	An occasional accessory mineral in enstatite achondrites	3,22
Carlsbergite (CrN)	*DA carlsbergite*	A rare accessory mineral in enstatite achondrites	23,24
Uakitite (VN)	*DA uakatite*	A rare accessory mineral in the Uakit (IIAB) iron meteorite	25
Roaldite [$(Fe,Ni)_4N$)]	*DA roaldite*	A scarce phase in iron meteorites	26
Sinoite (Si_2N_2O)	*DA sinoite*	A minor phase in the Zakłodzie enstatite achondrite	27
		Sulfides	
Troilite (FeS)	*DA troilite*	The most common sulfide phase in iron meteorites; also in stony-iron meteorites and achondrites	1,3,4,19,28–32
NaCl-type Monosulfide Group [(Mg,Fe,Ca,Mn)S]			
Niningerite [(Mg,Fe)S]	*DA niningerite*	Found in enstatite achondrites in association with other sulfides	27,33
Oldhamite (CaS)	*DA oldhamite*	Found in many enstatite achondrites with other sulfides	3,34
Alabandite (MnS)	*DA alabandite*	Found in many enstatite achondrites with other sulfides	3,35
Sphalerite Monosulfide Group [(Zn,Fe,Mn)S]			
Sphalerite (ZnS)	*DA sphalerite*	A rare phase in iron meteorites, possibly exsolved from alabandite	10
Browneite (MnS)	*DA browneite*	A minor phase in the Zakłodzie enstatite achondrite	37
Buseckite [(Fe,Zn,Mn)S]	*DA buseckite*	A minor phase in the Zakłodzie enstatite achondrite	27
Thiospinel Group [$(Fe,Mn,Cr,Zn)Cr_2S_4$]			
Daubréelite ($FeCr_2S_4$)	*DA daubréelite*	A common minor phase in iron and achondrite meteorites	1,3,29
Joegoldsteinite ($MnCr_2S_4$)	*DA joegoldsteinite*	Found in the Social Circle (IVA) iron meteorite	38
Kalininite ($ZnCr_2S_4$)	*DA kalininite*	Discovered as a trace phase in the Uakit (IIAB) iron meteorite	39
Wilkmanite Group [$(Fe,Cr)(Fe,Cr,Ti)_2S_4$]			
Brezinaite (Cr_3S_4)	*DA brezinaite*	A rare phase in iron and ureilite meteorites	40,41
Heideite [$(Fe,Cr)_{1.15}(Ti,Fe)_2S_4$]	*DA heideite*	Found in the Bustee enstatite achondrite with other sulfides	3,42
Other Sulfides			
Pentlandite [$(Ni,Fe)_9S_8$]	*DA pentlandite*	A rare phase in brachinites, coexisting with taenite and troilite	30,43
Caswellsilverite ($NaCrS_2$)	*DA caswellsilverite*	Occurs as inclusions in oldhamite in the Norton County aubrite	3,44
Unnamed ($CuCrS_2$)	*DA $CuCrS_2$*	A single occurrence from the Uakit (IIAB) iron meteorite	40
Djerfisherite [$K_6(Fe,Cu,Ni)_{25}S_{26}Cl$]	*DA djerfisherite*	Found in enstatite achondrites with other sulfides	3,45
		Phosphates	
Chlorapatite [$Ca_5(PO_4)_3Cl$]	*DA chlorapatite*	A common phosphate in iron and achondrite meteorites	4,30,46, 47
Whitlockite [$Ca_9Mg(PO_3OH)(PO_4)_6$]	*DA whitlockite*	A common phosphate in non-chondritic meteorites	1,46,48–53
Matyhite [$Ca_9(Ca_{0.5}\square_{0.5})Fe(PO_4)_7$]	*DA matyhite*	A rare phase from the D'Orbigny angrite	54
Graftonite [$(Fe,Mn)_3(PO_4)_3$]	*DA graftonite*	Occurs in troilite nodules in iron meteorites; often Mn-rich	55
Farringtonite [$(Fe,Mn)_3(PO_4)_3$]	*DA farringtonite*	Found in pallasites with fairfieldite and whitlockite	2,56
Sarcopside [$(Fe,Mn)_3(PO_4)_3$]	*DA sarcopside*	Occurs in troilite nodules of iron meteorites	57
Stanfieldite [$Ca_4Mg_5(PO_4)_6$]	*DA stanfieldite*	A minor phase in pallasites	2,56,58
Buchwaldite ($NaCaPO_4$)	*DA buchwaldite*	From troilite nodules in the Cape York (IIIAB) iron meteorite	10,59
Marićite ($NaFePO_4$)	*DA marićite*	From troilite nodules in the Cape York (IIIAB) iron meteorite	10
Moraskoite [$Na_2Mg(PO_4)F$]	*DA moraskoite*	A rare phase in the Morasko (IAB) iron meteorite	60
Xenophyllite [$Na_4Fe_7(PO_4)_6$]	*DA xenophyllite*	A rare phase in the Austinovka (IIIAB) iron meteorite	61
Brianite [$Na_2CaMg(PO_4)_2$]	*DA brianite*	A rare phase in iron meteorites associated with whitlockite	46,62,63
Panethite [$Na_2(Fe,Mn)_2(PO_4)_2$]	*DA panethite*	A rare phase in the Dayton (IAB) iron meteorite	46,62,64
Johnsomervilleite [$Na_2Ca(Fe,Mg,Mn)_7(PO_4)_6$]	*DA johnsomervilleite*	A rare phase in iron meteorites	57,65
Chladniite [$Na_2CaMg_7(PO_4)_6$]	*DA Chladniite*	Only known from the Carlton (IIICD) iron meteorite	64
Galileiite [$Na(Fe,Mn)_4(PO_4)_3$]	*DA galileiite*	A rare phase in iron meteorites	57
Tsangpoite [$Ca_5(PO_4)_2(SiO_4)$]	*DA tsangpoite*	A rare silico-phosphate from the D'Orbigny angrite	54

Uakitite has an observed composition of $[(V_{0.91}Cr_{0.07}Fe_{0.02})N]$ and is the earliest known vanadium mineral.

Roaldite [$(Fe,Ni)_4N$)]. *DA roaldite* occurs sparsely in the Jerslev and Youndegin (IAB) iron meteorites as exsolved platelets 1 to 2 μm thick and many millimeters in lateral extent in kamacite, as described by (Nielsen and Buchwald 1981). It contains ~6 mol% Ni substituted for Fe.

Sinoite (Si_2N_2O). The silicon oxy-nitride *DA sinoite* occurs as a rare minor phase in the Zakłodzie ungrouped enstatite achondrite, where it is associated with major enstatite, anorthite, and

TABLE 1.—*CONTINUED*

Group and Species (formula)	Natural kind	Characteristics	References
		Oxides	
Oxide Spinel Group [$(Mg,Fe^{2+})(Al,Fe^{3+},Cr^{3+},Ti)_2O_4$]			
Chromite ($Fe^{2+}Cr_2O_4$)	*DA chromite*	Often the most abundant oxide; found in all meteorite groups	1,2,4,31,43,66
Magnetite (Fe_3O_4)	*DA magnetite*	An accessory phase in angrites	67,68
Hercynite ($Fe^{2+}Al_2O_4$)	*DA hercynite*	A minor phase in angrites	67,68
Ulvöspinel ($Fe^{2+}_2Ti^{4+}O_4$)	*DA ulvöspinel*	A minor phase in angrites	69
Other Oxides			
Ilmenite ($FeTiO_3$)	*DA ilmenite*	Reported from diogenites, eucrites, and iron meteorites	48,70–72
Corundum (Al_2O_3)	*DA corundum*	One report from the LEW 88774 Cr-rich ureilite	73
Eskolaite (Cr_2O_3)	*DA eskolaite*	One report from the LEW 88774 Cr-rich ureilite	74
Rutile (TiO_2)	*DA rutile*	A minor phase in the Sombrerete (IAB) iron meteorite	48
Baddeleyite (ZrO_2)	*DA baddeleyite*	Found in the Angra dos Reis angrite as a minor phase	67
Perovskite ($CaTiO_3$)	*DA perovskite*	One report from an oxide inclusion in aubrite ALH 84008	75
Geilkeilite ($MgTiO_3$)	*DA geikeilite*	One report from an oxide inclusion in aubrite ALH 84008	75
Armalcolite [$(Mg,Fe^{2+})Ti_2O_5$]	*DA armalcolite*	A rare phase in silicate inclusions of iron meteorites	72,76
		Silicates	
Silica Group (SiO_2)			
Tridymite (SiO_2)	*DA tridymite*	Tridymite is the commonest silica polymorph; it is found in iron meteorites and in mafic meteorite lithologies	1,4,48,71,77
Cristobalite (SiO_2)	*DA cristobalite*	A minor phase in eucrites, aubrites, and iron meteorites	27,78,79
Quartz (SiO_2)	*DA quartz*	A minor phase in eucrites, aubrites, and iron meteorites	4,27,80
Silica glass (SiO_2)	*DA silica glass*	In silicate inclusions of iron meteorites	72
Olivine Group [$(Mg,Fe,Ca)_2SiO_4$]			
Forsterite [$(Mg,Fe)_2SiO_4$]	*DA forsterite*	A major meteorite mineral in many stony-irons and achondrites, comprising >98 vol % of some brachinites,	2–4,30,81
Fayalite (Fe_2SiO_4)	*DA fayalite*	Near end-member fayalite occurs in howardites and angrites	52,82,83
Kirschteinite ($CaFe^{2+}SiO_4$)	*DA kirschsteinite*	Occurs as a minor accessory phase in angrites	53,67,68
Pyroxene Group [$(Ca,Mg,Fe,Ti,Al)_2(Al,Si)_2O_6$]			
Orthoenstatite ($MgSiO_3$)	*DA orthoenstatite*	A major phase in several types of non-chondritic meteorites	3,4,31,71,84
Pigeonite [$(Mg,Fe,Ca)SiO_3$]	*DA pigeonite*	A major phase in many achondrites	4,30,85
Augite [$(Ca,Mg,Fe)_2Si_2O_6$]	*DA augite*	The major Ca-bearing phase in many achondrites	3,4,31,52,70,85
Hedenbergite ($CaFeSi_2O_6$)	*DA hedenbergite*	Near end-member examples occur in angrites	54,82
Fassaite [$Ca(Mg,Al,Ti^{3+},Ti^{4+})(Al,Si)SiO_6$]	*DA fassaite*	A common phase in angrite meteorites	53,68,86,87
Kosmochlor ($NaCr^{3+}Si_2O_6$)	*DA kosmochlor*	A minor phase in some iron meteorites	88,89
Amphibole Group			
Fluoro-richterite [$Na(NaCa)Mg_5Si_8O_{22}F_2$]	*DA fluoro-richterite*	A rare phase in iron and aubrite meteorites	90,91
Kaersutite [$NaCa_2(Mg_3AlTi^{4+})(Si_6Al_2)O_{22}O_2$]	*DA kaersutite*	Repoprted from the Sombrerete (IAB) iron meteorite	48
Feldspar Group [$(Ca,Na,K)Al(Al,Si)Si_2O_8$]			
Anorthite ($CaAl_2Si_2O_8$)	*DA anorthite*	A major phase in many non-chondritic meteorites	3,4,50,69
Albite ($NaAl_3SiO_8$)	*DA albite*	A common minor phase in brachinites, aubrites, and iron meteorites	4,6,51,72
Sanidine ($KAlSi_3O_8$)	*DA sanidine*	K-rich feldspars are rare in non-chondritic meteorites. They occur in silicate inclusions in iron meteorites as crystals and in antiperthite	92–94
Celsian ($BaAl_2Si_2O_8$)	*DA celsian*	Occurs as a minor phase in the Angra dos Reis angrite	67
Feldspathic glass (Na,K,Ca,Al,Si)	*DA feldspathic glass*	A significant phase in late-stage melt fractions from ureilites, brachinites, aubrites, and iron meteorites	8,48,72,92,95–97
Other Silicates			
Zircon ($ZrSiO_4$)	*DA zircon*	A rare phase in basaltic meteorite lithologies	83,98,99
Tranquillityite [$Fe^{2+}_8Ti_3Zr_2Si_3O_{24}$]	*DA tranquillityite*	One occurrence from NWA 11119 Si-rich achondrite	83
Yagiite [$NaMg_2(AlMg_2Si_{12})O_{30}$]	*DA yagiite*	A rare phase in iron meteorites	72,100
Kuratite [$Ca_2(Fe^{2+}_5Ti)O_2[Si_4Al_2O_{18}]$]	*DA kuratite*	Known only from the D'Orbigny angrite	101
Krinovite [$Na_4(Mg_8Cr^{3+}_4)O_4(Si_{12}O_{36})$]	*DA krinovite*	A rare mineral in iron meteorites	89
Roedderite [$(Na,K)_2Mg_5Si_{12}O_{30}$]	*DA roedderite*	A rare mineral in iron and enstatite achondrite meteorites	89,102,103
		Organic Solids	
Kerogen (C-H-O-N)	*DA kerogen*	An important carbon-bearing phase in many ureilites	104

References: 1. Buchwald (1977); 2. Buseck (1977); 3. Watters and Prinz (1979); 4. Mittlefehldt et al. (1998); 5. Benedix et al. (2014); 6. Rubin and Ma (2021); 7. Yang et al. (1997a); 8. Okada et al. (1988); 9. Yang et al. (1997b); 10. Ramdohr (1973); 11. Berkley & Jones (1982); 12. Treiman & Berkley (1994); 13. Goodrich & Berkley (1986); 14. Taylor et al. (1981); 15. Scott & Agrell (1971); 16. Ma & Rubin (2019); 17. Wasson & Wei (1970); 18. Garvie et al. (2020); 19. Benedix et al. (2000); 20. Buseck (1969); 21. Britvin et al. (2020a); 22. Bannister (1941); 23. Buchwald & Scott (1971); 24. Axon et al. (1981); 25. Sharygin et al. (2020); 26. Nielsen & Buchwald (1981); 27. Ma et al. (2012a); 28. Prinz et al. (1988); 29. Scott et al. (1996); 30. Nehru et al. (1992); 31. Bowman et al. (1997); 32. McCoy (1998); 33. McCoy et al. (1996); 34. Graham et al. (1977); 35. Keil & Fredriksson (1963); 36. Kracher et al. (1977); 37. Ma et al. (2012b); 38. Isa et al. (2016); 39. Sharygin (2020); 40. Bunch & Fuchs (1969a); 41. Nehru et al. (1982); 42. Keil & Brett (1974); 43. Nehru et al. (1983); 44. Okada & Keil (1982); 45. Ramdohr (1963); 46. McCoy et al. (1993); 47. Swindle et al. (1998); 48. Prinz et al. (1982); 49. Rubin & Mittlefehldt (1992); 50. Bunch et al. (1970); 51. Nehru et al. (1996); 52. Ikeda & Takeda (1985); 53. McKay et al. (1990); 54. Hwang et al. (2019); 55. Steele et al. (1991); 56. Buseck & Holdsworth (1977); 57. Olsen & Steele (1997); 58. Davis & Olsen (1991); 59. Olsen et al. (1977a); 60. Karwowski et al. (2015); 61. Britvin et al. (2020b); 62. Fuchs et al. (1967); 63. Scott & Bild (1974); 64. McCoy et al. (1994); 65. Olsen & Steele (1993); 66. Lovering (1975); 67. Prinz et al. (1977); 68. McKay et al. (1988); 69. Mikouchi et al. (1996); 70. Mittlefehldt & Lindstrom (1993); 71. Delany et al. (1984); 72. Ruzicka (2014); 73. Prinz et al. (1994); 74. Warren & Kallemeyn (1994); 75. Rosenshein et al. (2006); 76. Ebihara et al. (1997); 77. Nehru et al. (1980); 78. Marvin (1962); 79. Aoudjehane & Jambon (2007); 80. Marvin et al. (1997); 81. Ulff-Møller et al. (1998); 82. Yanai (1994); 83. Srinivasan et al. (2018); 84. Hiroi et al. (1993); 85. Takeda et al. (1992); 86. Prinz et al. (1986); 87. Prinz et al. (1990); 88. Frondel & Klein (1965); 89. Olsen & Fuchs (1968); 90. Olsen et al. (1973); 91. Bevan et al. (1977); 92. Wasserburg et al. (1968); 93. Wlotzka & Jarosewich (1977); 94. Olsen et al. (1994); 95. Goodrich (1986); 96. Fuchs (1974); 97. Fogel (2005); 98. Gomes & Keil (1980); 99. Ireland & Wlotzka (1992); 100. Bunch & Fuchs (1969b); 101. Hwang et al. (2016); 102. Hsu (1998); 103. Fogel (2001); 104. Vdovykin (1970).

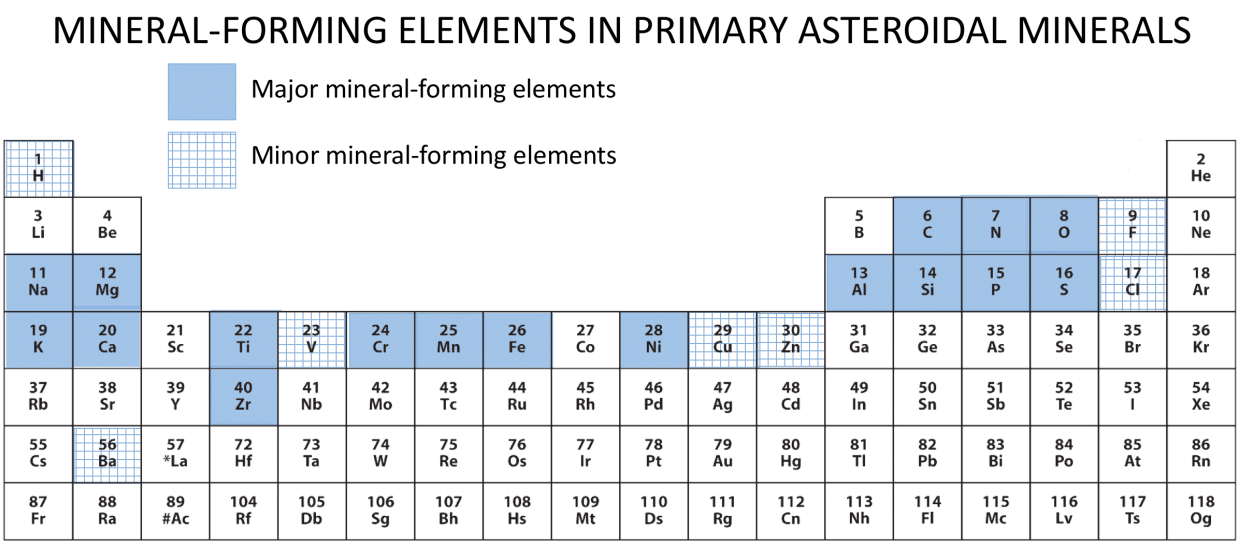

Figure 2. Essential mineral-forming elements in 90 primary asteroidal minerals. (Color online.)

troilite, and accessory silica polymorphs, schreibersite, keilite, buseckite, and other phases (Ma et al. 2012a).

Sulfides

The iron sulfide troilite is a common, and at times major, phase in non-chondritic meteorites [Mittlefehldt et al. (1998), Tables 2 and 29]. An additional suite of rare, highly reduced sulfides and associated phases occurs in enstatite achondrites (aubrites).

Some models of asteroidal differentiation suggest that predicted sulfide-rich meteorites may be missing from collections, based on the assumption that asteroid core formation should also result in late-stage sulfur-rich immiscible melts (Chabot and Drake 1999, 2000). However, the corresponding S-rich meteorites have not yet been found. One possibility is that sulfide-dominant meteors are selectively lost, as they will more easily decompose in space and fragment upon atmospheric entry than iron- or silicate-rich meteors (Kracher and Wasson 1982).

Troilite (FeS). *DA troilite*, the hexagonal (space group $P6_3/mmc$) polymorph of FeS, is by far the commonest sulfide mineral in non-chondritic meteorites, at times exceeding Fe-Ni metal in volume (Mittlefehldt et al. 1998). In iron meteorites, troilite occurs in several forms, most dramatically in nodules or veins in Fe-Ni alloys up to several centimeters in maximum dimension, in which it may occur in association with graphite, cohenite, and schreibersite. Other morphotypes in iron meteorites include oriented platelets up to a centimeter in maximum dimension but only a few millimeters thick, suggesting exsolution from the host Fe-Ni alloy (Buchwald 1975; Scott 1982; Casanova et al. 1995; Benedix et al. 2000).

Troilite is the dominant S-bearing phase in association with Fe-Ni alloys in stony-iron meteorites, including both pallasites (Buseck 1977) and mesosiderites, in which it can account for up to 14 vol% (Powell 1969; Floran 1978; Scott et al. 1996). Troilite occurs commonly as an accessory phase in achondrites, for example, in brachinites (Nehru et al. 1992), in HED group meteorites (Delaney et al. 1984; Takeda and Mori 1985; Bowman et al. 1997), and in angrites (Prinz et al. 1977, 1988, 1990; McKay et al. 1988, 1990). Troilite significantly enriched in Ti (with 17 to 25 wt% Ti, equivalent to 29 to 39 mol% TiS) occurs commonly in aubrites in association with a suite of highly reduced phases (Watters and Prinz 1979; McCoy 1998).

NaCl-type monosulfide group [(Mg,Fe,Ca,Mn)S]. Niningerite, keilite, oldhamite, and alabandite are monosulfides with the cubic (space group $Fd3m$) NaCl structure. All are rare, occurring with suites of unusual phases in enstatite chondrites and enstatite achondrites (also known as aubrites). These phases may represent a continuous solid solution among the Mg-Fe-Ca-Mn end-members, as all analyzed examples incorporate these four elements. However, until further data are available, we lump only niningerite-keilite (Fe-Mg-dominant) members.

Niningerite (MgS) and keilite (FeS). *DA niningerite* was originally described from enstatite chondrites by Keil and Snetsinger (1967) as a cubic monosulfide of Mg, with significant Fe substitution, in some instances with Fe > Mg. McCoy (1998) subsequently described niningerite with significant Mn and Fe (15 and 7 mol%, respectively) from the Bustee enstatite achondrite in association with a suite of highly reduced sulfides and other phases, while Shimizu et al. (2002) reported Fe-dominant analogs of niningerite from five different enstatite chondrites—a mineral species approved by the IMA as keilite. Ma et al. (2012a) then identified minor keilite in the Zakłodzie ungrouped enstatite achondrite, where it is associated with major enstatite, anorthite, and troilite, and accessory silica polymorphs, schreibersite, buseckite, and other phases. Because these occurrences suggest a continuous solid solution between the Mg and Fe end-members, and they always occur in association with troilite in enstatite achondrites, we lump these two species into DA niningerite with the general formula [(Mg,Fe,Mn)S].

Oldhamite (CaS). *DA oldhamite* occurs as a minor phase in enstatite achondrites (aubrites) as grains ~100 μm in diameter, typically in association with a suite of highly reduced phases (Graham et al. 1977; Watters and Prinz 1979). In aubrites, which lack phosphates, oldhamite is often the principal repository of rare-earth elements (Floss and Crozaz 1993; Wheelock et al. 1994). Note

that in some models of aubrite formation, which invoke partial melting of an enstatite chondrite precursor, oldhamite is thought to be a relict phase of nebular condensation processes rather than a product of asteroidal differentiation (Floss and Crozaz 1993; Lodders 1996). However, based on the very different trace element fractionation patterns in different samples, a combination of both nebular and igneous origins seems likely for different oldhamite occurrences (Wheelock et al. 1994; McCoy 1998).

Alabandite (MnS). *DA alabandite* with significant Fe^{2+} and Mg occurs as a minor phase in enstatite achondrites (aubrites), in association with a suite of highly reduced phases (Keil and Fredriksson 1963; Watters and Prinz 1979). For example, a specimen from the Mayo Belwa aubrite has composition [$(Mn_{0.52}Fe_{0.35}Mg_{0.02}Ca_{0.02}Cr_{0.03})S_{0.99}$] (Watters and Prinz 1979).

Sphalerite monosulfide group [(Zn,Fe,Mn)S]. The sphalerite group of cubic (space group $F\bar{4}3m$) monosulfides is represented in non-chondritic meteorites by two rare occurrences, including sphalerite and browneite. Solid solution occurs among the Zn-Fe-Mn end-members, but the two reported examples are close to Zn and Mn end-members. Therefore, we list them as discrete natural kinds.

Sphalerite (ZnS). *DA sphalerite* has been recorded by Kracher et al. (1977) as rare grains within troilite nodules, often in close association with Fe^{2+}-rich alabandite in the Cape York (IIIAB) iron meteorite. The average composition is [$(Zn_{0.82}Fe_{0.14}Mn_{0.04})S$]. Kracher et al. (1977) suggest that sphalerite may have exsolved from alabandite.

Browneite (MnS). *DA browneite* of approximate composition [$(Mn_{0.99}Fe_{0.01})S$] was reported by Ma et al. (2012b) from the Zakłodzie ungrouped enstatite achondrite, where it was found as a single 16 μm diameter crystal encased by plagioclase and in close association with troilite and enstatite. Browneite is metastable with respect to alabandite at all temperatures and pressures relevant to meteorite paragenesis; therefore, Ma et al. (2012b) speculated that browneite formed metastably at $T < 200$ °C, though the mechanism of formation is uncertain. Therefore, the possibility of a secondary origin through aqueous or weathering processes cannot be ruled out.

Buseckite [(Fe,Zn,Mn)S]. *DA buseckite* is the Fe^{2+}-dominant, hexagonal wurtzite-structure (space group $P6_3mc$) monosulfide. It was discovered by Ma et al. (2012a) in the Zakłodzie ungrouped enstatite achondrite, where it occurs as subhedral grains to 20 μm diameter in association with troilite, orthoenstatite, anorthite, and numerous other phases.

Thiospinel group [(Fe,Mn)Cr_2S_4]. Daubréelite, joegoldsteinite, and kalininite, the Fe, Mn, and Zn chromite members of the cubic (space group $Fd3m$) thiospinel group, are known exclusively from meteorites. Extensive solid solution may occur among these and other end-members; however, reported compositions are sufficiently close to end-member compositions to warrant three distinct natural kinds.

Daubréelite ($FeCr_2S_4$). *DA daubréelite* is found in numerous iron and achondrite meteorites as a minor accessory phase. It was reported as an exsolved phase in troilite from the Bishop Canyon (IVA) silicate-bearing iron meteorite (Scott et al. 1996) and as a minor component of silicate inclusions in a variety of iron meteorites (Buchwald 1975). It also occurs as a minor phase in aubrites with average composition [$(Fe_{0.89}Mg_{0.09}Mn_{0.07}Cr_{1.82})S_4$], in association with a suite of highly reduced phases (Graham et al. 1977; Watters and Prinz 1979).

Joegoldsteinite ($MnCr_2S_4$). *DA joegoldsteinite*, the Mn analog of daubréelite, was discovered by Isa et al. (2016) in the Social Circle (IVA) magmatic iron meteorite. The specimen, which occurs as two 13 to 15 μm maximum dimension inclusions in kamacite, has an empirical formula of [$(Mn_{0.82}Fe_{0.23})Cr_{1.99}S_{3.95}$].

Kalininite ($ZnCr_2S_4$). Sharygin (2020) lists *DA kalininite* as a trace phase in the Uakit (IIAB) iron meteorite in a preliminary report of its unusual accessory mineralogy, which also contains uakitite and an as yet unapproved Cu-Cr sulfide associated with troilite-rich inclusions.

Wilkmanite group [(Fe,Cr)$(Fe,Cr,Ti)_2S_4$]. Two new monoclinic (space group $I2/m$) sulfides discovered in meteorites, brezinaite and heidite, are isomorphous with wilkmanite (Ni_3Se_4).

Brezinaite (Cr_3S_4). The presence of the rare mineral *DA brezinaite* in the ungrouped Tucson iron meteorite is an indicator of its extremely reduced state, as revealed by coexisting Cr^{2+} and Cr^{3+} in this thiospinel (Bunch and Fuchs 1969a; Nehru et al. 1982). Brezinaite has also been reported from the anomalous Cr-rich ureilite LEW 88774 in association with chromite, eskolaite, a Cr-Fe carbide [~$(Fe,Cr)_2C$], and graphite (Prinz et al. 1994), as well as the Mt. Egerton aubrite (Casanova et al. 1993).

Heideite [$(Fe,Cr)_{1.15}(Ti,Fe)_2S_4$]. *DA heideite* was reported by Keil and Brett (1974) from the Bustee aubrite, in which it is associated with a suite of highly reduced sulfides and other phases (Watters and Prinz 1979).

Other sulfides

Pentlandite [$(Ni,Fe)_9S_8$]. *DA pentlandite* has been reported in brachinites, coexisting with Ni-rich troilite and taenite (Nehru et al. 1983, 1992).

Caswellsilverite ($NaCrS_2$). *DA caswellsilverite* occurs as inclusions in oldhamite in the Norton County enstatite achondrite in association with a suite of unusual highly reduced sulfides and other phases (Watters and Prinz 1979). Okada and Keil (1982) measured a composition of [$(Na_{0.95}Cr_{1.00}Ti_{0.05})S_{1.95}$].

Unnamed ($CuCrS_2$). Sharygin (2020) described an as yet unnamed sulfide, which we designate *DA* $CuCrS_2$, from the Uakit (IIAB) iron meteorite. Preliminary data, obtained on 10 μm maximum dimension crystals in phosphide-sulfide inclusions in kamacite and schreibersite, suggest that this phase may be a Cu^{1+} analog of caswellsilverite. The observed composition is [$(Cu_{0.94}Fe_{0.09}Cr_{0.97})S_2$].

Djerfisherite [$K_6(Fe,Cu,Ni)_{25}S_{26}Cl$]. *DA djerfisherite*, originally described by Fuchs (1966) from enstatite chondrites, also occurs in the Pena Blanca Springs enstatite achondrite as a minor mineral associated with a suite of highly reduced sulfides and other phases (Ramdohr 1963; Watters and Prinz 1979).

Phosphates

A diversity of phosphate minerals, both in P-rich nodules and in more widely dispersed grains, occur widely in non-chondritic meteorites [Fuchs (1969a), Mittlefehldt et al. (1998), Tables 2 and 16]. Phosphate minerals, which may comprise as much as 70 vol% of some inclusions in iron meteorites (McCoy et al. 1993), only occur in relatively oxidized iron meteorites (Olsen and Fredriksson 1966; Olsen et al. 1999); otherwise schreibersite is the dominant

P-bearing phase. Note that phosphates are particularly important components of pallasite stony-iron meteorites (Buseck 1977; Buseck and Holdsworth 1977).

Chlorapatite [$Ca_5(PO_4)_3Cl$]. *DA chlorapatite* is a significant phosphate mineral in several types of non-chondritic meteorites, including in phosphate-rich inclusions in the Carlton (IIICD) iron meteorite (McCoy et al. 1993); in brachinites (Nehru et al. 1992; Swindle et al. 1998); in polymict ureilites (Mittlefehldt et al. 1998); and in HED group meteorites (Mittlefehldt et al. 1998). Chlorapatite constitutes ~8 vol% of silicate inclusions in the ungrouped Somberrete (IAB) iron meteorite (Prinz et al. 1982).

Merrillite [$Ca_9NaMg(PO_4)_7$] and whitlockite [$Ca_9Mg(PO_3OH)(PO_4)_6$]. *DA merrillite*, including continuous solid solution with whitlockite, is a common phase in non-chondritic meteorites. It is an abundant phosphate mineral with brianite and panethite in the Dayton (IAB) iron meteorite (McCoy et al. 1993, 1994). Merrillite has been reported from pallasites (Buseck 1977; Buseck and Holdsworth 1977; Davis and Olsen 1991; Boesenberg et al. 1995), as a minor accessory mineral in mesosiderites (Floran 1978; Rubin and Mittlefehldt 1992), and from the unique Enon stony-iron (Bunch et al. 1970). In achondrites, merrillite occurs in brachinites in association with chlorapatite (Nehru et al. 1996; Swindle et al. 1998), in basaltic eucrites (Ikeda and Takeda 1985), and as a minor phase in angrites (McKay et al. 1990).

Matyhite [$Ca_9(Ca_{0.5}\square_{0.5})Fe(PO_4)_7$]. Hwang et al. (2019) characterized the new Ca-Fe phosphate mineral (presumed *DA*) *matyhite* from the D'Orbigny angrite, which is an analog of merrillite but with high Fe and low Na and Mg. Matyhite occurs as elongated crystallites up to ~10 mm maximum dimension in association with fayalite, kirchsteinite, and hedenbergite. It was previously reported from other angrites, including Angra do Reis (Prinz et al. 1977), LEW 86010 (McKay et al. 1988), Asuka 881371 (Prinz and Weisberg 1995), and NWA 1296 (Jambon et al. 2005). Hwang et al. (2019) suggest that matyhite formed as part of a residual melt assemblage that includes tsangpoite and kuratite. However, they could not rule out the possibility of formation by metasomatism.

Graftonite [$Fe^{2+}_3(PO_4)_3$] and beusite [$Mn^{2+}_3(PO_4)_2$]. *DA graftonite* was reported by Olsen and Steele (1993, 1997) from troilite nodules in iron meteorites in association with sarcopside, galileiite, and chromite. Steele et al. (1991) reported an intermediate composition ~[$(Fe_{1.5}Mn_{1.5})(PO_4)_3$], which they designated beusite. Their survey of more than a dozen graftonite-beusite analyses from the El Sampal (IIIA), Grant (IIIB), and other iron meteorites, revealed a range of Ca-free compositions from near end-member graftonite to samples with 33 to 58 mol% beusite. Because these compositions represent a continuous solid solution and the majority of specimens lie well within the Fe^{2+}-rich graftonite field, we designate all of these occurrences as *DA graftonite*.

Farringtonite [$(Mg,Fe)_3(PO_4)_3$]. *DA farringtonite* is found in pallasites, occurring with fairfieldite and whitlockite (Buseck 1977; Buseck and Holdsworth 1977).

Sarcopside [$(Fe,Mn)_3(PO_4)_2$]. *DA sarcopside* was reported by Olsen and Steele (1997) from troilite nodules in iron meteorites in association with graftonite, galileiite, and chromite.

Stanfieldite [$Ca_4Mg_5(PO_4)_6$]. *DA stanfieldite* was described by Fuchs (1967) and has been reported from several pallasites (Buseck 1977; Buseck and Holdsworth 1977; Davis and Olsen 1991).

Buchwaldite ($NaCaPO_4$). *DA buchwaldite* is a rare Na-Ca-phosphate described from a 40 μm diameter crystal by Olsen et al. (1977a). It occurs within troilite nodules associated with chromite and other phosphate minerals in the Cape York (IIIAB) iron meteorite (Kracher et al. 1977).

Marićite ($NaFePO_4$). *DA marićite* was reported by Kracher et al. (1977) from the Cape York (IIIAB) iron meteorite. This rare occurrence is in association with buchwaldite and two other unidentified alkali phosphates.

Moraskoite [$Na_2Mg(PO_4)F$]. *DA moraskoite* was described by Karwowski et al. (2015) in the Morasko (IAB) iron meteorite, in which it is associated with other primary phosphate minerals.

Xenophyllite [$Na_4Fe_7(PO_4)_6$]. Britvin et al. (2020b) reported the new phosphate *DA xenophyllite* from the Augustinovka (IIIAB) iron meteorite, associated with sarcopside, schreibersite, chromite, and pentlandite.

Brianite [$Na_2CaMg(PO_4)_2$]. *DA brianite* was discovered by Fuchs et al. (1967) as a minor phase in pockets up to 1.5 cm maximum dimensions with individual crystals up to 200 μm across from the Dayton (IAB) hexahedrite, where it occurs in association with whitlockite and panethite (McCoy et al. 1993, 1994). Scott and Bild (1974) reported brianite as scattered veins throughout silicate inclusions, but also commonly in contact with metal, in the San Cristobal (unique IAB) iron meteorite. Brianite has also been found in the Youndegin (IAB) low-Ni iron meteorite (Fuchs 1969a).

Panethite [$Na_2(Fe,Mn)_2(PO_4)_2$]. *DA panethite* occurs with whitlockite and brianite in the Dayton (IAB) iron meteorite in pockets up to 1.5 cm maximum dimensions, with individual crystals up to 200 μm diameter (Fuchs et al. 1967; McCoy et al. 1993, 1994).

Fillowite Group [$Na_2(Ca,Fe,Mg,Mn)_8(PO_4)_6$]. Three closely related members of the hexagonal (space group $R\bar{3}$) fillowite group—johnsomervilleite, chladniite, and galileiite—have been reported from troilite nodules in iron meteorites. We suspect that these three species may represent a single natural kind with a continuous solid solution and similar paragenetic mode. However, until more compositional data are available, we list these species as distinct natural kinds.

Johnsomervilleite [$Na_2Ca(Fe,Mg,Mn)_7(PO_4)_6$]. *DA johnsomervilleite* was reported by Olsen and Steele (1993, 1997) as rare accessory phases from troilite nodules in the Carlton (IIICD), Chupaderos (IIIB), Grant (IIIB), El Sampal (IIIA), and Sandtown (IIIAB) iron meteorites in association with chromite plus graftonite and/or sarcopside.

Chladniite [$Na_2CaMg_7(PO_4)_6$]. *DA Chladniite* was identified and named by McCoy et al. (1994) based on a single crystal ~1 mm in maximum dimension, which was found in a silicate-bearing inclusion in the Carlton (IIICD) iron meteorite in association with dominant chlorapatite (70 vol%), forsterite, orthoenstatite, and albite. McCoy et al. (1994) measured the chemical formula as [$Na_{1.77}Ca_{0.98}(Mg_{6.96}Fe_{0.26}Mn_{0.04})(PO_4)_6$].

Galileiite [$Na_2(Fe,Mn)_8(PO_4)_6$]. The Na-Fe-phosphate *DA galileiite* was described by Olsen and Steele (1997) from five different group III iron meteorites. It occurs as rare grains up to 30 μm in diameter in troilite nodules in association with graftonite, sarcopside, and chromite.

Tsangpoite [$Ca_5(PO_4)_2(SiO_4)$]. *DA tsangpoite* was characterized by Hwang et al. (2019) from the D'Orbigny angrite, where it occurs as numerous elongated hexagonal prismatic crystals to

tens of micrometers maximum dimension in association with hedenbergite, iron sulfide, and magnetite. Earlier reports of this rare Ca-silico-phosphate in angrites include occurrences in Asuka 881371 (Prinz and Weisberg 1995), NWA 1296 and 1670 (Jambon et al. 2005, 2008), NWA 4590 (Mikouchi et al. 2011), and NWA 11119 (Srinivasan et al. 2018).

Oxides

Oxides minerals are common, if usually minor, phases in non-chondritic meteorites [Mittlefehldt et al. (1998), Tables 17, 32, and 38]. The oxide spinels and ilmenite account for most reported occurrences, while instances of perovskite group oxides, corundum, eskolaite, rutile, and baddeleyite are rare.

Oxide spinel group [$(Mg,Fe^{2+})(Al,Fe^{3+},Cr^{3+},Ti)_2O_4$]. The oxide spinel group, the most ubiquitous oxide phases in non-chondritic meteorites, encompass a complex range of solid solutions, representing at least eight major idealized end-members: spinel ($MgAl_2O_4$), hercynite ($Fe^{2+}Al_2O_4$), magnesioferrite ($MgFe^{3+}_2O_4$), magnetite ($Fe^{2+}Fe^{3+}_2O_4$), magnesiochromite ($MgAl_2O_4$), chromite ($FeCr^{3+}_2O_4$), qandilite ($Mg_2Ti^{4+}O_4$), and ulvöspinel ($Fe^{2+}_2Ti^{4+}O_4$). In addition, some spinels incorporate significant amounts of Ca, Mn^{2+}, Zn, V^{3+}, Ti^{3+}, and/or Si. Given the compositional diversity and extensive solid solution among natural meteoritic samples of oxide spinels, it is challenging to determine how many distinct natural kinds are represented. In some instances, as with the angrites [Mittlefehldt et al. (1998), Table 38], two distinct oxide spinel compositions—one hercynitic and the other Al-poor, either magnetite or ulvöspinel—commonly coexist. We therefore recognize *DA hercynite*, *DA magnetite*, and *DA ulvöspinel* as distinct natural kinds. In other meteorite groups, including pallasites, brachinites, ureilites, diogneites, and eucrites, a range of Cr-rich spinel compositions usually closest to the chromite end-member is observed; we lump all such examples into *DA chromite*.

Chromite ($Fe^{2+}Cr_2O_4$). *DA chromite* is often the most abundant oxide mineral in non-chondritic meteorites. It is an important Cr-bearing phase in many iron meteorites (Buchwald 1975; Ulff-Møller et al. 1995; Scott et al. 1996), at times occurring as oriented thin "Reichenbach lamellae" encased by kamacite. Chromite is found in most pallasites (Buseck 1977), with modest substitution of Al for Cr^{3+} in some samples (Bunch and Keil 1971); as a minor phase in brachinites (up to ~3 vol%; Nehru et al. 1983); in ureilites (up to ~6 vol%; Mittlefehldt et al. 1998; Goodrich et al. 2014); as a common minor mineral up to 5 vol% in diogenites (Mittlefehldt 1994; Bowman et al. 1997); and in eucrites (Lovering 1975).

Magnetite (Fe_3O_4). The Angra dos Reis angrite holds accessory Ti-rich *DA magnetite* of average composition ($Fe^{2+}_{1.50}Mg_{0.06}Al_{0.15}Fe^{3+}_{0.51}Ti_{0.61}O_4$), which occurs in association with fassaite, forsterite, hercynite, and troilite, as well as an unusual suite of accessory phases including kirschsteinite, celsian, and baddeleyite (Prinz et al. 1977). A similar association was observed by McKay et al. (1988) in the LEW 86010 angrite, in which Ti-rich magnetite of average composition ($Fe^{2+}_{0.72}Mg_{0.06}Al_{0.19}Fe^{3+}_{1.01}Ti_{0.68}O_4$) occurs with hercynite.

Hercynite ($Fe^{2+}Al_2O_4$). *DA hercynite* is a minor phase in several angrite meteorites. Hercynite of average composition [$(Fe^{2+}_{0.75}Mg_{0.25})(Al_{1.80}Fe^{3+}_{0.07}Cr^{3+}_{0.07})O_4$] occurs in the Angra dos Reis angrite with fassaite, olivine, and troilite, as well as an unusual suite of accessory phases including kirschsteinite, celsian, Ti-rich magnetite, and baddeleyite (McKay et al. 1988; Prinz et al. 1977). In the Asuka 881371 angrite, hercynite of composition [$(Fe^{2+}_{0.80}Mg_{0.32})(Al_{1.35}Cr^{3+}_{0.50}Ti_{0.03})O_4$] coexists with ulvöspinel (Mikouchi et al. 1996), whereas in the LEW 86010 angrite hercynite of average composition [$(Fe^{2+}_{0.76}Mg_{0.25})(Al_{1.90}Fe^{3+}_{0.04}Cr^{3+}_{0.03}Ti_{0.02})O_4$] occurs with Ti-rich magnetite (McKay et al. 1988). Thus, meteoritic hercynite is commonly found in association with a second, Al-poor oxide spinel.

Ulvöspinel ($Fe^{2+}_2Ti^{4+}O_4$). Mikouchi et al. (1996) described *DA ulvöspinel* from the Asuka 881371 angrite, with reported average composition close to ($Fe^{2+}_{2.2}Al_{0.1}Ti_{0.8}O_4$). It co-occurs with Cr-rich hercynite [$(Fe^{2+}_{0.80}Mg_{0.32})(Al_{1.35}Cr_{0.50}Ti_{0.03})O_4$].

Other oxides

Ilmenite ($FeTiO_3$). *DA ilmenite* was reported by Mittlefehldt and Lindstrom (1993) from a lithic clast in a diogenite. Ilmenite is a common accessory mineral in eucrites, where it occurs as individual grains, as composite grains with chromite, and as an exsolved phase in chromite grains (Bunch and Keil 1971; Delaney et al. 1984), as well as in a variety of iron meteorites (Prinz et al. 1982; Ruzicka 2014).

Corundum (Al_2O_3). *DA corundum* was reported by Prinz et al. (1994) from the ureilite LEW 88774 as micrometer-scale grains with chromite and Cr-rich pyroxene.

Eskolaite (Cr_2O_3). *DA eskolaite* occurs in the LEW 88774 Cr-rich, anomalous ureilite in association with a reduced assemblage with carbides, chromite, brezinaite, and graphite (Prinz et al. 1994; Warren and Kallemeyn 1994).

Rutile (TiO_2). *DA rutile* is a minor phase in silicate inclusions in the Somberrete (IAB) iron meteorite, in which it is associated with albitic glass (the dominant phase), orthoenstatite, anorthite, chlorapatitie, and minor kaersutite, tridymite, and oxides (Prinz et al. 1982). Rutile was also reported in some mesosiderites (El Goresy 1971).

Baddeleyite (ZrO_2). *DA baddeleyite* occurs in the Angra dos Reis angrite as a minor mineral in association with major fassaite, forsterite, hercynite, and troilite, as well as an unusual suite of accessory phases including kirschsteinite, Ti-rich magnetite, and celsian (Prinz et al. 1977). It is also found in eucrites (Haba et al. 2014).

Perovskite ($CaTiO_3$). Rosenshein et al. (2006) reported a single occurrence of *DA perovskite* of composition [$(Ca_{0.94}Mg_{0.05}Fe_{0.02})Ti_{0.99}O_3$] in an unusual oxide clast in the Allan Hills 84008 aubrite. Perovskite occurs in association with geikeilite as inclusions in troilite.

Geikeilite ($MgTiO_3$). One occurrence of *DA geikeilite* close to end-member composition was described by Rosenshein et al. (2006) **{{AU: Reference not in list. Please add.}}** from an unusual oxide clast in the Allan Hills 84008 aubrite.

Armalcolite [$(Mg,Fe^{2+})Ti_2O_5$]. *DA armalcolite* is a rare phase in the silicate inclusions of iron meteorites (Ruzicka 2014). It has been reported from several IIE iron meteorites, including Elga, Colomera, and Miles (Prinz et al. 1983a; Ebihara et al. 1997; Rubin and Ma 2021).

Silicates

Forsteritic olivine, low- and high-Ca pyroxenes, and calcic plagioclase are major minerals in a wide range of achondrite,

stony-iron, and silicate-bearing iron meteorites (Bunch et al. 1970; McCoy et al. 1993; Benedix et al. 1998, 2000; Mittlefehldt et al. 1998; Rubin and Ma 2021). These and other silicates in supposedly non-chondritic meteorites underscore the difficulty of distinguishing minerals formed through asteroidal differentiation, as opposed to earlier and later events. For example, silicate inclusions in the Netschaëvo (IIE) iron meteorite appear to be relatively unaltered chondritic clasts, while those in Techado (IIE) are partially melted but undifferentiated. On the other hand, many non-chondritic meteorites display evidence for extensive impact alteration through brecciation and shock melting—processes that postdate asteroidal differentiation. In some instances, meteorites may represent a mixture of impact-induced metal melts surrounding fragmented and only partially melted silicates. Here we include all known phases from non-chondritic meteorites that appear to have formed by crystallization from a melt or vapor, or by subsequent solid-state reactions during cooling/annealing—i.e., minerals that were not formed directly by shock processes, aqueous alteration, or thermal metamorphism.

Silica group (SiO_2). Silica group minerals, including tridymite and less frequently cristobalite, quartz, and silica glass, are minor/trace phases in mafic lithologies.

Tridymite (SiO_2). *DA tridymite* is the most common silica polymorph in meteorites. It has been reported from a variety of iron meteorites (Buchwald 1975; Prinz et al. 1982; Scott et al. 1996), notably from the Gibeon and Steinbach (IVA) irons (Reid et al. 1974). The former contains a tridymite grain exceeding 2 cm maximum dimension (Marvin et al. 1997). Tridymite is also a common phase in mafic meteorite lithologies: it accounts for 5 to 14 vol% in mesosiderite basaltic clasts (Nehru et al. 1980) and up to 8 vol% in basaltic eucrites (Delaney et al. 1984; Ikeda and Takeda 1985; Mittlefehldt et al. 1998).

Cristobalite (SiO_2). *DA cristobalite* is a minor phase in several eucrites, where it occurs in association with other silica polymorphs (Aoudjehane and Jambon 2007), and as an accessory mineral in the troilite nodules of the Carbo (IID) iron meteorite (Marvin 1962). Ma et al. (2012a) record cristobalite as a rare accessory phase in the Zakłodzie ungrouped enstatite achondrite, where it co-occurs with more abundant tridymite and quartz.

Quartz (SiO_2). *DA quartz* has been reported as a minor phase in basaltic eucrites (Mittlefehldt et al. 1998). Marvin et al. (1997) described quartz-rich regions 3 to 4 mm in diameter occurring in the cracked core of a large (>2 cm maximum dimension) tridymite grain from the Gibeon (IVA) iron meteorite. Quartz also occurs with tridymite, rare cristobalite, and sinoite in the Zakłodzie ungrouped enstatite achondrite (Ma et al. 2012a).

Silica glass (SiO_2). Ruzicka (2014) summarizes silica-rich glass compositions, which are common in some silicate inclusions of iron meteorites. Of note are occurrences of *DA silica glass* with compositions exceeding 80 wt% SiO_2 in inclusions from Weekeroo Station and Miles (IIE) irons, in contrast to many glasses of more feldspathic compositions (see below).

Olivine group [$(Mg,Fe,Ca)_2SiO_4$]. Olivine is a major mineral in many types of non-chondritic meteorites [Mittlefehldt et al. (1998), Tables 7, 11, 13, 20, 24, 28, 31, 36, 43, and Figs. 17 and 58]. Note that while forsterite and fayalite form a continuous solid solution, the great majority of non-chondritic olivine occurrences fall in the range $Fo_{55–99}$. An exception is the occurrence of more fayalitic olivine in some angrites [$Fo_{32–86}$; Mittlefehldt et al. (1998), Table 36]; however, Prinz et al. (1990) and Mikouchi et al. (1996) reported that larger olivine grains are strongly zoned with magnesian cores ($Fo_{73–90}$) compared to more ferroan rims. Otherwise, the few outlier occurrences of fayalite are near end-member Fe_2SiO_4. For example, Yanai (1994, Fig. 8) summarized a bimodal distribution of olivine compositions in angrites, with most analyses in the range $Fo_{45–90}$, but a few analyses clustered at $Fo_{1–9}$. Therefore, we recognize *DA forsterite* and *DA fayalite* as distinct natural kinds.

Forsterite (Mg_2SiO_4). *DA forsterite* is a major silicate phase in many non-chondritic meteorites. The most olivine-rich meteorites are brachinites with as much as 98 vol% olivine with average 30 to 35 mol% fayalitic component (Kring et al. 1991; Nehru et al. 1992). Ureilites are ultramafic cumulates with up to >90 vol% olivine, typically with ~5 to 25 mol% Fe_2SiO_4 (Mittlefehldt et al. 1998, and references therein). Up to ~10 vol% of nearly pure end-member forsterite (typically $Fo_{99.99}$) is a common phase in highly reduced enstatite achondrites (aubrites), in which orthoenstatite is the dominant silicate phase (Watters and Prinz 1979).

Forsterite also occurs in pallasites with crystals of forsteritic olivine to >1 cm diameter that are typically close to Fo_{90} associated with Fe-Ni alloys (Buseck and Goldstein 1969; Buseck 1977; Ulff-Møller et al. 1998; Fig. 1b). In some instances, pallasite olivine incorporates P-rich zones, locally with up to 5 wt% P_2O_5 (Buseck 1977).

Fayalite (Fe_2SiO_4). Olivine close to fayalite in composition occurs rarely in non-chondritic meteorites. Ikeda and Takeda (1985) describe *DA fayalite* ($Fo_{10–14}$) associated with augite (~$Wo_{40}Fs_{40}$), tridymite, and plagioclase ($An_{~80}$) in unusual ferroan igneous clasts in howardites. Yanai (1994, Fig. 8) reported olivine compositions in angrites, with most analyses in the range $Fo_{45–90}$, but a few analyses clustered at $Fo_{1–9}$. Olivine in angrites are often Ca-rich, with up to 20 mol% of the Ca end-member in the most Fe-rich examples (Mittlefehldt et al. 2002). Fayalite was also reported by Srinivasan et al. (2018) as a minor phase in the unique silica-rich achondrite NWA 11119, which features millimeter-diameter vesicles comprising 30 vol% tridymite associated with an unusual mineralogical suite, including tranquillityite, zircon, and tsangpoite.

Kirschsteinite ($CaFe^{2+}SiO_4$). The calcic olivine *DA kirschsteinite* with average composition [$(Ca_{0.94}Fe^{2+}_{0.06})(Fe^{2+}_{0.60}Mg_{0.40})SiO_4$] is an accessory phase in the Angra dos Reis and other angrite achondrites, where it occurs as inclusions in low-Ca olivine in association with fassaite, hercynite, Ti-rich magnetite, and troilite (Prinz et al. 1977; McKay et al. 1988, 1990). In LEW 86010, kirschsteinite occurs as exsolution lamellae in Mg-Fe olivine (Mikouchi et al. 1995), while in D'Orbigny, it is observed as overgrowths on Mg-Fe olivine (Mittlefehldt et al. 2002).

Pyroxene group [$(Ca,Mg,Fe,Ti,Al)_2(Al,Si)_2O_6$]. Pyroxene group minerals are principal constituents of most types of achondrite and stony-iron meteorites [Mittlefehldt et al. (1998), Tables 7, 11, 15, 20, 25, 28, 30, 37, 42, and Fig. 42]. The nomenclature of meteoritic pyroxene group minerals is potentially confusing and replete with archaic and discredited terminology, owing to both chemical and structural complexities (Morimoto et al. 1988; Deer et al. 1997; Wenk and Bulakh 2003). Most meteoritic examples fall close to the familiar Mg-Fe-Ca pyroxene quadrilateral, bounded by end-members enstatite (En; $Mg_2Si_2O_6$), ferrosilite

(Fs; $Fe_2Si_2O_6$), diopside (Di; $CaMgSi_2O_6$), and hedenbergite (Hd; $CaFeSi_2O_6$). Pyroxene compositions are also commonly reported in terms of the mol% of their pure calcium component, wollastonite (Wo; $Ca_2Si_2O_6$). Four different pyroxene phase regions occur for Mg-Fe-Ca compositions near liquidus temperatures (e.g., Deer et al. 1997). Above ~1200 °C, a miscibility gap separates: (1) Ca-rich augites (all compositions with >Wo$_{\sim 30}$) and (2) Ca-poorer pigeonites (<Wo$_{\sim 15}$), both of which are monoclinic (space group $C2/c$). A second gap occurs between pigeonites (Wo$_{>10}$) and compositions close to the $MgSiO_3$-$FeSiO_3$ join (Wo$_{<05}$), for which the high-temperature pyroxene phases are: (3) protoenstatite (orthorhombic space group *Pbcn*) near the Mg-rich end-member and (4) orthopyroxene (orthorhombic space group *Pbca*) for more ferroan compositions.

Upon cooling, these four high-temperature pyroxene phases may undergo several types of solid-state transformations of significance to meteorite mineralogy—inversions that depend strongly on the thermal history of individual crystals. Some transitions are isochemical. For example, protoenstatite transforms to orthoenstatite below ~1000 °C and, given sufficient annealing time, may further transform to clinoenstatite (monoclinic $P2_1/c$) below ~600 °C. High-temperature $C2/c$ pigeonite similarly transforms to the low-temperature $P2_1/c$ form on cooling. Evidence for these isochemical transformations may be preserved in distinctive twinning (e.g., Takeda et al. 1989).

More commonly, shifting boundaries of miscibility gaps on cooling lead to exsolution of one pyroxene composition from another. Most significantly, the augite-pigeonite miscibility gap becomes wider with cooling below ~1200 °C, with coexisting equilibrium compositions approaching Wo$_5$ and Wo$_{45}$ below 1000 °C for some Mg-Fe compositions. Consequently, depending on cooling rates and annealing times, pigeonite with Wo$_{>5}$ may exsolve one or more generations of augite, while augite with Wo$_{<45}$ may exsolve pigeonite (Harlow et al. 1979; Mori and Takeda 1981a). Indeed, owing to multiple stages of exsolution, it is not uncommon for four different compositions of pyroxene to coexist in a single igneous rock (Deer et al. 1997).

This profligacy of potential compositional and morphological natural kinds of pyroxene creates challenges. We choose to simplify pyroxene nomenclature, lumping as much as possible pyroxenes that share their structure types within a continuous compositional field. Consequently, three natural kinds encompass the vast majority of pyroxenes in non-chondritic meteorites:

(1) *DA orthoenstatite*: Orthopyroxenes occur close to the En-Fs join with <5 mol% Wo. The official end-member names for this series are enstatite and orthoferrosilite. Almost all meteoritic examples, with the exception of orthopyroxenes with augite exsolution in some eucrites (En$_{35–75}$), are Mg-dominant. Therefore, we designate these occurrences as *DA orthoenstatite*; we employ "orthoenstatite" instead of the IMA-approved name "enstatite" (Morimoto et al. 1988) to reduce ambiguity.

(2) *DA pigeonite*: Low-calcium clinopyroxenes (monoclinic space group $P2_1/c$) encompass a range of Mg-Fe-Ca compositions, almost always with Mg > Fe in non-chondritic meteorites. The clinoenstatite-clinoferrosilite series is defined as having <5 mol% of the Wo component. However, these pyroxenes form a continuous solid solution with the somewhat more calcic pyroxenes (Wo$_{5–15}$) designated "pigeonite" by IMA conventions. Here we lump all low-Ca clinopyroxenes into *DA pigeonite*.

(3) *DA augite*: A similar somewhat arbitrary division is applied by IMA to Ca-rich pyroxenes, all of which are $C2/c$ monoclinic phases within a single-phase region. Therefore, we lump examples with Wo$_{45–50}$ close to the diopside-hedenbergite join together with somewhat less calcic clinopyroxenes (Wo$_{30–45}$), defined by IMA conventions as augite, into *DA augite*.

In addition to these common phases, we recognize three additional natural kinds of non-chondritic meteoritic pyroxene:

(4) Near end-member hedenbergite from the Asuka 881371 angrite represents a clear outlier [Yanai (1994), Fig. 8], which we name *DA hedenbergite*.

(5) The Na-Cr clinopyroxene *DA kosmochlor* ($NaCr^{3+}Si_2O_6$; formerly ureyite) occurs in some iron meteorites.

(6) Finally, calcic clinopyroxene nomenclature is further complicated by the occurrence of "fassaite," a Ca-Mg-dominant, Fe-poor clinopyroxene with Al and Ti, which result in compositions that lie significantly outside the pyroxene quadrilateral. Fassaite is closest compositionally to the IMA-approved species diopside ($CaMgSi_2O_6$), but it always incorporates significant fractions of other components, including kushiroite ($CaAl_2SiO_6$; also known as calcium-Tschermak's pyroxene), grossmanite ($CaTi^{3+}AlSiO_6$), and/or a hypothetical Ti^{4+} end-member ($CaMg_{0.5}Ti^{4+}_{0.5}AlSiO_6$). Sack and Ghiorso (2017) demonstrate that these compositions are separated by as many as three miscibility gaps from diopside; therefore, *DA fassaite*, though not officially recognized by the IMA, represents at least one additional pyroxene natural kind.

Orthoenstatite ($MgSiO_3$). *DA orthoenstatite* is a major primary igneous phase in several types of achondrites, with crystals sometimes exceeding 5 cm in maximum dimension (Mittlefehldt et al. 1998, and references therein). Orthoenstatite also forms through the inversion of pigeonite, which commonly leads to exsolution of augite lamellae (Deer et al. 1997). Diogenites incorporate from ~85 to 100 vol% orthoenstatite, typically with compositions close to En$_{75}$ [Mittlefehldt et al. (1998), Fig. 42 and Table 30]. Near end-member orthoenstatite (En$_{>98}$) is the dominant mineral in the unusual unbrecciated Shallowater enstatite achondrite, which has ~80 vol% orthoenstatite in crystals to 4.5 cm maximum dimension (Reid and Cohen 1967). This example contrasts with most aubrites, which have disordered enstatite, largely the result of impact alteration (Watters and Prinz 1979). Orthoenstatite also occurs in pallasites (Hiroi et al. 1993), in ureilites (Takeda 1987; Takeda et al. 1989), and in HED meteorites (Delaney et al. 1984; Mittlefehldt 1994; Bowman et al. 1997).

Pigeonite [$(Mg,Fe,Ca)SiO_3$]. *DA pigeonite*, including both pigeonite and samples close to end-member clinoenstatite with <5 mol% Wo, are significant minerals in many achondritic meteorites (Mittlefehldt et al. 1998). DA pigeonite is the dominant, and in some instances the only, pyroxene in ureilites, which are ultramafic restite achondrites (Takeda 1989; Takeda et al. 1992). In brachinites, which are olivine cumulate rocks, pigeonite is second in abundance to forsterite, constituting up to 15 modal percent (Kring et al. 1991; Nehru et al. 1992).

Augite [$(Ca,Mg,Fe)_2Si_2O_6$]. *DA augite*, including samples close to end-member diopside, occur as the principal calcium-bearing phase in several types of plagioclase-free ultramafic achondrites. Augite is found with pigeonite and/or orthopyroxene in some ureilites (Takeda 1989; Takeda et al. 1992). Unusually

ferroan augite (~$Wo_{40}Fs_{40}$) occurs in igneous clasts of howardites, associated with fayalite, tridymite, and plagioclase (Ikeda and Takeda 1985). Essentially iron-free diopsidic augite occurs in enstatite achondrites (aubrites) as a common minor phase, accounting for up to ~8 vol% of some examples (Olsen et al. 1977b; Watters and Prinz 1979). In many meteorites, for example diogenites (Bowman et al. 1997), pigeonite has inverted to orthoenstatite that has exsolution lamellae of a range of calcic clinopyroxenes, including diopsidic ($Di_{>90}$) and augitic ($Wo_{<45}Fs_{<25}$) examples (Mori and Takeda 1981b; Takeda and Mori 1985; Mittlefehldt and Lindstrom 1993).

Hedenbergite ($CaFeSi_2O_6$). Near end-member *DA hedenbergite* of composition [$(Ca_{0.99}Mg_{0.01}Fe_{1.00})Si_2O_6$], as well as other compositions on the Di-Hd join, occur in the Asuka 881371 angrite [Yanai (1994), Table 1], and in the D'Orbigny angrite (Hwang et al. 2019).

Fassaite [$Ca(Mg,Al,Ti^{3+},Ti^{4+})(Al,Si)SiO_6$]. The Al- and/or Ti-rich calcic pyroxene, *DA fassaite*, is the major phase (93 vol%) in the unusual Angra dos Reis angrite (Prinz et al. 1977). With average composition [$(Ca_{0.97}Mg_{0.59}Fe^{2+}_{0.21}Al_{0.16}Ti_{0.06})(Al_{0.28}Si_{1.72})O_6$], this clinopyroxene incorporates ~16 mol% Ca-Tschermak's and 21 mol% hedenbergite components, but only 6 mol% of the grossmanite component, in contrast to the more Ti-rich, Fe-poor fassaite in CAIs (Morrison and Hazen 2020). Fassaite occurs both as a groundmass of grains up to 0.5 mm maximum dimension and as larger grains to ~3 mm enclosing the groundmass. It occurs in association with olivine, hercynite, and troilite, as well as an unusual suite of accessory phases including kirschsteinite, celsian, Ti-rich magnetite, and baddeleyite. Fassaite is also present in other angrites (McKay et al. 1988, 1990; Prinz et al. 1988, 1990), as well as in angrite-like clasts in polymict ureilites (Prinz et al. 1983b, 1986).

Kosmochlor ($NaCr^{3+}Si_2O_6$). The Na-Cr clinopyroxene *DA kosmochlor* (formerly named ureyite; Morimoto et al. 1988) occurs in some iron meteorites, typically in association with graphite and chromite (Frondel and Klein 1965; Olsen and Fuchs 1968).

Amphibole group. Amphiboles, a major group of rock-forming double-chain silicates, make their earliest appearances as minor accessory phases in silicate inclusions in iron meteorites and in an aubrite. Two IMA-approved amphibole species, fluoro-richterite and kaersutite, have similar compositions and may represent end-members of a continuous solid solution. However, they occur in different contexts and only fluoro-richterite has measurable F. Therefore, we consider *DA fluoro-richterite* and *DA kaersutite* to be distinct natural kinds.

Fluoro-richterite [$Na(NaCa)Mg_5Si_8O_{22}F_2$]. *DA fluoro-richterite* was reported from the Canyon Diablo and Wichita County (IAB) iron meteorites (Olsen 1967; Olsen et al. 1973). In addition, Bevan et al. (1977) reported anhydrous fluoro-richterite in needle-like crystals to ~1 mm maximum dimension from the Mayo Belwa aubrite, which contains 5 vol% crystal-lined vugs. Rubin (2010) suggested that fluoro-richterite may be an impact-related phase, formed when F-rich gas condensed in shock-induced vugs.

Kaersutite [$NaCa_2(Mg_3AlTi^{4+})(Si_6Al_2)O_{22}O_2$]. A single occurrence of *DA kaersutite* has been reported from silicate inclusions in the Somberrete (IAB) iron meteorite (Prinz et al. 1982). DA kaersutite is associated with albitic glass (the dominant phase), orthoenstatite, anorthite, and chlorapatitie.

Feldspar group [$(Ca,Na,K)Al(Al,Si)Si_2O_8$]. Calcic plagioclase is an abundant primary igneous phase in many types of non-chondritic meteorites [Mittlefehldt et al. (1998), Tables 7, 11, 18, 20, 28, 33, 39, and 44]. Albite, sanidine, and celsian, by contrast, are extremely minor phases, typically associated with residual silica-rich melts. In spite of the continuous solid solution of the plagioclase series, we draw a distinction between *DA anorthite*, which is typically $An_{99–75}$ and, with the exception of brachinites, rarely displays compositions with $An_{<60}$, and *DA albite*, which is invariably close to the $NaAlSi_3O_8$ end-member ($An_{<10}$).

Anorthite ($CaAl_2Si_2O_8$). *DA anorthite* is an important component of many non-chondritic meteorites (Mittlefehldt et al. 1998, and references therein). It occurs in silicate inclusions in iron meteorites ($An_{57–93}$; Bunch and Olsen 1968; Bunch et al. 1970; Olsen et al. 1994); in aubrites ($An_{75–95}$; Watters and Prinz 1979); in HED group achondrites [$An_{72–95}$; Mittlefehldt et al. (1998), Table 33]; in angrites ($An_{–99}$; Prinz et al. 1977; Crozaz and McKay 1990; Mikouchi et al. 1996); in basaltic ($An_{>70}$) and cumulate eucrites [$An_{91–98}$; Mittlefehldt et al. (1998), Table 33], and in mesosiderites ($An_{91–93}$; Mittlefehldt et al. 1998).

Albite ($NaAl_3SiO_8$). Near end-member *DA albite* is a common, if minor, phase in non-chondritic meteorites. Albite occurs frequently in silica-rich clasts in numerous iron meteorites (Bunch and Olsen 1968; Wasserburg et al. 1968; Prinz et al. 1983a; Ruzicka 2014). For example, McCoy et al. (1994) report albite of composition ($Ab_{91}An_5Or_4$) from chlorapatite-dominant silicate inclusions in the Carlton (IIICD) iron meteorite.

Brachinites, which are dunites with up to 98 vol% forsterite, are an outlier with plagioclase compositions observed between An_{16} and An_{37} [Nehru et al. (1983, 1996); Mittlefehldt et al. (1998), Table 18], whereas aubrites typically contain minor albitic plagioclase (Rubin and Ma 2021).

Sanidine ($KAlSi_3O_8$). Potassic feldspars are rare phases in non-chondritic meteorites. Wasserburg et al. (1968) reported a sanidine crystal 11 cm in length from a silicate inclusion in the Colomera (IIE) iron meteorite, where it occurs in association with plagioclase-silica glass, clinoenstatite, and several minor phases. K feldspar is found in the Ni-rich San Cristobal (unique IAB) iron meteorite (Wlotzka and Jarosewich 1977), and as exsolution lamellae in "antiperthite" with an albitic host from the Watson (IIE) iron meteorite (Olsen et al. 1994). Potassic feldspar also occurs in the Bilanga diogenite (Domanik et al. 2004) and in some eucrites (Barrat et al. 2007).

Celsian ($BaAl_2Si_2O_8$). *DA celsian* [$(Ba_{0.90}Ca_{0.08}Na_{0.02})(Al_{1.98}Si_{2.02})O_8$] occurs in the Angra dos Reis angrite as a minor mineral in association with dominant fassaite, plus forsterite, hercynite, and troilite, as well as an unusual suite of accessory phases including kirschsteinite, Ti-rich magnetite, and baddeleyite (Prinz et al. 1977). Prinz et al. (1977) also describe minor coexisting anorthite from Angra dos Reis. This earliest known occurrence of a barium mineral may be the result of crystallization of a late-stage residual melt enriched in alkaline earth elements.

Feldspathic glass [Na-(K-Ca)-Al-Si]. *DA feldspathic glass*, in contrast to shock-induced maskelynite (see Part IVB below), occurs as a significant phase in a variety of silicate-rich inclusions that represent late-stage melt fractions (Ruzicka 2014). Sodium-dominant albitic glass is the major phase in silicate inclusions in the Somberrete (IAB) iron meteorite, in which it is associated

with enstatite, anorthite, chlorapatitie, and minor kaersutite, tridymite, and oxides (Prinz et al. 1982). Wasserburg et al. (1968) reported albitic glass from the Colomera (IIE) silicate-bearing iron meteorite, where it occurs in association with clinoenstatite, forsterite, and other phases. Na-K-Al-Si glass is reported from interstitial silicate assemblages in ureilites with clinoenstatite and augite (Goodrich 1986), while feldspathic glass with a significant anorthite content ($An_{5–50}$) occurs in lithic clasts from polymict ureilites (Prinz et al. 1986). Some brachinites contain Na-rich feldspathic glass (Nehru et al. 1983). Finally, feldspathic glass is a volumetrically minor component of some enstatite achondrites: Fuchs (1974) reported Na-K-Al-Si glass as ~5 μm diameter trapped melt inclusions in orthoenstatite in the Bishopville, Norton County, and Pena Blanca Springs aubrites, while Fogel (2005) described basaltic vitrophyre clasts in the Khor Temiki and LEW 87007 aubrite with 51 and 13 vol% albitic glass in the inclusions, respectively.

Other silicates

Zircon ($ZrSiO_4$). *DA zircon* is a rare phase in non-chondritic meteorites, reported in basaltic eucrites (Gomes and Keil 1980) and the unique andesitic (30 vol% tridymite) achondrite NWA 11119 (Srinivasan et al. 2018). Ireland and Wlotzka (1992) analyzed two zircon grains from the Vaca Muerta mesosiderite, from which they obtained a $^{207}Pb/^{206}Pb$ age of 4.563 ± 0.015 Ga.

Tranquillityite [$Fe_8^{2+}Ti_3Zr_2Si_3O_{24}$]. *DA tranquillityite* was identified by Srinivasan et al. (2018) as a minor phase in the unique NWA 11119 silica-rich achondrite—a silica-rich extrusive rock with numerous millimeter-diameter vesicles (comprising >1 vol%) surrounded by quenched melt and 30 vol% tridymite associated with an unusual mineralogical suite, including zircon, fayalite, and tsangpoite.

Yagiite [$NaMg_2(AlMg_2Si_{12})O_{30}$]. *DA yagiite* is member of the milarite group, originally described by Bunch and Fuchs (1969b) from silicate inclusions in the Colomera (IIE) iron meteorite. With average composition [$(Na_{1.20}K_{0.30})(Mg_{2.60}Fe_{0.34}Ti_{0.10}Al_{1.96})(Si_{10.22}Al_{1.78})O_{30}$], yagiite occurs as inclusions in fassaite and in association with whitlockite, tridymite, and albite. It has subsequently been identified in a similar inclusion in the Somberrete (IAB) iron meteorite (Ruzicka 2014).

Kuratite [$Ca_2(Fe_5^{2+}Ti)O_2(Si_4Al_2O_{18})$]. *DA kuratite* is a rare Fe^{2+} analog of rhönite that was characterized by Hwang et al. (2016) from the D'Orbigny angrite, where it occurs as euhedral to anhedral crystals up to ~20 μm maximum dimension in close association with hedenbergite, ulvöspinel, fayalite, kirschsteinite, and iron sulfide. Hwang et al. (2016) suggested that this assemblage represents rapid cooling of an interstitial melt from >1000 °C.

Krinovite [$Na_4(Mg_8Cr_4^{3+})O_4(Si_{12}O_{36})$]. Olsen and Fuchs (1968) described *DA krinovite*, a Cr-Mg isomorph of aenigmatite, from mineralogically unusual graphite-silicate inclusions in the Canyon Diablo, Wichita County, and Youndegin (IAB) iron meteorites. Subhedral grains up to 200 μm in diameter occur in association with graphite, albite, richterite, and roedderite.

Roedderite [$(Na,K)_2Mg_5Si_{12}O_{30}$]. *DA roedderite* was reported by Olsen and Fuchs (1968) from the Canyon Diablo and Wichita County (IAB) iron meteorites, where it occurs in graphite-silicate inclusions. Roedderite was also found in the Bustee aubrite by Hsu (1998) as an irregular ~500 × 200 μm grain associated with olivine and enstatite, as well as in the Khor Temiki and Pena Blanca Springs aubrites (Fogel 2001).

Organic solids

Kerogen (C-H-O-N). Condensed organic material, here termed *DA kerogen*, is an important carbon-bearing phase in many ureilites (Vdovykin 1970). It occurs along silicate grain boundaries, as well as in grain fractures and cleavage planes.

Part IVB: Impact mineralization of asteroidal bodies and their constituents

Among the earliest mineralizing processes in the solar nebula, commencing contemporaneously with asteroid formation at ~4.565 Ga and continuing throughout the history of the solar system, was shock alteration of preexisting phases (Buchwald 1975, 1977; Stöffler et al. 1988, 1991, 2018; Bischoff and Stöffler 1992; Scott et al. 1992; Rubin et al. 1997; Sharp and DeCarli 2006; Stöffler and Grieve 2007; Koeberl 2014; Rubin 2015a; Breen et al. 2016; Fritz et al. 2017; Tomioka and Miyahara 2017; Tschauner 2019). High-velocity collisions, as well as bow shocks in the early nebular environment, produced significant transient high-temperature and -pressure events that transformed materials through shattering (Bunch and Rajan 1988), impact melting (Dodd and Jarosewich 1979, 1982; Rubin 1985; Fagan et al. 2000; Lunning et al. 2016), vaporization (El Goresy et al. 1997), and a range of solid-state alterations (Ashworth 1980, 1985; Madon and Poirier 1980, 1983; Price 1983; Rubin 2006). Large-scale impacts also initiated more gradual asteroidal heating and fluidization that are manifest in asteroid metamorphism (Rubin and Ma 2021)—effects revealed by a significant correlation in meteorites between the extent of thermal metamorphism (to be reviewed in Part V) and the degree of shock alteration.

Here we focus on rapid, shock-related changes that produced new kinds of minerals in meteorites. Shock events recorded in meteorites represent transient temperatures and pressures that can exceed 3000 °C and 100 GPa (Fig. 3), with peak conditions lasting perhaps a few seconds [Ohtani et al. (2004); Xie et al. (2006); Tomioka and Miyahara (2017); Stöffler et al. (2018), Tables 4–11]. Under such extreme conditions, minerals transform in a variety of ways. Accordingly, Stöffler and colleagues have proposed a unified scale of shock metamorphism, with increasing stages of impact effects grading from S1 (for unshocked examples) to S7 (for whole-rock melting and/or vaporization). They enumerated separate mineralogical and textural criteria to codify shock stages for each major parent lithology (which can be applied equally to meteorites and to planetary impact structures): felsic (F), mafic (M), anorthositic (A), ultramafic (U), chondritic rocks (C), sedimentary rocks (SR), unconsolidated sediments (SE), and regolith (RE). Note that shock effects in iron meteorites were not considered by Stöffler et al. (2018); however, see previous work (Buchwald 1975, 1977; Bennett and McSween 1996; Tomkins 2009; Breen et al. 2016).

A range of effects, from undulose extinction with crossed polarizers in transmitted light and irregular fracturing at low degrees of shock, to mosaic extinction and planar fracturing at intermediate shock, to melting and/or transformation to new denser phases at the highest shock states, are observed in meteorites. Phases generated from impact melting and subsequent igneous processes are often

difficult to distinguish from minerals formed in molten differentiating asteroidal bodies; minerals that are thought to have crystallized at low pressure (<0.1 GPa) were considered in Part IVA above, for example in discussions of nonmagmatic achondrites. Likewise, minerals formed through condensation of impact-generated vapor are often similar to nebular condensates and are reviewed in previous sections of this evolutionary system. Here we focus exclusively on new high-pressure (>0.1 GPa) meteorite phases that arose from short-lived impact events, either through solid-state transformation or crystallization from a shock-induced melt.

Systematic impact alteration mineralogy

Minerals formed through shock processes and preserved in meteorites have been reviewed in the context of high-pressure mineralogy and/or meteorite mineralogy by several authors (Scott et al. 1992; Rubin et al. 1997; Mittlefehldt et al. 1998; Rubin and Ma 2017, 2021; Tomioka and Miyahara 2017; Ma 2018; Stöffler et al. 2018; Tschauner 2019). Here we list 40 kinds of dense, micrometer-scale phases (Table 2) that are thought to have formed rapidly as a byproduct of high-energy collisions between objects ranging in size from meters to hundreds of kilometers in diameter.

These impact minerals incorporate 14 different essential elements (Fig. 4), all of which are among the major essential elements in primary asteroidal and planetesimal minerals from which they formed (compare with Fig. 2).

We focus on irreversible high-pressure shock effects that likely occurred on asteroids and their precursors in the early solar nebula—events that led to new dense phases or diagnostic altered textures in preexisting minerals. However, unlike the time-restricted processes that formed minerals in CAIs, chondrules, or differentiated planetesimals in the earliest solar nebula, impact processes have continued throughout the 4.5 Ga history of the solar system. Accordingly, many of the phases listed in Table 2 are only known from examples that are significantly younger than 4560 Ma. Indeed, nine impact phases known thus far exclusively from martian meteorites (i.e., feiite, liebermannite, liuite, seifertite, stoeflerite, tissintite, tschaunerite, zagamiite, and an unnamed silicate) formed much more recently. Nevertheless, these shock minerals formed from precursor phases that were present on differentiated planetesimals and thus all of these impact phases were also likely to have formed during the earliest stages of the solar system.

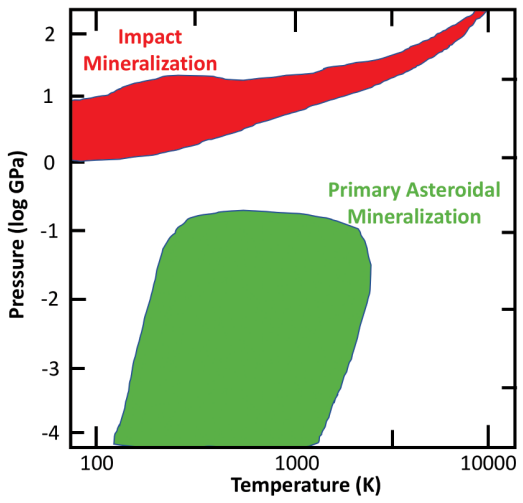

Figure 3. The ranges of pressure-temperature conditions for primary asteroidal mineralization (green) and impact mineralization (red) suggest that these processes represent distinct stages of mineral evolution. (Color online.)

We distinguish between shock effects preserved in chondritic, non-chondritic, and martian meteorites vs. more recent influences of meteor impacts on Earth, including effects of atmospheric passage. Terrestrial impact events have transformed a variety of crustal minerals that are not significant components of asteroids. Thus, high-pressure shock phases found exclusively in terrestrial impact structures, such as reidite ($ZrSiO_4$; Glass et al. 2002), akaogiite (TiO_2; El Goresy et al. 2010), maohokite ($MgFe_2O_4$; Chen et al. 2019), and reisite (TiO_2; Tschauner et al. 2020), will be considered in a later contribution. Note that we also defer to Part V discussion of enigmatic Al-bearing alloys and quasicrystals, for which extreme reduction associated with shock effects has been invoked as a possible origin (Hollister et al. 2014; Hu et al. 2019).

Several high-pressure minerals that are thus far known only as impact phases in meteorites likely occur as major phases in Earth's mantle, as well. A few examples—ringwoodite, majorite, and amorphous $CaSiO_3$, for example—have been reported from both meteorites and as inclusions in mantle-derived diamond. However, other presumed mantle phases, including akimotoite, hemleyite, and bridgmanite (likely the most abundant mineral on Earth in terms of volume; Tschauner et al. 2014), are to date known only from meteorites.

We employ a binomial nomenclature with IMA species names preceded by "impact," i.e., *impact stishovite*. We deviate from IMA conventions in a few instances. We lump members of five continuous Mg-Fe solid solutions—periclase-wüstite, wadsleyite-asimowite, ringwoodite-ahrensite, akimotoite-hemleyite, and bridgmanite-hiroseite—into *impact magnesiowüstite*, *impact wadsleyite*, *impact ringwoodite*, *impact akimotoite*, and *impact bridgmanite*, respectively. In each of these cases, Mg-dominant examples are much more abundant, Fe-dominant examples are typically close to intermediate compositions, and all examples formed by the same mechanism. We include four minerals that have been partially characterized but are not yet approved by the IMA: *impact martensite* (α_2-Fe,Ni), *impact* [$(Mg,Fe)SiO_3$], *impact* [$(Mg,Fe,Si)_2(Si,\square)O_4$], and *impact* [$(Fe,Mg,Cr,Ti,Ca,\square)_2(Si,Al)O_4$]. We also recognize three amorphous phases: impact silica glass, impact amorphous $CaSiO_3$, and impact maskelynite.

Native elements

Fe-Ni Alloys. Fe-Ni alloys commonly display significant shock effects (Buseck et al. 1966; Wood 1967; Begemann and Wlotzka 1969; Smith and Goldstein 1977; Bennett and McSween 1996). Etched samples of the Fe-Ni alloy kamacite often have shock-induced twinning known as Neumann bands (Buchwald 1975). These twins on the {211} planes of α-(Fe,Ni) form easily, perhaps in some cases on atmospheric entry. A range of more intense shock effects are observed in some meteoritic Fe-Ni alloys, including high-pressure transformation to the ε-iron phase, a high-density hexagonal close-packed structure requiring pressures >13 GPa, but which is not quenchable. Fe-Ni alloys experience extensive impact melting, as well as transformation of impact Fe-Ni melt

on cooling to the metastable α_2-Fe-Ni alloy called martensite.

Martensite (α_2-Fe,Ni). *Impact martensite* forms when shock heating of kamacite and taenite homogenizes the Fe-Ni alloy, which then cools rapidly to form the metastable (α_2-Fe,Ni) cubic form. Martensite, typically with 8 to 15 wt% Ni, is known from a range of chondritic and non-chondritic meteorites (Rubin and Keil 1983; Mittlefehldt et al. 1998; Rubin and Ma 2021). Martensite transforms to plessite, an intimate mixture of stable kamacite and taenite, upon reheating in the $\alpha+\gamma$ iron stability field (Taylor and Heymann 1970; Scott and Rajan 1979).

TABLE 2. Summary of 40 high-pressure impact phases in meteorites

GroupSpecies (Formula)	Natural Kind	Characteristics	References
	Native Elements and Alloys		
Martensite (α_2-Fe,Ni)	*Impact martensite*	Common in shocked meteorites; typically 8-15 wt. % Ni	1–3
Diamond (C)	*Impact diamond*	Often occurs as "lonsdaleite" with stacking faults	2,4–6
Chaoite (C)	*Impact chaoite*	Occurs in carbon-rich ureilite achondrites	7,8
	Silicides		
Suessite (Fe_3Si)	*Impact suessite*	A frequent minor phase in urelites	9,10
Xifengite (Fe_5Si_3)	*Impact xifengite*	A rare phase in urelites, in association with suessite	10
	Phosphides		
Allabogdanite [$(Fe,Ni)_2P$]	*Impact allabogdanite*	Occurs in shocked iron meteorites	11–13
	Sulfides		
Shenzhuangite ($NiFeS_2$)	*Impact shenzhuangite*	One occurrence in the Suizhou (L6) chondrite	14
	Phosphates		
Tuite [γ-$Ca_3(PO_4)_2$]	*Impact tuite*	One occurrence in the Suizhou (L6) chondrite	15
	Oxides		
Magnesiowüstite [(Mg,Fe)O]	*Impact magnesiowüstite*	In shocked chondrites in association with Mg-Fe-silicates	16,17
Wangdaodeite ($FeTiO_3$)	*Impact wangdaodeite*	One occurrence in the Suizhou (L6) chondrite	18
Liuite ($FeTiO_3$)	*Impact liuite*	From the shocked Tissint martian meteorite	19
Chenmingite ($FeCr_2O_4$)	*Impact chenmingite*	One occurrence in the Suizhou (L6) chondrite	20,21
Xieite ($FeCr_2O_4$)	*Impact xieite*	One occurrence in the Suizhou (L6) chondrite	22
Tschaunerite (Fe_2TiO_4)	*Impact tschaunerite*	From the shocked Tissint martian meteorite	23
Dmitryivanovite ($CaAl_2O_4$)	*Impact dmitryivanovite*	From the Northwest Africa 470 CH3 chondrite	24
Vestaite [$(Ti^{4+}Fe^{2+})Ti_3^{4+}O_9$]	*Impact vestaite*	Found in the eucrite NWA 8003	25
Feiite [$(Fe,Ti,Cr)_4O_5$]	*Impact feiite*	From the shocked Tissint martian meteorite	26
	Silicates		
Silica Polymorphs (SiO_2)			
Coesite (SiO_2)	*Impact coesite*	Identified in many meteorites	27–30
Stishovite (SiO_2)	*Impact stishovite*	Identified in many meteorites	6,29–32
Seifertite (SiO_2)	*Impact seifertite*	Found in shocked martian and lunar meteorites	33–36
Silica glass (SiO_2)	*Impact silica glass*	Found with other silica polymorphs in shocked meteorites	37,38
Olivine Polymorphs [$(Mg,Fe,Ca)_2SiO_4$]			
Wadsleyite [β-$(Mg,Fe)_2SiO_4$] & Asimowite [β-$(Fe,Mg)_2SiO_4$]	*Impact wadsleyite*	Found in varied shocked meteorites	30,39–42
Ringwoodite [γ-$(Mg,Fe)_2SiO_4$] & Ahrensite [γ-$(Fe,Mg)_2SiO_4$]	*Impact ringwoodite*	Found in varied shocked meteorites	30,43–47
Poirierite [$(Mg,Fe)_2SiO_4$]	*Impact poirierite*	One occurrence in the Suizhou (L6) chondrite	48
Pyroxene Polymorphs [$(Ca,Mg,Fe)_2Si_2O_6$]			
Clinoenstatite ($MgSiO_3$)	*Impact clinoenstatite*	From many meteorites by shock alteration of orthoenstatite	3,49–50
Majorite ($MgSiO_3$)	*Impact majorite*	From many shocked meteorites	30,44,51–58
Akimotoite [$(Mg,Fe)SiO_3$] & Hemleyite [$(Fe,Mg)SiO_3$]	*Impact akimotoite*	From many shocked meteorites	30,59–63
Bridgmanite [$(Mg,Fe)SiO_3$] & Hiroseite [$(Fe,Mg)SiO_3$]	*Impact bridgmanite*	From many shocked meteorites	17,30,64,65
Amorphous $CaSiO_3$	*Impact amorphous $CaSiO_3$*	Found as inversion of $CaSiO_3$ perovskite	57,66,67
Tissintite [$(Ca,Na,\square)AlSi_2O_6$]	*Impact tissinite*	From the shocked Tissint martian meteorite	66,67
Unnamed [$(Mg,Fe)SiO_3$]	*Impact unnamed [$(Mg,Fe)SiO_3$]*	From the Tenham (L6) chondrite	70
Feldspar Polymorphs [$(Ca,Na,K)Al(Al,Si)Si_2O_8$]			
Jadeite ($NaAlSi_2O_6$)	*Impact jadeite*	Formed by shock alteration of albite	30,71,72
Maskelynite [$(Ca,Na)Al(Al,Si)Si_2O_8$]	*Impact maskelynite*	Common form of impact glass	3,30,73–75
Lingunite [$(Na,Ca)AlSi_3O_8$]	*Impact lingunite*	From the shocked Sixiangkou (L6) chondrite meteorite	30,76
Liebermannite [$(K,Na)AlSi_3O_8$]	*Impact liebermannite*	From the shocked Zagami martian meteorite	77
Stöfflerite ($CaAl_2Si_2O_8$)	*Impact stöfflerite*	From the NWA 856 martian meteorite	78,79
Other Silicates			
Cordierite ($Mg_2Al_4Si_5O_{18}$)	*Impact cordierite*	From the Allende chondrite and Chaunskij mesosiderite	80,81
Zagamiite ($CaAl_2Si_{3.5}O_{11}$)	*Impact zagamiite*	Found in shocked martian meteorites	82,83
Unnamed [$(Fe,Mg,Cr,Ti,Ca,\square)_2(Si,Al)O_4$]	*Impact $(Fe,Mg,Cr,Ti,Ca,\square)_2(Si,Al)O_4$*	From the Tissint martian meteorite	84
Unnamed [$(Mg,Fe,Si)_2(Si,\square)O_4$]	*Impact $(Mg,Fe,Si)_2(Si,\square)O_4$*	Shock melt veins in Tenham and Suizhou chondrites	85

References: 1. Rubin & Keil (1983); 2. Mittlefehldt et al. (1998); 3. Rubin & Ma (2021); 4. Russell et al. (1992); 5. Rubin et al. (1997); 6. Garvie et al. (2011); 7. El Goresy & Donnay (1968); 8. Vdovykin (1970); 9. Keil et al. (1982); 10. Ross et al. (2019); 11. Britvin et al. (2002); 12. Britvin et al. (2019); 13. Litasov et al. (2019); 14. Bindi & Xie (2018); 15. Xie et al. (2003); 16. Chen et al. (1996); 17. Bindi et al. (2020); 18. Xie et al. (2020); 19. Ma & Tschauner (2018a); 20. Chen et al. (2003b); 21. Ma et al. (2019a); 22. Chen et al. (2008); 23. Ma & Prakapenka (2018); 24. Mikouchi et al. (2009); 25. Pang et al. (2018); 26. Ma & Tschauner (2018b); 27. Hollister et al. (2014); 28. Chao et al. (1960); 29. Ohtani et al. (2011); 30. Tomioka & Miyahara (2017); 31. Holtstam et al. (2003); 32. Kaneko et al. (2015); 33. Sharp et al. (1999); 34. Dera et al. (2002); 35. El Goresy et al. (2008); 36. Miyahara et al. (2013a); 37. Grieve et al. (1996); 38. Stöffler et al. (2018); 39. Price et al. (1983); 40. Malavergne et al. (2001); 41. Ozawa et al. (2009); 42. Bindi et al. (2019); 43. Binns et al. (1969); 44. Coleman (1977); 45. Feng et al. (2011); 46. Kimura et al. (2003); 47. Ma et al. (2016); 48. Tomioka et al. (2020); 49. Reid & Cohen (1967); 50. Tomioka & Fujino (1997); 51. Mason et al. (1968); 52. Smith & Mason (1970); 53. Walton (2013): 54. Kato et al. (2017); 55. Tomioka et al. (2002); 56. Ma & Tschauner (2016); 57. Xie & Sharp (2007); 58. Tomioka et al. (2016); 59. Sharp et al. (1997); 60. Tomioka & Fujino (1999); 61. Chen & Xie (2015); 62. Ferroir et al. (2008); 63. Bindi et al. (2017a); 64. Tschauner et al. (2014); 65. Vollmer et al. (2007); 66. Akaogi et al. (2004); 67. Tomioka & Kimura (2003); 68. Ma et al. (2015); 69. Rucks et al. (2018); 70. Xie et al. (2011); 71. Kimura et al. (2000); 72. Ozawa et al. (2014); 73. Stöffler et al. (1986); 74. Stöffler et al. (1991); 75. Rubin (2015b); 76. Gillet et al. (2000); 77. Langenhorst & Poirier (2000); 78. Spray & Boonsue (2016); 79. Tschauner & Ma (2017); 80. Fuchs (1969b); 81. Petaev et al. (2000); 82. Beck et al. (2004); 83. Ma et al. (2019b); 84. Ma et al. (2019c); 85. Ma et al. (2019d).

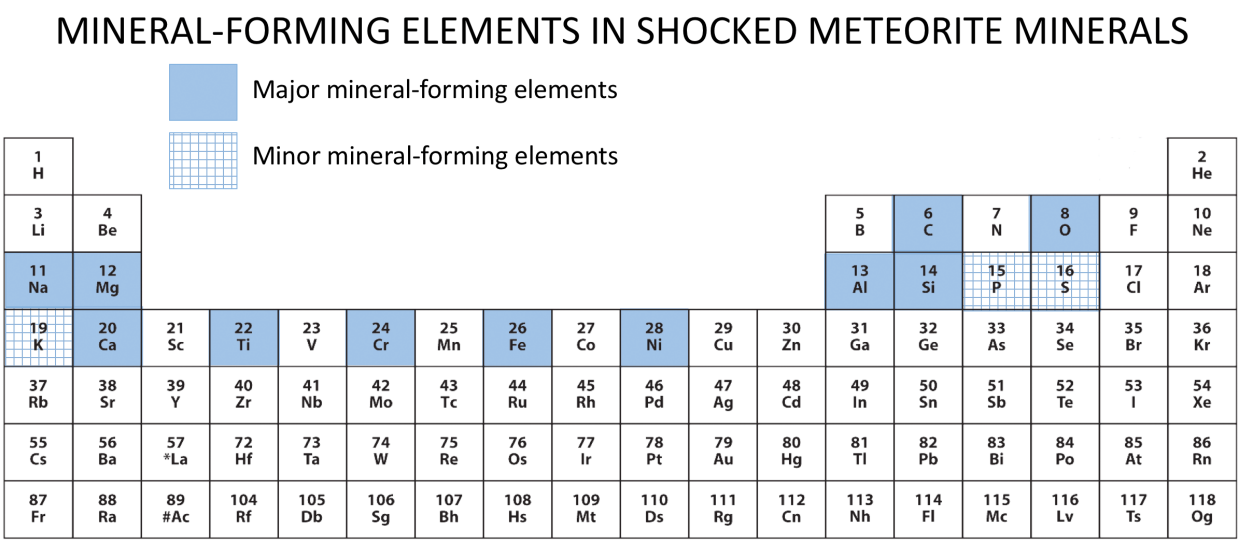

Figure 4. Essential mineral-forming elements in 40 shocked meteorite minerals. All of these 14 elements are major mineral-forming elements in primary asteroidal minerals (compare with Fig. 2). (Color online.)

Carbon allotropes. Allotropes of carbon display a range of shock-induced effects. Rubin (1997a) and Rubin and Scott (1997) describe graphite as an exsolution phase in impact metal melt, while partially disordered graphite has also been attributed to impact alteration (Rubin 1997b; Rubin and Scott 1997). Here we list two high-pressure forms of carbon, diamond and chaoite, as impact phases.

Diamond (C). *Impact diamond*, as well as its disordered form "lonsdaleite," is an important diagnostic mineralogical marker of high-pressure impacts. Diamond formed through terrestrial impacts has been recognized since detailed studies of the Meteor Crater, Arizona (Frondel and Marvin 1967). Impact diamond typically has a significant density of stacking faults. Impact diamond was subsequently described as a meteorite phase by several authors (Russell et al. 1992; Rubin et al. 1997; Mittlefehldt et al. 1998; Garvie et al. 2011). Note that "lonsdaleite," which was originally approved by the IMA as the hexagonal 2*H* variant of cubic diamond, has been shown by Németh et al. (2014) to be disordered diamond and is now discredited.

Chaoite (C). Chaoite, a high-pressure hexagonal (space group *P6*/*mmm*) form of carbon, was originally described by El Goresy and Donnay (1968) from the Reis Crater in Germany. *Impact chaoite* occurs in several carbon-rich ureilite achondrites (Vdovykin 1970).

Silicides

The origins of iron silicides, which are minor phases in many dimict and polymict ureilites, are enigmatic. Common occurrences of suessite (Fe_3Si; Keil et al. 1982; Ross et al. 2019) and rare xifengite (Fe_5Si_3; Ross et al. 2019), as well as unconfirmed reports of hapkeite (Fe_2Si; Smith et al. 2008) and naquite (FeSi; Moggi Cecchi et al. 2015), have been ascribed to reduction of Fe and Si from olivine (Keil et al. 1982) or Si-bearing metal (Ross et al. 2019), possibly in association with a reducing carbonaceous matrix, during shock-melting events and subsequent rapid quenching from high temperature.

Suessite (Fe_3Si). Keil et al. (1982) recorded *impact suessite* as a minor phase in the matrix of the North Haig polymict ureilite in association with troilite, kamacite, and a carbonaceous matrix. Ross et al. (2019) identified frequent occurrences of suessite, at times in association with rare xifengite, in several ureilites.

Xifengite (Fe_5Si_3). Ross et al. (2019) described rare grains of *impact xifengite* in association with suessite from the DaG 999 and EET 87720 ureilites.

Phosphides

Allabogdanite [$(Fe,Ni)_2P$]. *Impact allabogdanite* was discovered as elongated crystals in the Onello Ni-rich ataxite meteorite by Britvin et al. (2002), who originally ascribed it to primary asteroidal origins. Subsequent experimental research (Dera et al. 2008) and observations of natural material from several other occurrences (Britvin et al. 2019; Litasov et al. 2019) revealed allabogdanite to be a very-high-pressure impact phase in the Fe-Ni-P system.

Sulfides

Meteoritic sulfides display shock effects; notably, shocked troilite may have a "bubbly" texture, twinning, shearing, and transformation to polycrystalline aggregates (Scott et al. 1992; Bennett and McSween 1996; Joreau et al. 1996). However, with the possible exception of shenzhuangite (see below), new dense forms of sulfide minerals have not been reported from shocked meteorites.

Shenzhuangite ($NiFeS_2$). Bindi and Xie (2018) described a shock-induced sulfide from the Suizhou (L6) chondrite, *impact shenzhuangite* with the chalcopyrite structure. They argue that Ni is incompatible in the chalcopyrite structure at low pressure; therefore, shenzhuangite is included in our list of impact-generated phases (Tschauner 2019).

Phosphates

Tuite [γ-$Ca_3(PO_4)_2$]. Xie et al. (2002a, 2003) described *impact tuite*, a high-pressure transformation product of merrillite, which was discovered in shock veins from the Suizhou (L6) chondrite.

Experiments by Murayama et al. (1986) demonstrated that pressures in excess of 10 GPa are required to stabilize tuite.

Oxides

Magnesiowüstite [(Mg,Fe)O]. *Impact magnesiowüstite* occurs in several highly shocked meteorites in association with other high-pressure phases (Tschauner 2019; Bindi et al. 2020). For example, magnesiowüstite of average composition [$(Mg_{0.54}Fe_{0.46})O$], found in the shocked (S6) Sixiangkou chondrite as 5 μm diameter blebs in association with majorite (Chen et al. 1996), points to shock conditions exceeding 2050 °C at 20 to 24 GPa.

Wangdaodeite ($FeTiO_3$). *Impact wangdaodeite*, a high-pressure polymorph of ilmenite with the $LiNbO_3$ perovskite-type structure, was discovered by Xie et al. (2016, 2020) from the Suizhou (L6) chondrite. Experimental studies point to formation at shock pressures above 20 GPa.

Liuite ($FeTiO_3$). *Impact liuite* was reported by Ma and Tschauner (2018a) from a shock-melt pocket in the Tissint martian meteorite. The rare phase was found at the rim of a transformed ilmenite-ülvospinel grain in association with other impact phases, feiite and tschaunerite. Liuite is closely related to wangdaodeite, another ilmenite polymorph. However, liuite with the $GdFeO_3$ perovskite structure has a significant bridgmanite component, with a composition close to [$(Fe,Mg)(Ti_{0.6}Si_{0.4})O_3$].

Chenmingite ($FeCr_2O_4$). Two shock-induced polymorphs of chromite are known from the Shizhiu (L6) chondrite (Chen et al. 2003a). Chen et al. (2003b) and Ma et al. (2019a) characterized *impact chenmingite*, $FeCr_2O_4$ in the $CaFe_2O_4$-type structure. Experiments demonstrate that chemmingite formed at pressures above 17 GPa at temperatures exceeding 1300 °C.

Xieite ($FeCr_2O_4$). Chen et al. (2008) described *impact xieite*, a high-pressure polymorph of $FeCr_2O_4$ with the $CaTi_2O_4$ structure type found as lamellae in host chromite in the Shizhiu (L6) chondrite. Experiments suggest that shock pressures must have exceeded 17 GPa while temperatures were below 1300 °C.

Tschaunerite (Fe_2TiO_4). *Impact tschaunerite*, a polymorph of ülvospinel with the calcium ferrite structure, occurs in association with liuite and feiite from a shock-melt pocket in the Tissint martian meteorite (Ma and Prakapenka 2018).

Dmitryivanovite ($CaAl_2O_4$). Mikouchi et al. (2009) described a high-pressure polymorph of krotite, *impact dmitryivanovite*, from the Northwest Africa 470 CH3 chondrite.

Vestaite [$(Ti^{4+}Fe^{2+})Ti^{3+}_2O_9$]. *Impact vestaite* is a monoclinic high-pressure phase, identified in the eucrite NWA 8003, that crystallized from a shock melt at ≤10 GPa (Pang et al. 2018). It occurs in melt pockets and shock veins and presumably was produced after an impact on Vesta.

Feiite [$(Fe,Ti,Cr)_4O_5$]. *Impact feiite* from a shock-melt pocket in the Tissint martian meteorite was found at the rim of a transformed ilmenite-ülvospinel grain in association with other rare impact phases, liuite and tschaunerite (Ma and Tschauner 2018b).

Silicates

Virtually all silicates at room pressure have Si in tetrahedral coordination. A key to understanding many high-pressure transformations in silicates, including those caused by very high shock pressures, is the attainment of denser states through structures with Si partially or completely in octahedral coordination (i.e., Hazen and Finger 1978; Tschauner 2019). In this regard, shock minerals provide important insights to possible major phases of Earth's deep interior—notably dense variants of silica, olivine, pyroxene, and feldspar.

Silica polymorphs (SiO_2). Several high-pressure polymorphs of SiO_2 have been synthesized and observed in nature as shock phases (Swamy et al. 1994; Kuwayama 2008; Tschauner 2019). We include impact-formed coesite, stishovite, seifertite, and densified silica glass.

Coesite (SiO_2). *Impact coesite*, the natural analog of the high-pressure silica polymorph synthesized by Coes (1953), was first reported by Chao et al. (1960) from shock-altered sandstone at Meteor Crater, Arizona, where it was found in association with *impact stishovite*. Coesite was subsequently identified in several meteorites, providing early evidence that shock transformations played a significant role in the early solar system [Ohtani et al. (2011); Hollister et al. (2014); Tomioka and Miyahara (2017), Tables 2 and 3].

Stishovite (SiO_2). Chao et al. (1962) described *impact stishovite* from Meteor Crater, Arizona, with subsequent studies by Fahey (1964), following its initial synthesis by Stishov and Popova (1961). Numerous occurrences of this rutile isomorph have been reported from shocked meteorites and lunar rocks [Holtstam et al. (2003); Garvie et al. (2011); Ohtani et al. (2011); Kaneko et al. (2015); see Tomioka and Miyahara (2017), Tables 2 and 3].

Seifertite (SiO_2). *Impact seifertite* is an extremely high-pressure shock phase with the orthorhombic (space group *Pbcn*) α-PbO_2 structure. It was initially synthesized by German et al. (1973), recognized in nature by TEM observations (Sharp et al. 1999), and further characterized by Dera et al. (2002), El Goresy et al. (2008), and Miyahara et al. (2013a) from several shocked martian and lunar samples.

Silica glass (SiO_2). Dense *impact silica glass* is commonly associated with other high-pressure silica polymorphs (Grieve et al. 1996; Stöffler et al. 2018).

Olivine polymorphs [$(Mg,Fe)_2SiO_4$]. At high shock pressures, olivine undergoes a sequence of phase transitions, first to the modified spineloid polymorph wadsleyeite, then to the silicate spinel ringwoodite. Above ~25 GPa ringwoodite dissociates into perovskite-type [$(Mg,Fe)SiO_3$] plus masgnesiowüstite [(Mg,Fe)O] (e.g., Presnall 1995).

Wadsleyite [β-$(Mg,Fe)_2SiO_4$] and asimowite [β-$(Fe,Mg)_2SiO_4$]. *Impact wadsleyite*, the modified β-spinel form of Mg_2SiO_4, was described by Putnis and Price (1979) and Price et al. (1983) from the Tenham and Peace River (L6) chondrites. Impact wadsleyite has been reported from more than a dozen varied meteorites [Tomioka and Miyahara (2017), Tables 2 and 3], including shocked lunar and martian material (Malavergne et al. 2001). It evidently forms through transformation from olivine along grain boundaries and fractures (Ozawa et al. 2009).

The Fe-rich analog of wadsleyite, asimowite, was characterized by Bindi et al. (2019) in shock-melted silicate droplets of the Suizhou and Quebrada Chimborazo 001 chondrites. The reported composition of impact asimowite, [$(Fe_{1.10}Mg_{0.80}Cr_{0.04}Mn_{0.02}Ca_{0.02}Al_{0.02})(Si_{0.97}Al_{0.03})O_4$], is close to Fa_{55}. Given that a continuous solid solution exists between the Mg and Fe end-members (e.g., Presnall 1995), that the only known example of asimowite is of intermediate composition and coexists with more numerous

grains of wadsleyite (Fo_{30-45}), and that all meteoritic wadsleyite and asimowite grains were formed by similar shock processes, we lump asimowite with impact wadsleyite as a single natural kind.

Ringwoodite [γ-$(Mg,Fe)_2SiO_4$] and ahrensite [γ-$(Fe,Mg)_2SiO_4$]. Binns et al. (1969) discovered *impact ringwoodite*, the spinel-type (γ) form of Mg_2SiO_4 in a shock vein of the Tenham (L6) chondrite, and was subsequently reported from shock veins in numerous meteorites [Coleman (1977); Miyahara et al. (2008); Feng et al. (2011); Pittarello et al. (2015); Tomioka and Miyahara (2017), Tables 2 and 3]. Impact ringwoodite also occurs as lamellae in meteoritic olivine, from which it transformed either within olivine crystals or adjacent to grain boundaries (Kerschhofer et al. 1996, 1998; Chen et al. 2004; Miyahara et al. 2010; Tomioka and Miyahara 2017). Compositions of impact ringwoodite vary from Fo_{82} to Fo_{46} (Kimura et al. 2003; Feng et al. 2011; Ma et al. 2016; Tomioka and Miyahara 2017).

Ma et al. (2016) described an Fe-dominant analog of ringwoodite, named ahrensite, from the Tissint martian meteorite—a mineral also previously reported from the Umbarger (L6) chondrite by Xie et al. (2002b). Ahrensite of composition [$(Fe_{1.06}Mg_{0.91}Mn_{0.02})SiO_4$], i.e., close to Fo_{45}, coexists with more numerous grains of ringwoodite with average compositions near Fo_{55} [$(Mg_{1.11}Fe_{0.85}Mn_{0.02})SiO_4$]. In accordance with the conventions of our evolutionary system, we lump all meteoritic examples of the solid solution between ahrensite and ringwoodite as a single natural kind, *impact ringwoodite*.

Poirierite [$(Mg,Fe)_2SiO_4$]. Tomioka et al. (2020) characterized *impact poirierite*, an orthorhombic (space group *Pmma*) dense polymorph of forsterite from the Suizhou (L6) chondrite. Details of composition, structure, and occurrence will be forthcoming.

Pyroxene polymorphs [$(Ca,Mg,Fe)_2Si_2O_6$]. Pyroxene group minerals experience a variety of transformations under shock conditions (e.g., Gasparik 1990). At temperatures above ~1600 °C and ~16 GPa, end-member orthoenstatite ($MgSiO_3$) transforms initially to the garnet polymorph majorite with mixed tetrahedral and octahedral Si. Above ~17 GPa, majorite transforms to the ilmenite structure, akimotoite, and above ~22 GPa the perovskite form, bridgmanite with all Si in octahedral coordination appears. At high pressure below ~1600 °C, enstatite dissociates to wadsleyite or ringwoodite plus the stishovite form of SiO_2, but bridgmanite is the stable phase above 22 GPa.

Additional complexities arise at lower pressures because orthoenstatite can partially to completely transform to clinoenstatite at pressures from 7 to 12 GPa, depending on temperature. This ortho- to clinoenstatite transformation is often blurred because lamellae of the two polymorphs can occur intimately intermixed in a disordered structure as the result of shock deformation.

Clinoenstatite ($MgSiO_3$). *Impact clinoenstatite* forms through the transformation of *DA orthoenstatite* to a disordered monoclinic structure (Reid and Cohen 1967; Tomioka and Fujino 1997; Rubin and Ma 2021).

Majorite ($MgSiO_3$). Mason et al. (1968) reported a high-pressure form of $MgSiO_3$ with the cubic (space group $Ia\bar{3}d$) garnet structure from a shock vein in the Coorara (L6) chondrite. This phase, which can be represented by the structural formula [$Mg_3(MgSi)Si_3O_{12}$], was subsequently named majorite by Smith and Mason (1970). *Impact majorite* has been identified in more than 20 meteorites [Tomioka and Miyahara (2017), Tables 2 and 3], with compositions both close to the Mg-Fe join (Coleman 1977; Walton 2013; Kato et al. 2017) and in solid solution with other garnet components, including pyrope ($Mg_3Al_2Si_3O_{12}$; Chen et al. 1996), almandine ($Fe_3Al_2Si_3O_{12}$; Ma and Tschauner 2016), and calcic garnet (Xie and Sharp 2007).

The majorite story is complicated by the discovery of a few occurrences of unambiguously tetragonal (space group $I4_1/a$) high-pressure garnets, in contrast to the familiar cubic symmetry (Xie and Sharp 2007; Ma and Tschauner 2016; Tomioka et al. 2016)—a difference that is difficult to document without electron diffraction of individual micrometer-scale grains. The lower symmetry results from Mg-Si ordering in octahedral sites, which may be a pervasive feature of meteoritic majorites (Angel et al. 1989; Heinemann et al. 1997; Tomioka et al. 2002). At this stage, we do not distinguish between completely disordered cubic majorite, which might occur in some rapidly quenched examples, and the pseudo-cubic tetragonal variant, which would obtain for samples with any degree of Mg-Si order.

Akimotoite [$(Mg,Fe)SiO_3$] and hemleyite [$(Fe,Mg)SiO_3$]. The ilmenite structured polymorph of enstatite was reported by Sharp et al. (1997) from the Acfer 040 (L5-6) chondrite and by Tomioka and Fujino (1997) from the Tenham chondrite, and was subsequently named akimotoite (Tomioka and Fujino 1999). *Impact akimotoite* is now known from at least 17 meteorites [Tomioka and Miyahara (2017), Tables 2 and 3], including examples with significant Ca and minor Fe^{3+} (Ohtani et al. 2004; Xie and Sharp 2004; Xie et al. 2006; Miyajima et al. 2007; Ferroir et al. 2008; Chen and Xie 2015). Tomioka (2007) revealed the transformation mechanism from clinoenstatite to akimotoite as the result of oriented shear dislocations.

Bindi et al. (2017a, 2017b) described an Fe-dominant example of akimotoite in the shocked Suizhou (L6) chondrite—a phase they named hemleyite. Analyses span the range from 45 to 50 mol% $FeSiO_3$, with 33 to 39 mol% $MgSiO_3$, compared to reported akimotoite compositions from 20 to 30 mol% $FeSiO_3$, with 62 to 78 mol% $MgSiO_3$ (Bindi et al. 2017a, Fig. 5). Because there appears to be a continuous akimotoite-hemleyite solid solution and all examples are formed by similar shock transformation of clinopyroxene, we lump hemleyite with *impact akimotoite*.

Bridgmanite [$(Mg,Fe)SiO_3$] and hiroseite [$(Fe,Mg)SiO_3$]. Tschauner et al. (2014) characterized a natural occurrence of crystalline [$(Mg,Fe)SiO_3$] in the perovskite structure—a phase they named bridgmanite. The presence of this phase as a high-pressure shock mineral in meteorites was long suspected, based in part on amorphous regions of enstatite composition and the tendency of bridgmanite to invert to glass (Wang et al. 1992; Sharp et al. 1997), as well as transmission electron microscopy (TEM) evidence for the crystallinity of sub-micrometer grains of presumed $MgSiO_3$ perovskite coexisting with magnesiowüstite, which is the presumed post-ringwoodite assemblage (Tomioka and Fujino 1997).

Of note is the TEM description by Vollmer et al. (2007) of a 0.3 μm bridgmanite grain from the Acfer 094 carbonaceous chondrite. This grain has diagnostic isotopic anomalies, with extremely high-$^{17}O/^{16}O$ and low-$^{18}O/^{16}O$ characteristic of presolar grains from a low-mass AGB star. Consequently, Hazen and Morrison (2020) listed *AGB bridgmanite* as one of 41 stellar mineral natural kinds. However, we now consider this grain to be *impact bridgmanite* that formed from an isotopically anomalous *AGB enstatite* precursor grain.

Bindi and Xie (2019) and Bindi et al. (2020) characterized the Fe-dominant analog of bridgmanite of composition $[(Fe^{2+}_{0.44}Mg_{0.37}Fe^{3+}_{0.10}Al_{0.04}Ca_{0.03}Na_{0.02})(Si_{0.89}Al_{0.11})O_3]$, which they named hiroseite. Crystal inclusions in magnesiowüstite (~5 μm diameter) were found in the Suizhou (L6) chondrite in association with other high-pressure shock phases. Bindi et al. (2020) demonstrated that a significant fraction of iron in meteoritic bridgmanite undergoes charge disproportionation ($3Fe^{2+} \rightarrow Fe^0 + 2Fe^{3+}$), consistent with earlier analyses of experimental samples (McCammon 1997; Fialin et al. 2009; Sinmyo et al. 2017). This effect should be more pronounced in Fe-rich silicate perovskite; however, unless evidence is presented for a miscibility gap in the $[(Mg,Fe)SiO_3]$ solid solution, we lump all examples of meteoritic bridgmanite and hiroseite into *impact bridgmanite*.

Amorphous $CaSiO_3$. Shock transformation of Ca-rich pyroxene above ~17 GPa leads to the formation of a high-pressure Mg-silicate (wadsleyite + stishovite; majorite; ringwoodite + stishovite; akimotoite; or bridgmanite, depending on the temperature and pressure), plus $CaSiO_3$ perovskite (Akaogi et al. 2004). Therefore, perovskite-type $CaSiO_3$ must have formed in many augite-rich meteorites. However, the crystalline phase is unstable at room conditions and inverts to amorphous $CaSiO_3$ (Liu and Ringwood 1975)—a non-crystalline phase found in several meteorites (Tomioka and Kimura 2003; Xie and Sharp 2007), which we designate *impact amorphous $CaSiO_3$*.

Tissintite $[(Ca,Na,)AlSi_2O_6]$. Ma et al. (2015) discovered a monoclinic (space group *C*2/*c*) defect pyroxene in the shocked Tissint martian meteorite. *Impact tissintite* has an unusual defect structure, with vacancies in the M2 site. The phase was subsequently synthesized at 6 to 8.5 GPa and 1000 to 1350 °C by Rucks et al. (2018), who suggest it forms naturally from inversion of maskelynite.

Unnamed $[(Mg,Fe)SiO_3]$. Xie et al. (2011) presented TEM evidence for a high-pressure shock mineral with the olivine structure but with pyroxene stoichiometry from the Tenham (L6) chondrite. Further investigation of this intriguing phase, which we designate *impact unnamed* $[(Mg,Fe)SiO_3]$, is warranted.

Feldspar polymorphs $[(Ca,Na,K)Al(Al,Si)Si_2O_8]$. Feldspar-group minerals undergo a variety of high-pressure phase transformations under shock conditions, including meteorite minerals with the pyroxene, hollandite, and calcium ferrite structures, as well as amorphous shock phases (Liu 1978, 2006; Yagi et al. 1994; Liu and El Goresy 2007; Ozawa et al. 2014; Zhou et al. 2017).

Jadeite ($NaAlSi_2O_6$). Albite transforms to jadeite plus a silica phase (quartz, coesite, or stishovite, depending on the maximum pressure) at pressures above ~2.5 GPa. Jadeite plus stishovite is the stable assemblage to at least 20 GPa, above which pressure jadeite transforms to the calcium ferrite structure. Consequently, *impact jadeite* is known from numerous meteorites [Kimura et al. (2000); Ohtani et al. (2004); Ozawa et al. (2009, 2014); Tomioka and Miyahara (2017), Table 2]. In some instances, jadeite may represent a back reaction from crystallization of maskelynite (Miyahara et al. 2013b).

Maskelynite $[(Ca,Na)Al(Al,Si)Si_2O_8]$. The amorphous phase of plagioclase, *impact maskelynite*, is found in numerous shocked anorthite-bearing meteorites (Ostertag 1983; Stöffler et al. 1986, 1991; Brearley and Jones 1998; Mittlefehldt et al. 1998; Rubin 2015b; Rubin and Ma 2021).

Lingunite $[(Na,Ca)AlSi_3O_8]$. Alkali feldspars with the hollandite structure do not appear to have a high-pressure stability field; however, they can be quenched metastably from high pressure (Liu 2006; Zhou et al. 2017). The Na-rich end-member, first synthesized by Liu (2006), was characterized by Gillet et al. (2000) from the Sixiangkou meteorite and subsequently named lingunite. Natural examples of *impact lingunite* have been described from at least 20 shocked meteorites [Tomioka and Miyahara (2017), Tables 2 and 3].

Liebermannite $[(K,Na)AlSi_3O_8]$. A high-pressure hollandite structure polymorph of $KAlSi_3O_8$ was reported by Langenhorst and Poirier (2000) from the shocked Zagami meteorite—a phase synthesized by Liu and El Goresy (2007). Ma et al. (2018) characterized the mineral and named it liebermannite. *Impact liebermannite* with average composition $[(K_{0.6}Na_{0.2}Ca_{0.1})AlSi_3O_8]$ is found in close association with lingunite and maskelynite, both with compositions close to $\sim[Na_{0.5}K_{0.02}Ca_{0.4})Al(Al_{0.35}Si_{2.65}O_8]$.

Stöfflerite ($CaAl_2Si_2O_8$). The hollandite-structured high-pressure polymorph of anorthite was recognized by Spray and Boonsue (2016) from Raman spectra of material from a terrestrial impact structure. *Impact stöfflerite* was subsequently characterized by Tschauner and Ma (2017) from the NWA 856 martian meteorite.

Other silicates

Cordierite ($Mg_2Al_4Si_5O_{18}$). *Impact cordierite* is a rare phase in meteorites, first reported by Fuchs (1969b) from an unusual CAI in the Allende meteorite. It was subsequently identified in the Chaunskij anomalous mesosiderite, which was estimated to have equilibrated at 0.6 GPa (Petaev et al. 2000). Cordierite typically forms at pressures above 0.2 GPa (e.g., Deer et al. 1962), which is significantly greater than those of asteroid interiors; we thus assume a shock origin.

Zagamiite ($CaAl_2Si_{3.5}O_{11}$). Ma and colleagues (Ma and Tschauner 2017; Ma et al. 2017b, 2019b) characterized a high-pressure calcium aluminosilicate ($CaAl_2Si_{3.5}O_{11}$) found in shocked martian meteorites. *Impact zagamiite* was originally recognized by its distinctive Raman spectrum (Beck et al. 2004). This phase was synthesized by Irifune et al. (1994), who called it "CAS." It forms when calcic plagioclase is subjected to shock pressures greater than ~22 GPa (Akaogi et al. (2010).

Unnamed $[(Fe,Mg,Cr,Ti,Ca,\square)_2(Si,Al)O_4]$. Ma et al. (2019c) described a new high-pressure silicate phase, *impact* $(Fe,Mg,Cr,Ti,Ca,\square)_2(Si,Al)O_4$ with a tetragonal spinelloid structure, in a shock melt pocket from the Tissint Martian meteorite.

Unnamed $[(Mg,Fe,Si)_2(Si,\square)O_4]$. Ma et al. (2019d) reported a vacancy-rich, partially inverted spinelloid silicate, *impact* $(Mg,Fe,Si)_2(Si,\square)O_4$, as a major matrix phase in shock melt veins of the Tenham and Suizhou L6 chondrites.

Implications

Cosmic mineral evolution played out in a succession of stages, each of which explored new regimes of temperature, pressure, and composition while adding to the diversity of condensed solid phases. The 130 meteorite minerals reviewed above (Tables 1 and 2) complement the 41 stellar natural kinds (Hazen and Morrison 2020), 67 interstellar and primary nebular condensates (Morrison and Hazen 2020), and 44 primary chondrule minerals (Hazen et al. 2021) described in earlier parts of this series.

In Part IV of the evolutionary system of mineralogy, we encounter pressures significantly above 1 atm for the first time, both in the contexts of asteroidal interiors (to $P < 0.5$ GPa) and via shock events (to $P > 30$ GPa). The resulting inventory of meteorite minerals includes 90 kinds formed by primary asteroidal processes, as well as 40 high-pressure impact minerals. These 130 mineral natural kinds encompass 127 approved IMA mineral species, 10 of which are lumped with other species and thus do not appear as separate natural kinds in Tables 1 and 2. In addition, we include seven crystalline phases, either not recognized as valid IMA species (e.g., fassaite; magnesiowüstite; martensite) or awaiting possible approval (e.g., unnamed $CuCrS_2$ and Mg-Fe silicates), as well as six amorphous phases.

Asteroidal processes resulted in many new mineral phases. Of the 90 primary asteroidal natural kinds (Table 1), 48 minerals appear for the first time, including the earliest known members of the apatite and amphibole groups, as well as zircon, potassic feldspar, and numerous phosphate minerals. Of the 40 impact minerals listed in Table 2, 38 occur for the first time; only diamond and clinopyroxene also formed previously at low pressure. This total of 86 new minerals in Part IV almost doubles the total of 181 phases tabulated to this stage of mineral evolution.

The observed diversity and distribution of asteroidal minerals appear to be consistent with previous studies in "mineral ecology," by which patterns of mineral occurrences on Earth can be used to document the relative frequencies of common vs. rare species, as well as to predict Earth's "missing" minerals (Hazen et al. 2015a, 2015b, 2016; Hystad et al. 2015a, 2015b, 2017, 2019; Grew et al. 2017). Earlier studies demonstrate that the great majority of mineral occurrences (defined as a specific mineral species from one locality) represent a few abundant minerals, whereas the great majority of mineral species are rare (i.e., known from only a few localities). Meteorite minerals are no exception to this trend. Of the 90 asteroidal primary minerals, fewer than 20 phases constitute 99.9 vol% of almost all non-chondritic meteorites. By contrast, more than 50 of these minerals are rare and have only been reported as sub-millimeter- to sub-micrometer-scale grains, with at least two dozen of those phases only known as sub-micrometer crystals from a single meteorite. Accordingly, we estimate that the documented collective mass of these >50 rarest differentiated asteroidal minerals is no more than a few milligrams. We suggest that further statistical study of the diversity and distribution of meteorite minerals, employing the methods of mineral ecology, might provide estimates of the total diversity of meteorite minerals.

The characteristic "Large Numbers of Rare Events" (LNRE) distribution of minerals (Hystad et al. 2015a) observed for many mineralogical environments demonstrates that rare minerals play a disproportionate role in understanding natural processes (Hazen and Ausubel 2016), not unlike the role of trace elements and isotopes in petrology and geochemistry. In meteorites, rare minerals and their LNRE distributions document details of evolving pressure-temperature-composition niches and the important influence of transient and disequilibrium events while revealing many remarkable new structural topologies and compositional permutations. Furthermore, in the case of shock-induced minerals, phases that are intrinsically rare at Earth's surface provide perhaps our best natural view of mantle minerals that represent more than half of Earth's volume (Tschauner 2019). In Part V of this series, which will focus on secondary meteorite minerals formed by a range of aqueous and thermal processes, we will find a significant pulse of new phases characterized by the same type of skewed distribution—a few common kinds accompanied by many more rare minerals.

Acknowledgments

We are deeply grateful to Chi Ma, David Mittlefehldt, and Steven Simon, who provided detailed, thoughtful, and constructive reviews that significantly improved the manuscript. In addition, Timothy McCoy and Alan Rubin offered invaluable, detailed reviews of an earlier version of this contribution, while McCoy contributed photographs of important meteorite specimens. Luca Bindi, Chi Ma, and Alan Rubin provided access to highly relevant work in press. We are grateful to Asmaa Boujibar, Carol Cleland, Robert T. Downs, Olivier Gagné, Peter Heaney, Sergey Krivovichev, Glenn MacPherson, Anirudh Prabhu, Michael Walter, and Shuang Zhang for thoughtful discussions and comments.

Funding

This publication is a contribution to the Deep Carbon Observatory, the 4D Initiative, and the Deep-time Digital Earth (DDE) program. Studies of mineral evolution and mineral ecology have been supported by the Deep Carbon Observatory, the Alfred P. Sloan Foundation, the W.M. Keck Foundation, the John Templeton Foundation, the NASA Astrobiology Institute ENIGMA team, a private foundation, and the Carnegie Institution for Science. Any opinions, findings, or recommendations expressed herein are those of the authors and do not necessarily reflect the views of the National Aeronautics and Space Administration.

References cited

Akaogi, M., Yano, M., Tejima, Y., Iijima, M., and Kojitani, H. (2004) High-pressure transitions of diopside and wollastonite: Phase equilibria and thermochemistry of $CaMgSi_2O_6$, $CaSiO_3$ and $CaSi_2O_5$-$CaTiSiO_5$ system. Physics of the Earth and Planetary Interiors, 143, 145–156.

Akaogi, M., Haraguchi, M., Nakanishi, K., Ajiro, H., and Kojitani, H. (2010) High-pressure phase relations in the system $CaAl_4Si_2O_{11}$-$NaAl_3Si_3O_{11}$ with implication for Na-rich CAS phase in shocked Martian meteorites. Earth and Planetary Science Letters, 289, 503–508.

Angel, R.J., Finger, L.W., Hazen, R.M., Kanzaki, M., Weidner, D.J., Liebermann, R.C., and Veblen, D.R. (1989) Structure and twinning of single-crystal $MgSiO_3$ garnet synthesized at 17 GPa and 1800 °C. American Mineralogist, 74, 509–512.

Aoudjehane, H.C., and Jambon, A. (2007) Determination of silica polymorphs in eucrites by cathodoluminescence. Lunar and Planetary Science, 38, 1714.

Ashworth, J.R. (1980) Deformation mechanisms in mildly shocked chondritic diopside. Meteoritics, 15, 105–115.

——— (1985) Transmission electron microscopy of L-group chondrites: 1. Natural shock effects. Earth and Planetary Science Letters, 73, 17–32.

Axon, H.J., Kinder, J., Haworth, C.W., and Horsfield, J.W. (1981) Carlsbergite, CrN, in troilite, FeS, of the Sikhote Alin meteoritic iron. Mineralogical Magazine, 44, 107–109.

Bailey, K.D. (1994) Typologies and taxonomies: An introduction to classification techniques. Studies in Quantitative Applications in the Social Sciences, 102. SAGE Publications.

Bannister, F.A. (1941) Osbornite, meteoritic titanium nitride. Mineralogical Magazine, 26, 36–44.

Barrat, J.-A., Yamaguchi, A., Greenwood, R.C., Bohn, M., Cotten, J., Benoit, M., and Franchi, I.A. (2007) The Stannern trend eucrites: Contamination of main group eucritic magmas by crustal partial melts. Geochimica et Cosmochimica Acta, 71, 4108–4124.

Beck, P., Gillet, P., Gautron, L., Daniel, I., and El Goresy, A. (2004) A new natural high-pressure (Na,Ca)-hexaluminosilicate [$(Ca_xNa_{1-x})Al_{3+x}Si_{3-x}O_{11}$] in shocked Martian meteorites. Earth and Planetary Science Letters, 219, 1–12.

Beck, A.W., Mittlefehldt, D.W., McSween, H.Y. Jr., Rumble, D. III, Lee, C.-T., and Bodnar, R.J. (2011) MIL 03443, a dunite from asteroid 4 Vesta: Evidence for its classification and cumulate origin. Meteoritics & Planetary Science, 46, 1133–1151.

Begemann, F., and Wlotzka, F. (1969) Shock induced thermal metamorphism and mechanical deformations in the Ramsdorf chondrite. Geochimica et Cosmochimica Acta, 33, 1351–1370.

Benedix, G.K., McCoy, T.J., Keil, K., Bogard, D.D., and Garrison, D.H. (1998) A petrologic and isotopic study of winonaites: Evidence for early partial melting, brecciation, and metamorphism. Geochimica et Cosmochimica Acta, 62, 2535–2553.

Benedix, G.K., McCoy, T.J., Love, S.G., and Keil, K. (2000) A petrologic study of IAB iron meteorites: Constraints on the formation of the IAB-winonaite parent body. Meteoritics & Planetary Science, 35, 1127–1141.

Benedix, G.K., Haack, H., and McCoy, T.J. (2014) Iron and stony-iron meteorites. Treatise on Geochemistry, 2nd ed., 1, 267–285.

Bennett, M.E.I., and McSween, H.Y. Jr. (1996) Shock features in iron-nickel metal and troilite of L-group ordinary chondrites. Meteoritics & Planetary Science, 31, 255–264.

Benz, W., and Asphaug, E. (1999) Catastrophic disruptions revisited. Icarus, 142, 5–20.
Berkley, J.L., and Jones, J.H. (1982) Primary igneous carbon in ureilites: Petrological implications. Journal of Geophysical Research, 87, A353–A364.
Bevan, A.W.R., Bevan, J.C., and Francis, J.G. (1977) Amphibole in the Mayo Belwa meteorite: First occurrence in an enstatite achondrite. Mineralogical Magazine, 41, 531–534.
Bild, R.W., and Wasson, J.T. (1977) Netschaëvo: A new class of chondritic meteorite. Science, 197, 58–62.
Bindi, L., and Xie, X.D. (2018) Shenzhaungite, $NiFeS_2$, the Ni-analogue of chalcopyrite from the Suizhou L6 chondrite. European Journal of Mineralogy, 30, 165–169.
——— (2019) Hiroseite, IMA 2019-019. Mineralogical Magazine, 83, 615–620.
Bindi, L., Steinhardt, P.J., Yao, N., and Lu, P.J. (2011) Icosahedrite, $Al_{63}Cu_{24}Fe_{13}$, the first natural quasicrystal. American Mineralogist, 96, 928–931.
Bindi, L., Eiler, J.M., Guan, Y., Hollister, L.S., MacPherson, G., Steinhardt, P.J., and Yao, N. (2012) Evidence for the extraterrestrial origin of a natural quasicrystal. Proceedings of the National Academy of Sciences, 109, 1396–1401.
Bindi, L., Lin, C., Ma, C., and Steinhardt, P.J. (2016) Collisions in outer space produced an icosahedral phase in the Khatyrka meteorite never observed previously in the laboratory. Scientific Reports, 6, 38117.
Bindi, L., Chen, M., and Xie, X. (2017a) Discovery of the Fe-analogue of akimotoite in the shocked Suizhou L6 chondrite. Scientific Reports, 7, 42674, 1–8.
——— (2017b) Hemleyite, IMA 2016-085. Mineralogical Magazine, 81, 209–213.
Bindi, L., Brenker, F.E., Nestola, F., Koch, T.E., Prior, D.J., Lilly, K., Krot, A.N., Bizzarro, M., and Xie, X. (2019) Discovery of asimowite, the Fe-analog of wadsleyite, in shock-melted silicate droplets of the Suizhou L6 and the Quebrada Chimborazo 001 CB3.0 chondrites. American Mineralogist, 104, 775–778.
Bindi, L., Shim, S-H., Sharp, T.G., and Xie, X. (2020) Evidence for the charge disproportionation of iron in extraterrestrial bridgmanite. Science Advances, 6, eaay7893 (6 p.).
Binns, R.A., Davis, R.J., and Reed, S.J.B. (1969) Ringwoodite, natural $(Mg,Fe)_2SiO_4$ spinel in the Tenham meteorite. Nature, 221, 943–944.
Bischoff, A., and Stöffler, D. (1992) Shock metamorphism as a fundamental process in the evolution of planetary bodies: Information from meteorites. European Journal of Mineralogy, 4, 707–755.
Blichert-Toft, J., Moynier, F., Lee, C-T.A., Telouk, P., and Albarède, F. (2010) The early formation of the IVA iron meteorite parent body. Earth and Planetary Science Letters, 296, 469–480.
Bogard, D., Burnett, D., Eberhardt, P., and Wasserburg, G.J. (1967) ^{40}Ar-^{40}K ages of silicate inclusions in iron meteorites. Earth and Planetary Science Letters, 3, 275–283.
Bogard, D.D., Burnett, D.S., and Wasserburg, G.J. (1969) Cosmogenic rare gases and the ^{40}K-^{40}Ar age of the Kodaikanal iron meteorite. Earth and Planetary Science Letters, 5, 273–281.
Boesenberg, J.S., Prinz, M., Weisberg, M.K., Davis, A.M., Clayton, R.N., Mayeda, T.K., and Wasson, J.T. (1995) Pyroxene-pallasites: A new pallasite grouplet. Meteoritics, 30, 488–489.
Boesenberg, J.S., Delaney, J.S., and Hewins, R.H. (2012) A petrological and chemical reexamination of Main Group pallasite formation. Geochimica et Cosmochimica Acta, 89, 134–158.
Bowman, L.E., Spilde, M.N., and Papike, J.J. (1997) Automated energy dispersive spectrometer modal analysis applied to the diogenites. Meteoritics & Planetary Science, 32, 869–875.
Boyd, R. (1991) Realism, anti-foundationalism and the enthusiasm for natural kinds. Philosophical Studies, 61, 127–148.
Brearley, A.J., and Jones, R.H. (1998) Chondritic meteorites. Reviews in Mineralogy, 36, 3.01–3.398.
Breen, J.P., Rubin, A.E., and Wasson, J.T. (2016) Variations in impact effects among IIIE iron meteorites. Meteoritics & Planetary Science, 51, 1611–1631.
Britvin, S.N., Rudashevsky, N.S., Krivovichev, S.V., Burns, P.C., and Polekhovsky, Y.S. (2002) Allabogdanite, $(Fe,Ni)_2P$, a new mineral from the Onello meteorite: The occurrence and crystal structure. American Mineralogist, 87, 1245–1249.
Britvin, S.N., Shilovskikh, V.V., Pagano, R., Vlasenko, N.S., Zaitsev, A.N., Krzhizhanovskaya, M.G., Lozhkin, M.S., Zolotarev, A.A., and Gurzhiy, V.V. (2019) Allabogdanite, the high-pressure polymorph of $(Fe,Ni)_2P$, a stishovite-grade indicator of impact processes in the Fe-Ni-P system. Scientific Reports, 9, 1047 (8 p.).
Britvin, S.N., Murashko, M.N., Vapnik, Y., Polekhovsky, Y.S., Krivovichev, S.V., Krzhizhanovskaya, M.O., Vereshchagin, O.S., Shilovskikh, V.V., and Vlasenko, N.S. (2020a) Transjordanite, Ni_2P, a new terrestrial and meteoritic phosphide, and natural solid solutions barringerite-transjordanite (hexagonal Fe_2P–Ni_2P). American Mineralogist, 105, 428–436.
Britvin, S.N., Krivovichev, S.V., Obolonskaya, E.V., Vlasenko, N.S., Bocharov, V.N., and Bryukhanova, V.V. (2020b) Xenophyllite, $Na_4Fe_7(PO_4)_6$, an exotic meteoritic phosphate: New mineral description, Na-ions mobility and electrochemical implications. Minerals, 10, 300 (13 pp.).
Buchwald, V.F. (1975) Handbook of Iron Meteorites. University of California Press.
——— (1977) The mineralogy of iron meteorites. Philosophical Transactions of the Royal Society of London, A, 286, 453–491.
Buchwald, V.F., and Scott, E.R.D. (1971) First nitride (CrN) in iron meteorites. Nature Physical Science, 233, 113–114.
Bunch, T.E., and Fuchs, L.H. (1969a) A new mineral: Brezinaite, Cr_3S_4, and the Tucson meteorite. American Mineralogist, 54, 1509–1518.
——— (1969b) Yagiite, a new sodium-magnesium analogue of osumilite. American Mineralogist, 54, 14–18.
Bunch, T.E., and Keil, K. (1971) Chromite and ilmenite in non-chondritic meteorites. American Mineralogist, 56, 146–157.
Bunch, T.E., and Olsen, E. (1968) Potassium feldspar in Weekeroo Station, Kodaikanal, and Colomera iron meteorites. Science, 160, 1223–1225.
Bunch, T.E., and Rajan, R.S. (1988) Meteorite regolith breccias. In J.F. Kerridge and M.S. Matthews, Eds., Meteorites and the Early Solar System, pp. 144–164. University of Arizona Press.
Bunch, T.E., Keil, K., and Olsen, E. (1970) Mineralogy and petrology of silicate inclusions in iron meteorites. Contributions to Mineralogy and Petrology, 25, 297–240.
Burke, E.A.J. (2006) The end of CNMMN and CCM—Long live the CNMNC! Elements, 2, 388.
Burkhardt, C., Kleine, T., Oberli, F., Pack, A., Bourdon, B., and Wieler, R. (2011) Molybdenum isotopic anomalies in meteorites: Constraints on solar nebula evolution and the origin of the Earth. Earth and Planetary Science Letters, 312, 390–400.
Buseck, P.R. (1969) Phosphide from meteorites: Barringerite, a new iron-nickel mineral. Science, 165, 169–171.
——— (1977) Pallasite meteorites-mineralogy, petrology, and geochemistry. Geochimica et Cosmochimica Acta, 41, 711–740.
Buseck, P.R., and Goldstein, J.I. (1969) Olivine compositions and cooling rates of pallasitic meteorites. Geological Society of America Bulletin, 80, 2141–2158.
Buseck, P.R., and Holdsworth, E. (1977) Phosphate minerals in pallasite meteorites. Mineralogical Magazine, 41, 91–102.
Buseck, P.R., Mason, B., and Wiik, H.-B. (1966) The Farmington meteorite-mineralogy and petrology. Geochimica et Cosmochimica Acta, 30, 1–8.
Casanova, I., McCoy, T.J., and Keil, K. (1993) Metal-rich meteorites from the aubrite parent body. Lunar and Planetary Science, 24, 259–260.
Casanova, I., Graf, T., and Marti, K. (1995) Discovery of an unmelted H-chondrite inclusion in an iron meteorite. Science, 268, 540–542.
Chabot, N.L., and Drake, M.J. (1999) Crystallization of magmatic iron meteorites: The role of mixing in the molten core. Meteoritics & Planetary Science, 34, 235–246.
——— (2000) Crystallization of magmatic iron meteorites: The effects of phosphorus and liquid immiscibility. Meteoritics & Planetary Science, 35, 807–816.
Chao, E.C.T., Shoemaker, E.M., and Madsen, B.M. (1960) First natural occurrence of coesite. Science, 132, 220–222.
Chao, E.C.T., Fahey, J.J., Littler, J., and Milton, D.J. (1962) Stishovite, SiO_2, a very high pressure new mineral from Meteor Crater, Arizona. Journal of Geophysical Research, 67, 419–421.
Chen, M., and Xie, X.D. (2015) Shock-produced akimotoite in the Suizhou L6 chondrite. Science China Earth Sciences, 58, 876–880.
Chen, M., Sharp, T.G., El Goresy, A., Wopenka, B., and Xie, X. (1996) The majorite-pyrope-magnesiowustite assemblage: Constraints on the history of shock veins in chondrites. Science, 271, 1570–1573.
Chen, M., Shu, J., Mao, H.-K., Xie, X., and Hemley, R.J. (2003a) Natural occurrence and synthesis of two new post-spinel polymorphs of chromite. Proceedings of the National Academy of Sciences, 100, 14651–14654.
Chen, M., Shu, J., Xie, X., and Mao, H.-K. (2003b) Natural $CaTi_2O_4$-structured $FeCr_2O_4$ polymorph in the Suizhou meteorite and its significance in mantle mineralogy. Geochimica et Cosmochimica Acta, 67, 3937–3942.
Chen, M., El Goresy, A., and Gillet, P. (2004) Ringwoodite lamellae in olivine: Clues to olivine-ringwoodite phase transition mechanisms in shocked meteorites and subducting slabs. Proceedings of the National Academy of Sciences, 101, 15033–15037.
Chen, M., Shu, J., and Mao, H.K. (2008) Xieite, a new mineral of high-pressure $FeCr_2O_4$ polymorph. Chinese Science Bulletin, 53, 3341–3345.
Chen, M., Shu, J., Xie, X., and Tan, D. (2019) Maohokite, a post-spinel polymorph of $MgFe_2O_4$ in shocked gneiss from the Xiuyan crater in China. Meteoritics & Planetary Science, 54, 495–502.
Choi, B.-G., Ouyang, X., and Wasson, J.T. (1995) Classification and origin of IAB and IIICD iron meteorites. Geochimica et Cosmochimica Acta, 59, 593–612.
Clarke, R.S. Jr., and Scott, E.R.D. (1980) Tetrataenite—ordered FeNi, a new mineral in meteorites. American Mineralogist, 65, 624–630.
Clayton, R.N., and Mayeda, T.K. (1996) Oxygen-isotope studies of achondrites. Geochimica et Cosmochimica Acta, 60, 1999–2018.
Clayton, D.D., and Nittler, L.R. (2004) Astrophysics with presolar stardust. Annual Reviews of Astronomy and Astrophysics, 42, 39–78.
Coes, L. (1953) A new dense crystalline silica. Science, 118, 131–132.
Cohen, B.A., Goodrich, C.A., and Keil, K. (2004) Feldspathic clast populations in polymict ureilites: Stalking the missing basalts from the ureilite parent body. Geochimica et Cosmochimica Acta, 68, 4249–4266.
Coleman, L.C. (1977) Ringwoodite and majorite in the Catherwood meteorite. Canadian Mineralogist, 15, 97–101.
Crozaz, G., and McKay, G. (1990) Rare earth elements in Angra dos Reis and Lewis Cliff 86010, two meteorites with similar but distinct magma evolutions. Earth and Planetary Science Letters, 97, 369–381.
Davis, A.M. (2011) Stardust in meteorites. Proceedings of the National Academy of Sciences, 108, 19142–19146.
——— (2014) Meteorites and cosmochemical processes: Treatise on geochemistry,

Volume 1, Second edition. Elsevier-Pergamon.
Davis, A.M., and Olsen, E.J. (1991) Phosphates in pallasite meteorites as probes of mantle processes in small planetary bodies. Nature, 353, 637–640.
Davison, T.M., Collins, G.S., and Ciesla, F.J. (2010) Numerical modeling of heating in porous planetesimal collisions. Icarus, 208, 468–481.
Day, J.M.D., Ash, R.D., Liu, Y., Bellucci, J.J., Rumble, D., McDonough, W.F., Walker, R.J., and Taylor, L.A. (2009) Early formation of evolved asteroidal crust. Nature, 457, 179–182.
Day, J.M.D., Walker, R.J., Ash, R.D., Liu, Y., Rumble, D., Irving, A.J., Goodrich, C.A., Tait, K., McDonough, W.F., and Taylor, L.A. (2012) Origin of felsic achondrites Graves Nunataks 06128 and 06129, and ultramafic brachinites and brachinite-like achondrites by partial melting of volatile-rich primitive parent bodies. Geochimica et Cosmochimica Acta, 81, 94–128.
Deer, W.A., Howie, R.A., and Zussman, J. (1962) Rock-Forming Minerals. Volume 1B. Disilicates and ring silicates. Longman.
——— (1997) Rock-Forming Minerals. Volume 2A. Single-chain silicates. The Geological Society of London.
Delaney, J.S., Prinz, M., and Takeda, H. (1984) The polymict eucrites. Journal of Geophysical Research, 89, C251–C288.
Dera, P., Prewitt, C.T., Boctor, N.Z., and Hemley, R.J. (2002) Characterization of a high-pressure phase of silica from the Martian meteorite Shergotty. American Mineralogist, 87, 1018–1023.
Dera, P., Lavina, B., Borkowski, L.A., Prakapenka, V.B., Sutton, S.R., Rivers, M.L., Downs, R.T., Boctor, N.Z., and Prewitt, C.T. (2008) High-pressure polymorphism of Fe_2P and its implications for meteorites and Earth's core. Geophysical Research Letters, 35, L10301.
Dodd, R.T., and Jarosewich, E. (1979) Incipient melting in and shock classification of L-group chondrites. Earth and Planetary Science Letters, 44, 335–340.
——— (1982) The composition of incipient shock melts in L6 chondrites. Earth and Planetary Science Letters, 59, 355–363.
Domanik, K., Kolar, S., Musselwhite, D., and Drake, M.J. (2004) Accessory silicate mineral assemblages in the Bilanga diogenite: A petrographic study. Meteoritics & Planetary Science, 39, 567–579.
Downes, H., Mittlefehldt, D.W., Kita, N.T., and Valley, J.W. (2008) Evidence from polymict ureilite meteorites for a disrupted and re-accreted single ureilite parent asteroid gardened by several distinct impactors. Geochimica et Cosmochimica Acta, 72, 4825–4844.
Drake, M.J. (2001) The eucrite/Vesta story. Meteoritics & Planetary Science, 36, 501–513.
Dupré, J. (1981) Natural kinds and biological taxa. Philosophical Review, 90, 66–90.
Ebihara, M., Ikeda, Y., and Prinz, M. (1997) Petrology and chemistry of the Miles IIE iron. II: Chemical characteristics of the Miles silicate inclusions. Proceedings of the NIPR Symposium on Antarctic Meteorites, 21, 373–388.
El Goresy, A. (1971) Meteoritic rutile: A niobium bearing mineral. Earth and Planetary Science Letters, 11, 359–361.
El Goresy, A., and Donnay, G. (1968) A new allotropic form of carbon from the Ries Crater. Science, 161, 363–364.
El Goresy, A., Wopenka, B., Chen, M., Weinbruch, S., and Sharp, T. (1997) Evidence for two different shock induced high-pressure events and alkali-vapor metasomatism in Peace River and Tenham (L6) chondrites. Lunar and Planetary Science, 28, 1044.
El Goresy, A., Dera, P., Sharp, T.G., Prewitt, C.T., Chen, M., Dubrovinsky, L., Wopenka, B., Boctor, N.Z., and Hemley, R.J. (2008) Seifertite, a dense orthorhombic polymorph of silica from the Martian meteorites Shergotty and Zagami. European Journal of Mineralogy, 20, 523–528.
El Goresy, A., Dubrovinsky, L., Gillet, P., Graup, G., and Chen, M. (2010) Akaogiite: An ultra-dense polymorph of TiO_2 with the baddeleyite-type structure, in shocked garnet gneiss from the Ries Crater, Germany. American Mineralogist, 95, 892–895.
Fagan, T.J., Scott, E.R.D., Keil, K., Cooney, T.F., and Sharma, S.K. (2000) Formation of feldspathic and metallic melts by shock in enstatite chondrite Reckling Peak A80259. Meteoritics & Planetary Science, 35, 319–329.
Fahey, J.J. (1964) Recovery of coesite and stishovite from Coconino Sandstone of Meteor Crater, AZ. American Mineralogist, 49, 1643–1647.
Feng, L., Lin, Y., Hu, S., Xu, l., and Miao, B. (2011) Estimating compositions of natural ringwoodite in the heavily shocked Grove Mountains 052049 meteorite from Raman spectra. American Mineralogist, 96, 1480–1489.
Ferroir, T., Beck, P., Van de Moortèle, B., Bohn, M., Reynard, B., Simonovici, A., El Goresy, A., and Gillet, P. (2008) Akimotoite in the Tenham meteorite: Crystal chemistry and high-pressure transformation mechanisms. Earth and Planetary Science Letters, 275, 26–31.
Fialin, M., Catillon, G., and Andrault, D. (2009) Disproportionation of Fe^{2+} in Al-free silicate perovskite in the laser heated diamond anvil cell as recorded by electron probe microanalysis of oxygen. Physics and Chemistry of Minerals, 36, 183–191.
Floran, R.J. (1978) Silicate petrography, classification, and origin of the mesosiderites: Review and new observations. Proceedings of the Lunar and Planetary Science Conference, 9, 1053–1081.
Floss, C., and Crozaz, G. (1993) Heterogeneous REE patterns in oldhamite from the aubrites: Their nature and origin. Geochimica et Cosmochimica Acta, 57, 4039–4057.
Fogel, R.A. (2001) The role of roedderite in the formation of aubrites. Lunar and Planetary Science, 32, 2177.
——— (2005) Aubrite basalt vitrophyres: The missing basaltic component and high-sulfur silicate melts. Geochimica et Cosmochimica Acta, 69, 1633–1648.
Fritz, J., Greshake, A., and Fernandes, V.A. (2017) Revising the shock classification of meteorites. Meteoritics & Planetary Science, 52, 1216–1232.
Frondel, C., and Klein, C. (1965) Ureyite, $NaCrSi_2O_6$: A new meteoritic pyroxene. Science, 149, 742–744.
Frondel, C., and Marvin, U.B. (1967) Lonsdaleite, a hexagonal polymorph of diamond. Nature, 214, 587–589.
Fuchs, L.H. (1966) Djerfisherite, alkali copper-iron sulfide, a new mineral from the Kota-Kota and St. Mark's enstatite chondrites. Science, 153, 166–167.
——— (1967) Stanfieldite: A new phosphate mineral from stony-iron meteorites. Science, 158, 910–911.
——— (1969a) The phosphate mineralogy of meteorites. In P.M. Millman, Ed., Meteorite Research, pp. 683–695. Reidel.
——— (1969b) Occurrence of cordierite and aluminous orthoenstatite in the Allende meteorite. American Mineralogist, 4, 1645–1653.
——— (1974) Glass inclusions of granitic compositions in orthopyroxene from three enstatite achondrites. Meteoritics, 9, 342.
Fuchs, L.H., Olsen, E., and Henderson, E.P. (1967) On the occurrence of brianite and panethite, two new phosphate minerals from the Dayton meteorite. Geochimica et Cosmochimica Acta, 31, l71l–1719.
Garvie, L.A.J., Németh, P., and Buseck, P.R. (2011) Diamond, bucky-diamond, graphite-diamond, Al-silicate, and stishovite in the Gujba CB chondrite. Meteoritics & Planetary Science, 46, Supplement, 1, 5227.
Garvie, L.A.J., Ma, C., Ray, S., Domanik, K., Wittmann, A., and Wadhwa, M. (2021) Carletonmooreite, Ni_3Si, a new silicide from the Norton County, aubrite meteorite. American Mineralogist, in press. **{{AU: staff Update? 7645}}**
Gasparik, T. (1990) Phase relations in the transition zone. Journal of Geophysical Research, 95, 15751–15769.
German, V.N., Podurets, M.A., and Trunin, R.F. (1973) Shock compression of quartz to 90 GPa. Soviet Physics, Journal of Experimental and Theoretical Physics, 37, 107–115.
Gillet, P., Chen, M., Dubrovinsky, L., and El Goresy, A. (2000) Natural $NaAlSi_3O_8$-hollandite in the shocked Sixiangkou meteorite. Science, 287, 1633–1636.
Glass, B.P., Liu, S., and Leavens, P.B. (2002) Reidite: An impact-produced high-pressure polymorph of zircon found in marine sediments. American Mineralogist, 87, 562–565.
Goldstein, J.I., and Michael, J.R. (2006) The formation of plessite in meteoritic metal. Meteoritics & Planetary Science, 41, 553–570.
Goldstein, J.I., Scott, E.R.D., and Chabot, N.L. (2009) Iron meteorites: Crystallization, thermal history, parent bodies, and origin. Chemie der Erde, 69, 293–325.
Gomes, C.B., and Keil, K. (1980) Brazilian Stone Meteorites. University of New Mexico Press.
Goodrich, C.A. (1986) Trapped primary silicate liquid in ureilites. Lunar and Planetary Science, 17, 273–274.
——— (1992) Ureilites: A critical review. Meteoritics, 27, 252–327.
Goodrich, C.A., and Berkley, J.L. (1986) Primary magmatic carbon in ureilites: Evidence from cohenite-bearing spherules. Geochimica et Cosmochimica Acta, 50, 681–691.
Goodrich, C.A., Scott, E.R.D., and Fioretti, A.M. (2004) Ureilitic breccias: Clues to the petrologic structure and impact disruption of the ureilite parent asteroid. Chemie der Erde—Geochemistry, 64, 283–327.
Goodrich, C.A., Van Orman, J.A., and Wilson, L. (2007) Fractional melting and smelting on the ureilite parent body. Geochimica et Cosmochimica Acta, 71, 2876–2895.
Goodrich, C.A., Hutcheon, I.D., Kita, N.T., Huss, G.R., Cohen, B.A., and Keil, K. (2010) ^{53}Mn-^{53}Cr and ^{26}Al-^{26}Mg ages of a feldspathic lithology in polymict ureilites. Earth and Planetary Science Letters, 295, 531–540.
Goodrich, C.A., Wilson, L., Van Orman, J.A., and Michel, P. (2013) Comment on 'Parent body depth-pressure-temperature relationships and the style of the ureilite anatexis' by P.H. Warren (MAPS 47, 209–227). Meteoritics & Planetary Science, 48, 1096–1106.
Goodrich, C.A., Harlow, G.E., Van Orman, J.A., Sutton, S.R., Jercinovic, M.J., and Mikouchi, T. (2014) Petrology of chromite in ureilites: Deconvolution of primary oxidation states and secondary reduction processes. Geochimica et Cosmochimica Acta, 135, 126–169.
Göpel, C., Manhès, G., and Allègre, C.J. (1985) Concordant 3,676 Ma U-Pb formation age for the Kodaikanal iron meteorite. Nature, 317, 341–344.
Grady, M.M., and Wright, I. (2006) Types of extraterrestrial material available for study. In D.S. Lauretta and H.Y. McSween Jr., Eds., Meteorites and the Early Solar System II, pp. 3–18. University of Arizona Press.
Graham, A.L., Easton, A.J., and Hutchison, R. (1977) The Mayo Belwa meteorite: A new enstatite achondrite fall. Mineralogical Magazine, 41, 487–492.
Grew, E.S., Yates, M.G., Beane, R.J., Floss, C., and Gerbi, C. (2010) Chopinite-sarcopside solid solution, $[(Mg,Fe)_3\square](PO_4)_2$, in GRA95209, a transitional acapulcoite: Implications for phosphate genesis in meteorites. American Mineralogist, 95, 260–272.
Grew, E.S., Hystad, G., Hazen, R.M., Krivovichev, S.V., and Gorelova, L.A. (2017) How many boron minerals occur in Earth's upper crust? American Mineralogist, 102, 1573–1587.
Grieve, R.A.F., Langenhorst, F., and Stöffler, D. (1996) Shock metamorphism of quartz in nature and experiment. 2. Significance in geoscience. Meteoritics & Planetary

Science, 31, 6–35.
Haack, H., Rasmussen, K.L., and Warren, P.H. (1990) Effects of regolith/megaregolith insulation on the cooling histories of differentiated asteroids. Journal of Geophysical Research, 95, 5111–5124.
Haba, M.K., Yamaguchi, A., Horie, K., and Hidaka, H. (2014) Major and trace elements of zircons from basaltic eucrites: Implications for the formation of zircons on the eucrite parent body. Earth and Planetary Science Letters, 387, 10–21.
Harlow, G.E., Nehru, C.E., Prinz, M., Taylor, G.J., and Keil, K. (1979) Pyroxenes in Serra de Mage: Cooling history in comparison with Moama and Moore County. Earth and Planetary Science Letters, 43, 173–181.
Hawley, K., and Bird, A. (2011) What are natural kinds? Philosophical Perspectives, 25, 205–221.
Hazen, R.M. (2019) An evolutionary system of mineralogy: Proposal for a classification based on natural kind clustering. American Mineralogist, 104, 810–816.
Hazen, R.M., and Ausubel, J.H. (2016) On the nature and significance of rarity in mineralogy. American Mineralogist, 101, 1245–1251.
Hazen, R.M., and Finger, L.W. (1978) Crystal chemistry of silicon-oxygen bonds at high pressure: Implications for the Earth's mantle mineralogy. Science, 201, 1122–1123.
Hazen, R.M., and Morrison, S.M. (2020) An evolutionary system of mineralogy, Part I: stellar mineralogy (>13 to 4.6 Ga). American Mineralogist, 105, 627–651.
Hazen, R.M., Papineau, D., Bleeker, W., Downs, R.T., Ferry, J.M., McCoy, T.L., Sverjensky, D.A., and Yang, H. (2008) Mineral evolution. American Mineralogist, 93, 1693–1720.
Hazen, R.M., Grew, E.S., Downs, R.T., Golden, J., and Hystad, G. (2015a) Mineral ecology: Chance and necessity in the mineral diversity of terrestrial planets. Canadian Mineralogist, 53, 295–323.
Hazen, R.M., Hystad, G., Downs, R.T., Golden, J., Pires, A., and Grew, E.S. (2015b) Earth's "missing" minerals. American Mineralogist, 100, 2344–2347.
Hazen, R.M., Hummer, D.R., Hystad, G., Downs, R.T., and Golden, J.J. (2016) Carbon mineral ecology: Predicting the undiscovered minerals of carbon. American Mineralogist, 101, 889–906.
Hazen, R.M., Morrison, S.M., and Prabhu, A. (2021) An evolutionary system of mineralogy, part III: Primary chondrule mineralogy (4.566 to 4.561 Ga). American Mineralogist, 106, 325–350.
Heinemann, S., Sharp, T.G., Seifert, F., and Rubie, D.C. (1997) The cubic-tetragonal phase transition in the system majorite ($Mg_4Si_4O_{12}$)–pyrope ($Mg_3Al_2Si_3O_{12}$), and garnet symmetry in the Earth's transition zone. Physics and Chemistry of Minerals, 24, 206–221.
Henderson, E.P. (1941) Chilean hexahedrites and the composition of all hexahedrites. American Mineralogist, 26, 546–550.
Herrin, J.S., Zolensky, M.E., Ito, M., Le, L., Mittlefehldt, D.W., Jenniskens, P., Ross, A.J., and Shaddad, M.H. (2010) Thermal and fragmentation history of ureilitic asteroids: insights from the Almahata Sitta fall. Meteoritics & Planetary Science, 45, 1789–1803.
Hewins, R.H. (1983) Impact versus internal origins for mesosiderites. Journal of Geophysical Research, 88, B257–B266.
Hewins, R.H., Jones, R.H., and Scott, E.R.D., Eds. (1996) Chondrules and the Protoplanetary Disk. Cambridge University Press.
Hiroi, T., Bell, J.F., Takeda, H., and Pieters, C.M. (1993) Spectral comparison between olivine-rich asteroids and pallasites. Proceedings of the NIPR Symposium on Antarctic Meteorites, 6, 234–245.
Hollister, L.S., Bindi, L., Yao, N., Poirier, G.R., Andronicos, C.L., MacPherson, G.J., Lin, C., Distler, V.V., Eddy, M.P., Kostin, A., and others (2014) Impact-induced shock and the formation of natural quasicrystals in the early solar system. Nature Communications, 5, 4040.
Holtstam, D., Broman, C., Söderhielm, J., and Zetterqvist, A. (2003) First discovery of stishovite in an iron meteorite. Meteoritics & Planetary Science, 38, 1579–1583.
Hsu, W. (1998) Geochemical and petrographic studies of oldhamite, diopside, and roedderite in enstatite meteorites. Meteoritics & Planetary Science, 33, 291–301.
Hu, J., Asimow, P.D., and Ma, C. (2019) First shock synthesis of khatyrkite, stolperite and a newly found natural quasicrystal: Implications for the impact origin of quasicrystals from the Khatyrka meteorite. Lunar and Planetary Science, 50, 3126.
Hubbard, A. (2016) Ferromagnetism and particle collisions: Applications to protoplanetary disks and the meteoritical record. The Astrophysical Journal, 826, 152 (10 pp).
Hutchison, R. (2004) Meteorites: A petrologic, chemical and isotopic synthesis. Cambridge University Press.
Hwang, S.L., Shen, P., Chu, H.T., Yui, T.F., Varela, M.E., and Iizuka, Y. (2016) Kuratite, $Ca_4(Fe^{2+}_{10}Ti_2)O_4[Si_8Al_4O_{36}]$, the Fe^{2+}-analogue of rhönite, a new mineral from the D'Orbigny angrite meteorite. Mineralogical Magazine, 80, 1067–1076.
——— (2019) New minerals tsangpoite $Ca_5(PO_4)_2(SiO_4)$ and matyhite $Ca_9(Ca_{0.5}\square_{0.5})Fe(PO_4)_7$ from the D'Orbigny angrite. Mineralogical Magazine, 83, 293–313.
Hystad, G., Downs, R.T., and Hazen, R.M. (2015a) Mineral frequency distribution data conform to a LNRE model: Prediction of Earth's "missing" minerals. Mathematical Geosciences, 47, 647–661.
Hystad, G., Downs, R.T., Grew, E.S., and Hazen, R.M. (2015b) Statistical analysis of mineral diversity and distribution: Earth's mineralogy is unique. Earth and Planetary Science Letters, 426, 154–157.
Hystad, G., Downs, R.T., Hazen, R.M., and Golden, J.J. (2017) Relative abundances for the mineral species on Earth: A statistical measure to characterize Earth-like planets based on Earth's mineralogy. Mathematical Geosciences, 49, 179–194.
Hystad, G., Eleish, A., Downs, R.T., Morrison, S.M., and Hazen, R.M. (2019) Bayesian estimation of Earth's undiscovered mineralogical diversity using noninformative priors. Mathematical Geosciences, 51, 401–417.
Ikeda, Y., and Takeda, H. (1985) A model for the origin of basaltic achondrites based on the Yamato 7308 howardite. Journal of Geophysical Research, 90, C649–C663.
Ireland, T.R., and Wlotzka, F. (1992) The oldest zircons in the solar system. Earth and Planetary Science Letters, 109, 1–10.
Irifune, T., Ringwood, A.E., and Hibberson, W.O. (1994) Subduction of continental crust and terrigenous and pelagic sediments: An experimental study. Earth and Planetary Science Letters, 126, 351–368.
Isa, J., Ma, C., and Rubin, A.E. (2016) Joegoldsteinite: A new sulfide mineral ($MnCr_2S_4$) from the Social Circle IVA iron meteorite. American Mineralogist, 101, 1217–1221.
Ivanov, A.V., Zolensky, M.E., Saito, A., Ohsumi, K., MacPherson, G.J., Yang S.V., Kononkova, N.N., and Mikouchi, T. (2000) Florenskyite, FeTiP, a new phosphide from the Kaidun meteorite. American Mineralogist, 85, 1082–1086.
Jambon, A., Barrat, J.A., Boudouma, O., Fonteilles, M., Badia, D., Göpel, C., and Bohn, M. (2005) Mineralogy and petrology of the angrite Northwest Africa 1296. Meteoritics & Planetary Science, 40, 361–375.
Jambon, A., Boudouma, O., Fonteilles, M., Le Guillou, C., Badia, D., and Barrat, J.A. (2008) Petrology and mineralogy of the angrite Northwest Africa 1670. Meteoritics & Planetary Science, 43, 1783–1795.
Johansen, A., Oishi, J.S., Mac Low, M.-M., Klahr, H., Henning, T., and Youdin, A. (2007) Rapid planetesimal formation in turbulent circumstellar disks. Nature, 448, 1022–1025.
Joreau, P., Leroux, H., and Doukhan, J.C. (1996) A transmission electron microscopy (TEM) investigation of opaque phases in shocked chondrites. Meteoritics, 31, 305–312.
Kaneko, S., Miyahara, M., Ohtani, E., Arai, T., Hirao, N., and Sato, K. (2015) Discovery of stishovite in Apollo 15299 sample. American Mineralogist, 100, 1308–1311.
Karwowski, Ł., Kusz, J., Muszyński, A., Kryza, R., Sitarz, M., and Galuskin, E.V. (2015) Moraskoite, $Na_2Mg(PO_4)F$, a new mineral from the Morasko IAB-MG iron meteorite (Poland). Mineralogical Magazine, 79, 387–398.
Kato, Y., Sekine, T., Kayama, M., Miyahara, M., and Yamaguchi, A. (2017) High-pressure polymorphs in Yamato-790729 L6 chondrite and their significance for collisional conditions. Meteoritics & Planetary Science, 52, 2570–2585.
Keil, K. (2000) Thermal alteration of asteroids: Evidence from meteorites. Planetary and Space Science, 48, 887–903.
——— (2010) Enstatite achondrite meteorites (aubrites) and the histories of their asteroidal parent bodies. Chemie der Erde—Geochemistry, 70, 295–317.
——— (2012) Angrites, a small but diverse suite of ancient, silica-undersaturated asteroidal volcanic-plutonic mafic meteorites, and the history of their parent asteroid. Chemie der Erde—Geochemistry, 72, 191–218.
Keil, K., and Brett, R. (1974) Heideite, $(Fe,Cr)_{1+x}(Ti,Fe)_2S_4$: a new mineral in the Bustee enstatite achondrite. American Mineralogist, 59, 465–470.
Keil, K., and Fredriksson, K. (1963) Electron microprobe analysis of some rare minerals in the Norton County achondrite. Geochimica et Cosmochinca Acta, 27, 939–947.
Keil, K., and Snetsinger, K.G. (1967) Niningerite, a new meteoritic sulfide. Science, 155, 451–453.
Keil, K., Berkley, J.L., and Fuchs, L.H. (1982) Suessite, Fe_3Si: A new mineral in the North Haig ureilite. American Mineralogist, 67, 126–131.
Keil, K., Haack, H., and Scott, E.R.D. (1994) Catastrophic fragmentation of asteroids—Evidence from meteorites. Planetary and Space Science, 42, 1109–1122.
Kelly, W.R., and Larimer, J.W. (1977) Chemical fractionation in meteorites-VII. Iron meteorites and the cosmochemical history of the metal phase. Geochimica et Cosmochimica Acta, 41, 93–111.
Kerridge, J.F., and Matthews, M.S. (1988) Meteorites and the early Solar System. University of Arizona Press.
Kerschhofer, L., Sharp, T.G., and Rubie, D.C. (1996) Intracrystalline transformation of olivine to wadsleyite and ringwoodite under subduction zone conditions. Science, 274, 79–81.
Kerschhofer, L., Dupas, C., Liu, M., Sharp, T.G., Durham, W.B., and Rubie, D.C. (1998) Polymorphic transformations between olivine, wadsleyite and ringwoodite: Mechanisms of intracrystalline nucleation and the role of elastic strain. Mineralogical Magazine, 62, 617–638.
Kimura, M., Suzuki, A., Kondo, T., Ohtani, E., and El Goresy, A. (2000) Natural occurrence of high-pressure phases jadeite, hollandite, wadsleyite, and majorite-pyrope garnet in an H chondrite, Yamato 75100. Meteoritics & Planetary Sciences, 35, A87–A88.
Kimura, M., Chen, M., Yoshida, T., El Goresy, A., and Ohtani, E. (2003) Back-transformation of high-pressure phases in a shock melt vein of an H-chondrite during atmospheric passage: Implications for the survival of high-pressure phases after decompression. Earth and Planetary Science Letters, 217, 141–150.
Koeberl, C. (2014) The geochemistry and cosmochemistry of impacts. Treatise on Geochemistry, 2nd ed., 1, 73–118.
Kracher, A., and Wasson, J.T. (1982) The role of S in the evolution of the parental cores of the iron meteorites. Geochimica et Cosmochimica Acta, 46, 2419–2426.
Kracher, A., Kurat, G., and Buchwald, V.F. (1977) Cape York: The extraordinary mineralogy of an ordinary iron meteorite and its implication for the genesis of III AB

irons. Geochemical Journal, 11, 207–217.
Kring, D.A., Boynton, W.V., Hill, D.H., and Haag, R.A. (1991) Petrologic description of Eagles Nest: A new olivine achondrite. Meteoritics, 26, 360.
Krot, A.N., Keil, K., Scott, E.R.D., Goodrich, C.A., and Weisberg, M.K. (2014) Classification of meteorites and their genetic relationships. Treatise on Geochemistry, 2nd ed., 1, 2–63.
Kruijer, T.S., Burkhardt, C., Budde, G., and Kleine, T. (2017) Age of Jupiter from the distinct genetics and formation times of meteorites. Proceedings of the National Academy of Sciences, 114, (5 p.). DOI: 10.1073/pnas.1704461114.
Kuwayama, Y. (2008) Ultrahigh pressure and high temperature experiments using a laser heated diamond anvil cell in multimegabar pressures region. The Review of High-Pressure Science and Technology, 18, 3–10.
Langenhorst, F., and Poirier, J.-P. (2000) 'Eclogitic' minerals in a shocked basaltic meteorite. Earth and Planetary Science Letters, 176, 259–265.
Litasov, K.D., Teplyakova, S.N., Shatskiy, A., and Kuper, K.E. (2019) Fe-Ni-PS melt pockets in Elga IIE iron meteorite: Evidence for the origin at high pressures up to 20 GPa. Minerals, 9, 616 (11 p.).
Liu, L.G. (1978) High-pressure phase transformations of albite, jadeite and nepheline. Earth and Planetary Science Letters, 37, 438–444.
Liu, X. (2006) Phase relations in the system $KAlSi_3O_8$-$NaAlSi_3O_8$ at high pressure-high temperature conditions and their implication for the petrogenesis of lingunite. Earth and Planetary Science Letters, 246, 317–325.
Liu, L.G., and El Goresy, A. (2007) High-pressure phase transitions of the feldspars, and further characterization of lingunite. International Geology Review, 49, 854–860.
Liu, L.G., and Ringwood, A.E. (1975) Synthesis of a perovskite-type polymorph of $CaSiO_3$. Earth and Planetary Science Letters, 28, 209–211.
Lodders, K. (1996) An experimental and theoretical study of rare-earth-element partitioning between sulfides (FeS,CaS) and silicate and applications to enstatite achondrites. Meteoritics & Planetary Science, 31, 749–766.
Lodders, K., and Amari, S. (2005) Presolar grains from meteorites: Remnants from the early times of the solar system. Chemie der Erde, 65, 93–166.
Longhi, J. (1999) Phase equilibrium constraints on angrite petrogenesis. Geochimica et Cosmochimica Acta, 63, 573–585.
Lovering, J.F. (1975) The Moama eucrite—A pyroxene-plagioclase adcumulate. Meteoritics, 10, 101–114.
Lugaro, M. (2005) Stardust from Meteorites: An introduction to presolar grains. World Scientific.
Lunning, N.G., Corrigan, C.M., McSween, H.Y., Tenner, T.J., Kita, N.T., and Bodnar, R.J. (2016) CV and CM chondrite impact melts. Geochimica et Cosmochimica Acta, 189, 338–358.
Ma, C. (2018) A closer look at shock meteorites: Discovery of new high-pressure minerals. American Mineralogist, 103, 1521–1522.
Ma, C., and Prakapenka, V. (2018) Tschaunerite, IMA 2017-032a. Mineralogical Magazine, 82, 1369–1379.
Ma, C., and Rubin, A.E. (2019) Edscottite, Fe_5C_2, a new iron carbide mineral from the Ni-rich Wedderburn IAB meteorite. American Mineralogist, 104, 1351–1355.
Ma, C., and Tschauner, O. (2016) Discovery of tetragonal almandine, $(Fe,Mg,Ca,Na)_3(Al,Si,Mg)_2Si_3O_{12}$, a new high-pressure mineral in Shergotty. Meteoritics & Planetary Science, 51, Supplement 1, 6124.
——— (2017) Zagamiite, IMA 2015-022a. European Journal of Mineralogy, 29, 339–344.
——— (2018a) Liuite, IMA 2017-042a. Mineralogical Magazine, 82, 1369–1379.
——— (2018b) Feiite, IMA 2017-041a. Mineralogical Magazine, 82, 1369–1379.
Ma, C., Beckett, J.R., and Rossman, G.R. (2012a) Buseckite, (Fe,Zn,Mn)S, a new mineral from the Zakłodzie meteorite. American Mineralogist, 97, 1226–1233.
——— (2012b) Browneite, MnS, a new sphalerite-group mineral from the Zakłodzie meteorite. American Mineralogist, 97, 2056–2059.
Ma, C., Tschauner, O., Beckett, J.R., Liu, Y., Rossman, G.R., Zhuravlev, K., Prakapenka, V., Dera, P., and Taylor, L.A. (2015) Tissintite, $(Ca,Na,)AlSi_2O_6$, a highly-defective, shock-induced, high-pressure clinopyroxene in the Tissint martian meteorite. Earth and Planetary Science Letters, 422, 194–205.
Ma, C., Tschauner, O., Beckett, J.R., Liu, Y., Rossman, G.R., Sinogeikin, S.V., Smith, J.S., and Taylor, L.A. (2016) Ahrensite, γ-Fe_2SiO_4, a new shock-metamorphic mineral from the Tissint meteorite: Implications for the Tissint shock event on Mars. Geochimica et Cosmochimica Acta, 184, 240–256.
Ma, C., Lin, C., Bindi, L., and Steinhardt, P.J. (2017a) Hollisterite (Al_3Fe), kryachkoite $(Al,Cu)_6(Fe,Cu)$, and stolperite (AlCu): Three new minerals from the Khatyrka CV3 carbonaceous chondrite. American Mineralogist, 102, 690–693.
Ma, C., Tschauner, O., and Beckett, J.R. (2017b) A new high-pressure calcium aluminosilicate ($CaAl_2Si_{3.5}O_{11}$) in martian meteorites: Another after-life for plagioclase and connections to the CAS phase. Lunar and Planetary Science, 48, 1128.
Ma, C., Tschauner, O., Beckett, J.R., Rossman, G.R., Prescher, C., Prakapenka, V.B., Bechtel, H.A., and MacDowell, A. (2018) Liebermannite, $KAlSi_3O_8$, a new shock-metamorphic, high-pressure mineral from the Zagami Martian meteorite. Meteoritics & Planetary Science, 53, 50–61.
Ma, C., Tschauner, O., Beckett, J.R., Liu, Y., Greenberg, E., and Prakapenka, V.B. (2019a) Chenmingite, $FeCr_2O_4$ in the $CaFe_2O_4$-type structure, a shock-induced, high-pressure mineral in the Tissint martian meteorite. American Mineralogist, 104, 1521–1525.
Ma, C., Tschauner, O., and Beckett, J.R. (2019b) A closer look at Martian meteorites: Discovery of the new mineral zagamiite, $CaAl_2Si_{3.5}O_{11}$, a shock-metamorphic, high-pressure, calcium aluminosilicate. International Conference on Mars, 9, 6138.
——— (2019c) Discovery of a new high-pressure silicate phase, $(Fe,Mg,Cr,Ti,Ca,\square)_2(Si,Al)O_4$ with a tetragonal spinelloid structure, in a shock melt pocket from the Tissint Martian meteorite. Lunar and Planetary Science Conference, 50, 1460.
Ma, C., Tschauner, O., Bindi, L., Beckett, J.R., and Xie, X. (2019d) A vacancy-rich, partially inverted spinelloid silicate, $(Mg,Fe,Si)_2(Si,\square)O_4$, as a major matrix phase in shock melt veins of the Tenham and Suizhou L6 chondrites. Meteoritics & Planetary Science, 54, 1907–1918.
Madon, M., and Poirier, J.P. (1980) Dislocations in spinel and garnet high-pressure polymorphs of olivine and pyroxene: Implications for mantle rheology. Science, 207, 66–68.
——— (1983) Transmission electron microscope observation of α, β and γ $(Mg,Fe)_2SiO_4$ in shocked meteorites: Planar defects and polymorphic transitions. Physics of the Earth and Planetary Interiors, 33, 31–44.
Magnus, P.D. (2012) Scientific enquiry and natural kinds: From mallards to planets. Palgrave MacMillan.
Malavergne, V., Guyot, F., Benzerara, K., and Martinez, I. (2001) Description of new shock-induced phases in the Shergotty, Zagami, Nakhla and Chassigny meteorites. Meteoritics & Planetary Science, 36, 1297–1305.
Marvin, U.B. (1962) Cristobalite in the Carbo Iron Meteorite. Nature, 196, 634–636.
Marvin, U.B., Petaev, M.I., Croft, W.J., and Killgore, M. (1997) Silica minerals in the Gibeon IVA iron meteorite. Lunar and Planetary Science, 28, 879–880.
Mason, B., Nelen, J., and White, J.S. Jr. (1968) Olivine-garnet transformation in a meteorite. Science, 160, 66–67.
McCammon, C.A. (1997) Perovskite as a possible sink for ferric iron in the lower mantle. Nature, 387, 694–696.
McCord, T.B., Adams, J.B., and Johnson, T.V. (1970) Asteroid Vesta: Spectral reflectivity and compositional implications. Science, 168, 1445–1447.
McCoy, T.J. (1998) A pyroxene-oldhamite clast in Bustee: Igneous aubritic oldhamite and a mechanism for the Ti enrichment in aubritic troilite. Antarctic Meteorite Research, 11, 34–50.
McCoy, T.J., Scott, E.R.D., and Haack, H. (1993) Genesis of the IIICD iron meteorites: Evidence from silicate-bearing inclusions. Meteoritics, 28, 552–560.
McCoy, T.J., Steele, I.M., Keil, K., Leonard, B.F., and Endress, M. (1994) Chladniite, $Na_2CaMg_7(PO_4)_6$: A new mineral from the Carlton (IIICD) iron meteorite. American Mineralogist, 79, 375–380.
McCoy, T.J., Ehlmann, A.J., Benedix, G.K., Keil, K., and Wasson, J.T. (1996) The Lueders, Texas, IAB iron meteorite with silicate inclusions. Meteoritics and Planetary Science, 31, 419–422.
McCoy, T.J., Mittlefehldt, D., and Wilson, L. (2006) Asteroid differentiation. In D.S. Lauretta and H.Y. McSween Jr., Eds., Meteorites and the Early Solar System II, pp. 733–745. University of Arizona Press.
McKay, G., Lindstrom, D., Yang, S.-R., and Wagstaff, J. (1988) Petrology of a unique achondrite Lewis Cliff 86010. Lunar and Planetary Science, 19, 762–763.
McKay, G., Crozaz, G., Wagstaff, J., Yang, S.-R., and Lundberg, L. (1990) A petrographic, electron microprobe, and ion microprobe study of mini-angrite Lewis Cliff 87051. Lunar and Planetary Science, 21, 771–772.
McSween, H.Y. Jr. (1999) Meteorites and their Parent Planets, 2nd ed. Cambridge University Press.
McSween, H.Y., Mittlefehldt, D.W., Beck, A.W., Mayne, R.G., and McCoy, T.J. (2011) HED meteorites and their relationship to the geology of Vesta and the Dawn Mission. Space Science Reviews, 163, 141–174.
Mikouchi, T., Takeda, H., Miyamoto, M., Ohsumi, K., and McKay, G.A. (1995) Exsolution lamellae of kirschsteinite in magnesium-iron olivine from an angrite meteorite. American Mineralogist, 80, 585–592.
Mikouchi, T., Miyamoto, M., and McKay, G.A. (1996) Mineralogical study of angrite Asuka-881371: Its possible relation to angrite LEW87051. Proceedings of the NIPR Symposium on Antarctic Meteorites, 9, 174–188.
Mikouchi, T., Zolensky, M.E., Ivanova, M., Tachikawa, O., Komatsu, M., Le, L., and Gounelles, M. (2009) Dmitryivanovite: A new high-pressure calcium aluminum oxide from the Northwest Africa 470 CH3 chondrite characterized using electron back-scatter diffraction analysis. American Mineralogist, 94, 746–750.
Mikouchi, T., Sugiyama, K., Satake, W., and Amelin, Y. (2011) Mineralogy and crystallography of calcium silico-phosphate in Northwest Africa 4590 angrite. Lunar and Planetary Science, 42.
Mills, S.J., Hatert, F., Nickel, E.H., and Ferrais, G. (2009) The standardization of mineral group hierarchies: Application to recent nomenclature proposals. European Journal of Mineralogy, 21, 1073–1080.
Mittlefehldt, D.W. (1994) The genesis of diogenites and HED parent body petrogenesis. Geochimica et Cosmochimica Acta, 58, 1537–1552.
——— (2014) Achondrites. Treatise on Geochemistry, 2nd ed., 1, 235–266.
Mittlefehldt, D.W., and Lindstrom, M.M. (1990) Geochemistry and genesis of the angrites. Geochimica et Cosmochimica Acta, 54, 3209–3218.
——— (1993) Geochemistry and petrology of a suite of ten Yamato HED meteorites. Proceedings of the NIPR Symposium on Antarctic Meteorites, 6, 268–292.
Mittlefehldt, D.W., McCoy, T.J., Goodrich, C.A., and Kracher, A. (1998) Non-chondritic meteorites from asteroidal bodies. Reviews in Mineralogy, 36, 4.1–4.195.
Mittlefehldt, D.W., Killgore, M., and Lee, M.T. (2002) Petrology and geochemistry of

D'Orbigny, geochemistry of Sahara 99555, and the genesis of angrites. Meteoritics & Planetary Science, 37, 345–369.
Miyahara, M., El Goresy, A., Ohtani, E., Nagase, T., Nishijima, M., Vashaei, Z., Ferroir, T., Gillet, P., Dubrovinsky, L., and Simionovici, A. (2008) Evidence for fractional crystallization of wadsleyite and ringwoodite from olivine melts in chondrules entrained in shock-melt veins. Proceedings of the National Academy of Sciences, 105, 8542–8547.
Miyahara, M., Ohtani, E., Kimura, M., El Goresy, A., Ozawa, S., Nagase, T., Nishijima, M., and Hiraga, K. (2010) Coherent and subsequent incoherent ringwoodite growth in olivine of shocked L6 chondrites. Earth and Planetary Science Letters, 295, 321–327.
Miyahara, M., Kaneko, S., Ohtani, E., Sakai, T., Nagase, T., Kayama, M., Nishido, H., and Hirao, N. (2013a) Discovery of seifertite in a shocked lunar meteorite. Nature Communications, 4, 1737.
Miyahara, M., Ozawa, S., Ohtani, E., Kimura, M., Kubo, T., Sakai, T., Nagase, T., Nishijima, M., and Hirao, N. (2013b) Jadeite formation in shocked ordinary chondrites. Earth and Planetary Science Letters, 373, 102–108.
Miyajima, N., El Goresy, A., Dupas-Bruzek, C., Seifert, F., Rubie, D.C., Chen, M., and Xie, X. (2007) Ferric iron in Al-bearing akimotoite coexisting with iron-nickel metal in a shock-melt vein in an L-6 chondrite. American Mineralogist, 92, 1545–1549.
Moggi Cecchi, V., Caporali, S., and Pratesi, G. (2015) DaG 1066: A newfound anomalous ureilite with chondritic inclusions. Meteoritics & Planetary Science, 50, Supplement, 1, 5252.
Moore, C.B., Lewis, C.F., and Nava, D. (1969) Superior analysis of iron meteorites. In P.M. Millman, Ed., Meteorite Research, pp. 738–748. Reidel.
Mori, H., and Takeda, H. (1981a) Thermal and deformational histories of diogenites as inferred from their microtextures of orthopyroxene. Earth and Planetary Science Letters, 53, 266–274.
——— (1981b) Evolution of the Moore County pyroxenes as viewed by an analytical transmission electron microprobe (ATEM). Meteoritics, 16, 362–363.
Morimoto, N., Fabries, J., Ferguson, A.K., Ginzburg, I.V., Ross, M., Seifert, F.A., Zussman, J., Aoki, K., and Gottardi, G. (1988) Nomenclature of pyroxenes. American Mineralogist, 73, 1123–1133.
Morrison, S.M., and Hazen, R.M. (2020) An evolutionary system of mineralogy, Part II: interstellar and solar nebula primary condensation mineralogy (>4.565 Ga). American Mineralogist, 105, 1508–1535.
Mostefaoui, S., Lugmair, G.W., and Hoppe, P. (2005) ^{60}Fe: A heat source for planetary differentiation from a nearby Supernova explosion. The Astrophysical Journal, 625, 271–277.
Murayama, J.K., Nakai, S., Kato, M., and Kumazawa, M. (1986) A dense polymorph of $Ca_3(PO_4)_2$: A high pressure phase of apatite decomposition and its geochemical significance. Physics of the Earth and Planetary Interiors 44, 293–303.
Nehru, C.E., Delaney, J.S., Harlow, G.E., and Prinz, M. (1980) Mesosiderite basalts and the eucrites. Meteoritics, 15, 337–338.
Nehru, C.E., Prinz, M., and Delaney, J.S. (1982) The Tucson iron and its relationship to enstatite meteorites. Journal of Geophysical Research, B87, Supplement I, A365–A373.
Nehru, C.E., Prinz, M., Delaney, J.S., Dreibus, G., Palme, H., Spettel, B., and Wanke, H. (1983) Brachina: A new type of meteorite, not a Chassignite. Journal of Geophysical Research, 88, B237–B244.
Nehru, C.E., Prinz, M., Weisberg, M.K., Ebihara, M.E., Clayton, R.N., and Mayeda, T.K. (1992) Brachinites: A new primitive achondrite group. Meteoritics, 27, 267.
——— (1996) A new brachinite and petrogenesis of the group. Lunar and Planetary Science, 27, 943–944.
Németh, P., Garvie, L.A., Aoki. T., Dubrovinskaia, N., Dubrovinsky, L., and Buseck, P.R. (2014) Lonsdaleite is faulted and twinned cubic diamond and does not exist as a discrete material. Nature Communications, 5, 5447.
Nielsen, H.P., and Buchwald, V.F. (1981) Roaldite, a new nitride in iron meteorites. Geochimica et Cosmochimica Acta, Supplement, 16, 1343–1348.
Niemeyer, S. (1979a) I-Xe dating of silicate and troilite from IAB iron meteorites. Geochimica et Cosmochimica Acta, 43, 843–860.
——— (1979b) ^{40}Ar-^{39}Ar dating of inclusions from IAB iron meteorites. Geochimica et Cosmochimica Acta, 43, 1829–1840.
Nittler, L.R., and Ciesla, F. (2016) Astrophysics with extraterrestrial materials. Annual Reviews of Astronomy and Astrophysics, 54, 53–93.
Ohtani, E., Kimura, Y., Kimura, M., Takata, T., Kondo, T., and Kubo, T. (2004) Formation of high-pressure minerals in shocked L6 chondrite Yamato 791384: Constraints on shock conditions and parent body size. Earth and Planetary Science Letters, 227, 505–515.
Ohtani, E., Ozawa, S., Miyahara, M., Ito, Y., Mikouchi, T., Kimura, M., Arai, T., Sato, K., and Hiraga, K. (2011) Coesite and stishovite in a shocked lunar meteorite, Asuka-881757, and impact events in lunar surface. Proceedings of the National Academy of Sciences, 108, 463–466.
Okada, A., and Keil, K. (1982) Caswellsilverite, $NaCrS_2$: A new mineral in the Norton County enstatite achondrite. American Mineralogist, 67, 132–136.
Okada, A., Keil, K., Taylor, G.J., and Newsom, H. (1988) Igneous history of the aubrite parent asteroid: Evidence from the Norton County enstatite achondrite. Meteoritics, 23, 59–74.
Olsen, E.J. (1967) Amphibole: First occurrence in a meteorite. Science, 156, 61–62.
Olsen, E.J., and Fredriksson, K. (1966) Phosphates in iron and pallasite meteorites. Geochimica et Cosmochimica Acta, 30, 459–470.
Olsen, E.J., and Fuchs, L. (1968) Krinovite, $NaMg_2CrSi_3O_{10}$: A new meteorite mineral. Science, 161, 786–787.
Olsen, E.J., and Jarosewich, E. (1971) Chondrules: First occurrence in an iron meteorite. Science, 174, 583–585.
Olsen, E.J., and Steele, I.A. (1993) New alkali phosphates and their associations in the IIIAB iron meteorites. Meteoritics, 28, 415.
Olsen, E.J., and Steele, I.A. (1997) Galileiite: A new meteoritic phosphate mineral. Meteoritics & Planetary Science, 32, AI55–A156.
Olsen, E.J., Huebner, J.S., Douglas, J.A.V., and Plant, A.G. (1973) Meteoritic amphibole. American Mineralogist, 58, 869–872.
Olsen, E.J., Erlichman. J., Bunch, T.E., and Moore, P.B. (1977a) Buchwaldite, a new meteoritic phosphate mineral. American Mineralogist, 63, 362–364.
Olsen, E.J., Bunch, T.E., Jarosewich, E., Noonan, A.F., and Huss, G.I. (1977b) Happy Canyon: A new type of enstatite achondrite. Meteoritics, 12, 109–123.
Olsen, E.J., Davis, A., Clarke, R.S. Jr., Schultz, L., Weber, H.W., Clayton, R., Mayeda, T., Jarosewich, E., Sylvester, P., Grossman, L., and others (1994) Watson: A new link in the IIE iron chain. Meteoritics, 29, 200–213.
Olsen, E.J., Kracher, A., Davis, A.M., Steele, I.M., Hutcheon, I.D., and Bunch, T.E. (1999) The phosphates of IIIAB iron meteorites. Meteoritics & Planetary Science, 34, 285–300.
Ostertag, R. (1983) Shock experiments on feldspar crystals. Journal of Geophysical Research, 88, 364–376.
Ozawa, S., Ohtani, E., Miyahara, M., Suzuki, A., Kimura, M., and Ito, Y. (2009) Transformation textures, mechanisms of formation of high-pressure minerals in shock melt veins of L6 chondrites, and pressure-temperature conditions of the shock events. Meteoritics & Planetary Sciences, 44, 1771–1786.
Ozawa, S., Miyahara, M., Ohtani, E., Koroleva, O.N., Ito, Y., Litasov, K.D., and Pokhilenko, N.P. (2014) Jadeite in Chelyabinsk meteorite and the nature of an impact event on its parent body. Scientific Reports, 4, 5033. https://doi.org/10.1038/srep05033.
Pang, R.-L., Harries, D., Pollok, K., Zhang, A.-C., and Langenhorst, F. (2018) Vestaite, $(Ti^{4+}Fe^{2+})Ti^{4+}_3O_9$, a new mineral in the shocked eucrite Northwest Africa 8003. American Mineralogist, 103, 1502–1511.
Petaev, M.I., Clarke, R.S. Jr., Jarosewich, E., Zaslavskaya, N.I., Kononkova, N.N., Wang, M.-S., Lipschutz, M.E., Olsen, E.J., Davis, A.M., Steele, I.M., and others (2000) The Chaunskij anomalous mesosiderite: Petrology, chemistry, oxygen isotopes, classification and origin. Geochemistry International, 38, S322–S350.
Pittarello, L., Ji, G., Yamaguchi, A., Schryvers, D., Debaille, V., and Claeys, P. (2015) From olivine to ringwoodite: A TEM study of a complex process. Meteoritics & Planetary Science, 50, 944–957.
Powell, B.N. (1969) Petrology and chemistry of meso siderites-I. Textures and composition of nickel-iron. Geochimica et Cosmochimica Acta, 33, 789–810.
Pratesi, G., Bindi, L., and Moggi-Cecchi, V. (2006) Icosahedral coordination of phosphorus in the crystal structure of melliniite, a new phosphide mineral from the Northwest Africa 1054 acapulcoite. American Mineralogist, 91, 451–454.
Presnall, D.C. (1995) Phase diagrams of Earth-forming minerals. In T.J. Ahrens, Ed., Mineral Physics & Crystallography: A Handbook of Physical Constants, pp. 248–268. American Geophysical Union.
Price, G.D. (1983) The nature and significance of stacking faults in wadsleyite, natural β-$(Mg, Fe)_2SiO_4$ from the Peace River meteorite. Physics of the Earth and Planetary Interiors, 33, 137–147.
Price, G.D., Putnis, A., Agrell, S.O., and Smith, D.G.W. (1983) Wadsleyite, natural β-$(Mg,Fe)_2SiO_4$ from the Peace River meteorite. Canadian Mineralogist, 21, 29–35.
Prinz, M., and Weisberg, M.K. (1995) Asuka 881371 and the angrites: Origin in a heterogeneous, CAI-enriched, differentiated, volatile depleted body. Antarctic Meteorites, 20, 207–210.
Prinz, M., Keil, K., Hlava, P.F., Berkley, J.L., Gomes, C.B., and Curvello, W.S. (1977) Studies of Brazilian meteorites, III. Origin and history of the Angra dos Reis achondrite. Earth and Planetary Science Letters, 35, 317–330.
Prinz, M., Nehru, C.E., and Delaney, J.S. (1982) Sombrerete: An iron with highly fractionated amphibole-bearing Na-P-rich silicate inclusions. Lunar and Planetary Science, 13, 634–635.
Prinz, M., Nehru, C.E., Delaney, J.S., Weisberg, M., and Olsen, E. (1983a) Globular silicate inclusions in IIE irons and Sombrerete: Highly fractionated minimum melts. Lunar and Planetary Science, 14, 618–619.
Prinz, M., Delaney, J.S., Nehru, C.E., and Weisberg, M.K. (1983b) Enclaves in the Nilpena polymict ureilite. Meteoritics, 18, 376–377.
Prinz, M., Weisberg, M.K., and Nehru, C.E. (1986) North Haig and Nilpena: Paired polymict ureilites with Angra dos Reis-related and other clasts. Lunar and Planetary Science, 17, 681–682.
——— (1988) LEW86010, a second angrite: Relationship to CAI's and opaque matrix. Lunar and Planetary Science, 19, 949–950.
——— (1990) LEW 87051, a new angrite: Origin in a Ca-Al-enriched eucritic planetesimal? Lunar and Planetary Science, 21, 979–980.
——— (1994) LEW88774: A new type of Cr-rich ureilite. Lunar and Planetary Science, 25, 1107–1108.
Putnis, A., and Price, G.D. (1979) High-pressure $(Mg,Fe)_2SiO_4$ phases in the Tenham chondritic meteorite. Nature, 280, 217–218.

Ramdohr, P. (1963) The opaque minerals in stony meteorites. Journal of Geophysical Research, 68, 2011–2036.
——— (1973) The opaque minerals in stony meteorites. Akademie Verlag.
Randich, E., and Goldstein, J.I. (1978) Cooling rates of seven hexahedrites. Geochimica et Cosmochimica Acta, 42, 221–234.
Rasmussen, K.L. (1989) Cooling rates and parent bodies of iron meteorites from group IIICD, IAB, and IVB. Physica Scripta, 39, 410–416.
Reid, A.M., and Cohen, A.J. (1967) Some characteristics of enstatite from enstatite achondrites. Geochimica et Cosmochimica Acta, 31, 661–672.
Reid, A.M., Williams, R.J., and Takeda, H. (1974) Coexisting bronzite and clinobronzite and the thermal evolution of the Steinbach meteorite. Earth and Planetary Science Letters, 22, 67–74.
Reuter, K.B., Williams, D.B., and Goldstein, J.I. (1988) Low temperature phase transformations in the metallic phases of iron and stony-iron meteorites. Geochimica et Cosmochimica Acta, 52, 617–626.
Rosenshein, E.B., Ivanova, M.A., Dickinson, T.L., McCoy, T.J., Lauretta, D.S., Guan, Y., Leshin, L.A., and Benedix, G.K. (2006) Oxide-bearing and FeO-rich clasts in aubrites. Meteoritics & Planetary Science, 41, 495–503.
Ross, A.J., Downes, H., Herrin, H.S., Mittlefehldt, D.W., Humayun, M., and Smith, C. (2019) The origin of iron silicides in ureilite meteorites. Geochemistry, 79, 125539 (15 pp).
Rubin, A.E. (1985) Impact melt products of chondritic material. Reviews of Geophysics, 23, 277–300.
——— (1997a) Igneous graphite in chondritic meteorites. Mineralogical Magazine, 61, 699–703.
——— (1997b) Mineralogy of meteorite groups. Meteoritics & Planetary Science, 32, 231–247.
——— (2006) Shock, post-shock annealing and post-annealing shock in ureilites. Meteoritics & Planetary Science, 41, 125–133.
——— (2010) Impact melting in the Cumberland Falls and Mayo Belwa aubrites. Meteoritics & Planetary Science, 45, 265–275.
——— (2015a) Impact features of enstatite-rich meteorites. Chemie der Erde, 75, 1–28.
——— (2015b) Maskelynite in asteroidal, lunar and planetary basaltic meteorites: An indicator of shock pressure during impact ejection from their parent bodies. Icarus, 257, 221–229.
Rubin, A.E., and Keil, K. (1983) Mineralogy and petrology of the Abee enstatite chondrite breccia and its dark inclusions. Earth and Planetary Science Letters, 64, 118–131.
Rubin, A.E., and Ma, C. (2017) Meteoritic minerals and their origins. Chemie der Erde, 77, 325–385.
——— (2021) Meteorite Mineralogy. Cambridge University Press.
Rubin, A.E., and Mittlefehldt, D.W. (1992) Classification of mafic clasts from mesosiderites: Implications for endogenous igneous processes. Geochimica et Cosmochimica Acta, 56, 827–840.
Rubin, A.E., and Scott, E.R.D. (1997) Abee and related EH chondrite impact-melt breccias. Geochimica et Cosmochimica Acta, 61, 425–435.
Rubin, A.E., Scott, E.R.D., and Keil, K. (1997) Shock metamorphism of enstatite chondrites. Geochimica et Cosmochimica Acta, 61, 847–858.
Rucks, M.J., Whitaker, M.L., Glotch, T.D., Parise, J.B., Jaret, S.J., Catalano, T., and Dyar, M.D. (2018) Making tissintite: Mimicking meteorites in the multi-anvil. American Mineralogist, 103, 1516–1519.
Russell, S.S., Pillinger, C.T., Arden, J.W., Lee, M.R., and Ott, U. (1992) A new type of meteoritic diamond in the enstatite chondrite Abee. Science, 256, 206–209.
Russell, S.A., Connelly, H.C., and Krot, A.N., Eds. (2018) Chondrules: Records of protoplanetary disk processes. Cambridge University Press.
Ruzicka, A. (2014) Silicate-bearing iron meteorites and their implications for the evolution of asteroidal parent bodies. Chemie der Erde, 74, 3–48.
Sack, R.O., and Ghiorso, M.S. (2017) Ti^{3+}- and Ti^{4+}-rich fassaites at the birth of the solar system: Thermodynamics and applications. American Journal of Science, 317, 807–845.
Schertl, H.-P., Mills, S.J., and Maresch, W.V. (2018) A compendium of IMA-approved mineral nomenclature. International Mineralogical Association.
Scott, E.R.D. (1972) Chemical fractionation in iron meteorites and its interpretation. Geochimica et Cosmochimica Acta, 36, 1205–1236.
——— (1977a) Pallasites-metal composition, classification and relationships with iron meteorites. Geochimica et Cosmochimica Acta, 41, 349–360.
——— (1977b) Formation of olivine-metal textures in pallasite meteorites. Geochimica et Cosmochimica Acta, 41, 693–710.
——— (1979) Origin of anomalous iron meteorites. Mineralogical Magazine, 43, 415–421.
——— (1982) Origin of rapidly solidified metal-troilite grains in chondrites and iron meteorites. Geochimica et Cosmochimica Acta, 46, 813–823.
Scott, E.R.D., and Agrell, S.O. (1971) The occurrence of carbides in iron meteorites. Meteoritics, 6, 312–131.
Scott, E.R.D., and Bild, R.W. (1974) Structure and formation of the San Cristobal meteorite, other IB irons and group I1ICD. Geochimica et Cosmochimica Acta, 38, 1379–1391.
Scott, E.R.D., and Krot, A.N. (2014) Chondrites and their components. In A.M. Davis, H.D. Holland, and K.K. Turekian, Eds., Treatise on Geochemistry, Vol. 1: Meteorites, Comets, and Planets, Second Edition, pp. 65–137. Elsevier-Pergamon.
Scott, E.R.D., and Rajan, R.S. (1979) Thermal history of the Shaw chondrite. Proceedings of the Lunar and Planetary Science Conference, 10, 1031–1043.
Scott, E.R.D., and Wasson, J.T. (1975) Classification and properties of iron meteorites. Reviews of Geophysics and Space Physics, 13, 527–546.
Scott, E.R.D., Keil, K., and Steffler, D. (1992) Shock metamorphism of carbonaceous chondrites. Geochimica et Cosmochimica Acta, 56, 4281–4293.
Scott, E.R.D., Haack, H., and McCoy, T.J. (1996) Core crystallization and silicate-metal mixing in the parent body of the IVA iron and stony-iron meteorites. Geochimica et Cosmochimica Acta, 60, 1615–1631.
Scott, E.R.D., Haack, H., and Love, S.G. (2001) Formation of mesosiderites by fragmentation and reaccretion of a large differentiated asteroid. Meteoritics & Planetary Science, 36, 869–881.
Sharp, T.G., and DeCarli, P.S. (2006) Shock effects in meteorites. In D.S. Lauretta and H.Y. McSween Jr., Eds., Meteorites and the Early Solar System II, pp. 653–677. University of Arizona Press.
Sharp, T.G., Lingemann, C.M., Dupas, C., and Stöffler, D. (1997) Natural occurrence of $MgSiO_3$-ilmenite and evidence for $MgSiO_3$-perovskite in a shocked chondrite. Science, 277, 352–355.
Sharp, T.G., El Goresy, A., Wopenka, B., and Chen, M. (1999) A post-stishovite SiO_2 polymorph in the meteorite Shergotty: Implications for impact events. Science, 284, 1511–1513.
Sharygin, V.V. (2020) Phase $CuCrS_2$ in iron meteorite Uakit (IIAB), Buryatia, Russia: Preliminary data. In S. Votyakov, D. Kiseleva, V. Grokhovsky, and Y. Shchapova, Eds., Minerals: Structure, properties, methods of investigation: 9th Geoscience Conference for Young Scientists, Ekaterinburg, Russia, February 5–8, pp. 229–234. Springer.
Sharygin, V.V., Ripp, G.S., Yakovlev, G.A., Seryotkin, Y.V., Karmanov, N.S., Izbrodin, I.A., Grokhovsky, V.I., and Khromova, E.A. (2020) Uakitite VN, a new mononitride mineral from Uakit iron meteorite (IIAB). Minerals, 10, 150. https://doi.org/10.3390/min10020150.
Shearer, C.K., Burger, P.V., Neal, C., Sharp, Z., Spivak-Birndorf, L., Borg, L., Fernandes, V.A., Papike, J.J., Karner, J., Wadha, M., and others (2010) Non-basaltic asteroidal magmatism during the earliest stages of Solar System evolution. A view from Antarctic achondrites Graves Nunataks 06128 and 06129. Geochimica et Cosmochimica Acta, 74, 1172–1199.
Shimizu, M., Yoshida, H., and Mandarino, J.A. (2002) The new mineral species keilite, (Fe,Mg)S, the iron-dominant analogue of niningerite. Canadian Mineralogist, 40, 1687–1692.
Singletary, S., and Grove, T.L. (2006) Experimental constraints on ureilite petrogenesis. Geochimica et Cosmochimica Acta, 70, 1291–1308.
Sinmyo, R., McCammon, C.A., and Dubrovinsky, L. (2017) The spin state of Fe^{3+} in lower mantle bridgmanite. American Mineralogist, 102, 1263–1269.
Shukolyukov, A., and Lugmair, G. (1992) ^{60}Fe-Light my fire. Meteoritics, 27, 289.
Smith, B.A., and Goldstein, J.I. (1977) The metallic microstructures and thermal histories of severely reheated chondrites. Geochimica et Cosmochimica Acta, 41, 1061–1072.
Smith, J.V., and Mason, B. (1970) Pyroxene-garnet transformation in Coorara meteorite. Science, 168, 832–833.
Smith, C.L., Downes, H., and Jones, A.P. (2008) Metal and sulphide phases in interstitial veins in "dimict" ureilites—Insights into the history and petrogenesis of the ureilite parent body. Lunar and Planetary Science, 39, 1669.
Spray, J.G., and Boonsue, S. (2016) Monoclinic and tetragonal plagioclase (An54) in shock veins from the central uplift of the Manicougan impact structure. Meteoritics & Planetary Science, 51, A590.
Srinivasan, G., Goswami, J.N., and Bhandari, N. (1999) ^{26}Al in eucrite Piplia Kalan: Plausible heat source and formation chronology. Science, 284, 1348–1350.
Srinivasan, P., Dunlap, D.R., Agee, C.B., Wadhwa, M., Coleff, D., Ziegler, K., Ziegler, R., and McCubbin, F.M. (2018) Silica-rich volcanism in the early solar system dated at 4.565 Ga. Nature Communications, 9, 3036 (8 pp.).
Steele, I.M., Olsen, E., Pluth, J., and Davis, A.M. (1991) Occurrence and crystal structure of Ca-free beusite in the El Sampal IIIA iron meteorite. American Mineralogist, 76, 1985–1989.
Stewart, B., Papanastassiou, D.A., and Wasserburg, G.J. (1996) Sm-Nd systematics of a silicate inclusion in the Caddo IAB iron meteorite. Earth and Planetary Science Letters, 143, 1–12.
Stishov, S.M., and Popova, S.V. (1961) A new dense modification of silica. Geokhimiya, 10, 837–839.
Stöffler, D., and Grieve R.A.F. (2007) Impactites. In D. Fettes and J. Desmons, Eds., Metamorphic rocks: A classification and glossary of terms, recommendations of the International Union of Geological Sciences Cambridge, pp. 82–92. Cambridge University Press.
Stöffler, D., Ostertag, R., Jammes, C., Pfannschmidt, G., Sen Gupta, P.R., Simon, S.B., Papike, J.J., and Beauchamp, R.H. (1986) Shock metamorphism and petrography of the Shergotty achondrite. Geochimica et Cosmochimica Acta, 50, 889–903.
Stöffler, D., Bischoff, A., Buchwald, V., and Rubin, A.E. (1988) Shock effects in meteorites. In J.F. Kerridge and M.S. Matthews, Eds., Meteorites and the Early Solar System, pp.165–202. University of Arizona Press.
Stöffler, D., Keil, K., and Scott, E.R.D. (1991) Shock metamorphism of ordinary chondrites. Geochimica et Cosmochimica Acta, 55, 3845–3867.
Stöffler, D., Hamann, C., and Metzler, K. (2018) Shock metamorphism of planetary

silicate rocks and sediments: Proposal for an updated classification system. Meteoritics & Planetary Science, 53, 5–49.
Swamy, V., Saxena, S.K., Sundman, B., and Zhang, J. (1994) A thermodynamic assessment of silica phase diagram. Journal of Geophysical Research, 99, 11,787–11,794.
Swindle, T.D., Kring, D.A., Burkland, M.K., Hill, D.H., and Boynton, W.V. (1998) Noble gases, bulk chemistry, and petrography of olivine-rich achondrites Eagles Nest and Lewis Cliff 88763: Comparison to brachinites. Meteoritics & Planetary Science, 33, 31–48.
Takeda, H. (1987) Mineralogy of Antarctic ureilites and a working hypothesis for their origin and evolution. Earth and Planetary Science Letters, 81, 358–370.
——— (1989) Mineralogy of coexisting pyroxenes in magnesian ureilites and their formation conditions. Earth and Planetary Science Letters, 93, 181–194.
Takeda, H., and Mori, H. (1985) The diogenite-eucrite links and the crystallization history of a crust of their parent body. Journal of Geophysical Research, 90, C636–C648.
Takeda, H., Mori, H., and Ogata, H. (1989) Mineralogy of augite-bearing ureilites and the origin of their chemical trends. Meteoritics, 24, 73–81.
Takeda, H., Babi, T., and Mori, H. (1992) Mineralogy of a new orthopyroxene-bearing ureilite LEW88201 and the relationship between magnesian ureilites and lodranites. Lunar and Planetary Science, 23, 1403–1404.
Takeda, H., Mori, H., Hiroi, T., and Saito, J. (1994) Mineralogy of new Antarctic achondrites with affinity to Lodran and a model of their evolution in an asteroid. Meteoritics, 29, 830–842.
Takeda, H., Yugami, K., Bogard, D., and Miyamoto, M. (1997a) Plagioclase-augite-rich gabbro in the Caddo County IAB Iron and the missing basalts associated with iron meteorites. Lunar and Planetary Science, 28, 1409–1410.
Takeda, H., Ishii, T., Arai, T., and Miyamoto, M. (1997b) Mineralogy of the Asuka 87 and 88 eucrites and the crustal evolution of the HED parent body. Antarctic Meteorite Research, 10, 401–413.
Taylor, G.J., and Heymann, D. (1970) Electron microprobe study of metal particles in the Kingfisher meteorite. Geochimica et Cosmochimica Acta, 34, 677–687.
Taylor, G.J., Okada, A., Scott, E.R.D., Rubin, A.E., Huss, G.R., and Keil, K. (1981) The occurrence and implications of carbide-magnetite assemblages in unequilibrated ordinary chondrites. Lunar and Planetary Science Conference, 12, 1076–1078.
Tomioka, N. (2007) A model for the shear mechanism in the enstatite-akimotoite phase transition. Journal of Mineralogical and Petrological Sciences, 102, 226–232.
Tomioka, N., and Fujino, K. (1997) Natural $(Mg,Fe)SiO_3$-ilmenite and -perovskite in the Tenham meteorite. Science, 277, 1084–1086.
——— (1999) Akimotoite, $(Mg,Fe)SiO_3$, a new silicate mineral of the ilmenite group in the Tenham chondrite. American Mineralogist, 84, 267–271.
Tomioka, N., and Kimura, M. (2003) The breakdown of diopside to Ca-rich majorite and glass in a shocked H chondrite. Earth and Planetary Science Letters, 208, 271–278.
Tomioka, N., and Miyahara, M. (2017) High-pressure minerals in shocked meteorites. Meteoritics & Planetary Science, 52, 2017–2039.
Tomioka, N., Fujino, K., Ito, E., Katsura, T., Sharp, T., and Kato, T. (2002) Microstructures and structural phase transition in $(Mg,Fe)SiO_3$ majorite. European Journal of Mineralogy, 14, 7–14.
Tomioka, N., Miyahara, M., and Ito, M. (2016) Discovery of natural $MgSiO_3$ tetragonal garnet in a shocked chondritic meteorite. Science Advances, 2, e1501725.
Tomioka, N., Okuchi, T., Iitaka, T., Miyahara, M., Bindi, L., and Xie, X. (2020) Poirierite, IMA No. 2018-026b. European Journal of Mineralogy, 32, 275–283.
Tomkins, A.G. (2009) What metal-troilite textures can tell us about post-impact metamorphism in chondrite meteorites. Meteoritics & Planetary Science, 44, 1133–1149.
Tonks, W.B., and Melosh, H.J. (1992) Core formation by giant impacts. Icarus, 100, 326–346.
Treiman, A.H., and Berkley, J.L. (1994) Igneous petrology of the new ureilites Nova 001 and Nullarbor 010. Meteoritics, 29, 843–848.
Trinquier, A., Birck, J., and Allegre, C.J. (2007) Widespread ^{54}Cr heterogeneity in the inner solar system. The Astrophysical Journal, 655, 1179–1185.
Trinquier, A., Elliott, T., Ulfbeck, D., Coath, C., Krot, A.N., and Bizzarro, M. (2009) Origin of nucleosynthetic isotope heterogeneity in the solar protoplanetary disk. Science, 324, 374–376.
Tschauner, O. (2019) High-pressure minerals. American Mineralogist, 104, 1701–1731.
Tschauner, O., and Ma, C. (2017) Stöfflerite, IMA 2017-062. Mineralogical Magazine, 81, 1279–1286.
Tschauner, O., Ma, C., Beckett, J.R., Prescher, C., Prakapenka, V.B., and Rossman, G.R. (2014) Discovery of bridgmanite, the most abundant mineral in Earth, in a shocked meteorite. Science, 346, 1100–1102.
Tschauner, O., Ma, C., Lanzirotti, A., and Newville, M.G. (2020) Riesite, a new high pressure polymorph of TiO_2 from the Ries impact structure. Minerals, 10, 78 (8 pp.).
Ulff-Møller, F., Rasmussen, K.L., Prinz, M., Palme, H., Spettel, B., and Kallemeyn, G.W. (1995) Magmatic activity on the IVA parent body: Evidence from silicate-bearing iron meteorites. Geochimica et Cosmochimica Acta, 59, 4713–4728.
Ulff-Møller, F., Tran, J., Choi, B.-G., Haag, R., Rubin, A.E., and Wasson, J.T. (1997) Esquel: Implications for pallasite formation processes based on the petrography of a large slab. Lunar and Planetary Science, 28, 1465–1466.
Ulff-Møller, F., Choi, B.-G., Rubin, A.E., Tran, J., and Wasson, J.T. (1998) Paucity of sulfide in a large slab of Esquel: New perspectives on pallasite formation. Meteoritics & Planetary Science, 33, 221–227.
van Kooten, E.M.M.E., Schiller, M., and Bizzarro, M. (2017) Magnesium and chromium isotope evidence for initial melting by radioactive decay of ^{26}Al and late stage impact-melting of the ureilite parent body. Geochimica et Cosmochimica Acta, 208, 1–23.
Vdovykin, G.P. (1970) Ureilites. Space Science Reviews, 10, 483–510.
Vollmer, C., Hoppe, P., Brenker, F.E., and Holzapfel, C. (2007) Stellar $MgSiO_3$ perovskite: A shock-transformed stardust silicate found in a meteorite. The Astrophysical Journal Letters, 666, L49–L52.
Wallner, A., Bichler, M., Buczak, K., Dressler, R., Fifield, L.K., Schumann, D., Sterba, J.H., Tims, S.G., Wallner, G., and Kutschera, W. (2015) Settling the half-life of ^{60}Fe: Fundamental for a versatile astrophysical chronometer. Physical Review Letters, 114, 041101 (6 pp).
Walton, E.L. (2013) Shock metamorphism of Elephant Moraine A79001: Implications for olivine-ringwoodite transformation and the complex thermal history of heavily shocked Martian meteorites. Geochimica et Cosmochimica Acta, 107, 299–315.
Wang, Y., Guyot, F., and Liebermann, R.C. (1992) Electron microscopy of $(Mg,Fe)SiO_3$ perovskite: Evidence for structural phase transitions and implications for the lower mantle. Journal of Geophysical Research, 97,12,327–12,347.
Warren, P. (2011) Stable-isotopic anomalies and the accretionary assemblage of the Earth and Mars: A subordinate role for carbonaceous chondrites. Earth and Planetary Science Letters, 311, 93–100.
Warren, P.H. (2012) Parent body depth–pressure–temperature relationships and the style of the ureilite anatexis. Meteoritics & Planetary Science, 47, 209–227.
Warren, P.H., and Kallemeyn, G.W. (1994) Petrology of LEW88774: An extremely chromium-rich ureilite. Lunar and Planetary Science, 25, 1465–1466.
Wasserburg, G.J., Sanz, H.G., and Bence, A.E. (1968) Potassium-feldspar phenocrysts in the surface of Colomera, an iron meteorite. Science, 161, 684–687.
Wasson, J.T. (1967) Chemical classification of iron meteorites: I. A study of iron meteorites with low concentrations of gallium and germanium. Geochimica et Cosmochimica Acta, 31, 161–180.
——— (1970) Chemical classification of iron meteorites: IV. Irons with Ge concentrations greater than 190 ppm and other meteorites associated with group I. Icarus, 12, 407–423.
——— (1971) Chemical classification of iron meteorites: V. Groups IIIC and IIID and other irons with germanium concentrations between 1 and 25 ppm. Icarus, 14, 59–70.
——— (1974) Meteorites: Classification and properties. Springer-Verlag.
——— (1990) Ungrouped iron meteorites in Antarctica: Origin of anomalously high abundance. Science, 249, 900–902.
——— (2016) Formation of the Treysa quintet and the main-group pallasites by impact-generated processes in the IIIAB asteroid. Meteoritics & Planetary Science, 51, 773–784.
Wasson, J.T., and Choe, W.H. (2009) The IIG iron meteorites: Probable formation in the IIAB core. Geochimica et Cosmochimica Acta, 73, 4879–4890.
Wasson, J.T., and Kallemeyn, G.W. (2002) The IAB iron-meteorite complex: A group, five subgroups, numerous grouplets, closely related, mainly formed by crystal segregation in rapidly cooling melts. Geochimica et Cosmochimica Acta, 66, 2445–2473.
Wasson, J.T., and Rubin, A.E. (1985) Formation of mesosiderites by low-velocity impacts as a natural consequence of planet formation. Nature, 318, 168–170.
Wasson, J.T., and Wang, J.M. (1986) A nonmagmatic origin of group IIE iron meteorites. Geochimica et Cosmochimica Acta, 50, 725–732.
Wasson, J.T., and Wei, C.M. (1970) Composition of metal, schreibersite and perryite of enstatite achondrites and the origin of enstatite chondrites and achondrites. Geochimica et Cosmochimica Acta, 31, 169–184.
Wasson, J.T., Willis, J., Wai, C.M., and Kracher, A. (1980) Origin of iron meteorite groups IAB and IIICD. Zeitschrift für Naturforschung, 35A, 781–795.
Wasson, J.T., Ouyang, X.W., Wang, J.M., and Jerde, E. (1989) Chemical classification of iron meteorites: XI. Multi-element studies of 38 new irons and the high abundance of ungrouped irons from Antarctica. Geochimica et Cosmochimica Acta, 53, 735–744.
Wasson, J.T., Choi, B.G., Jerde, E.A., and Ulff-Møller, F. (1998) Chemical classification of iron meteorites: XII. New members of the magmatic groups. Geochimica et Cosmochimica Acta, 62, 715–724.
Watters, T.R., and Prinz, M. (1979) Aubrites: Their origin and relationship to enstatite chondrites. Proceedings of the Lunar and Planetary Science Conference, 10, 1073–1093.
Weisberg, M.K., McCoy, T.J., and Krot, A.N. (2006) Systematics and evaluation of meteorite classification. In D.S. Lauretta and H.Y. McSween, Jr., Eds., Meteorites and the Early Solar System II, pp. 19–52. University of Arizona Press.
Wenk, H.-R., and Bulakh, A. (2003) Minerals: Their constitution and origin. Cambridge University Press.
Wheelock, M.M., Keil, K., Floss, C., Taylor, G.J., and Crozaz, G. (1994) REE geochemistry of oldhamite-dominated clasts from the Norton County aubrite: Igneous origin of oldhamite. Geochimica et Cosmochimica Acta, 58, 449–458.
Willis, J. (1980) The bulk composition of iron meteorite parent bodies. Ph.D. dissertation, University of California at Los Angeles, 208 p.
Wlotzka, F., and Jarosewich, E. (1977) Mineralogical and chemical compositions of silicate inclusions in the El Taco, Camp del Cielo, iron meteorite. Smithsonian Contributions to Earth Science, 19, 104–125.
Wood, J.A. (1967) Chondrites: Their metallic minerals, thermal histories, and parent planets. Icarus, 6, 1–49.
Woolum, D., and Cassen, P. (1999) Astronomical constraints on nebular temperatures: Implications for planetesimal formation. Meteoritics & Planetary Science, 34,

897–907.
Xie, Z., and Sharp, T.G. (2004) High-pressure phases in shock-induced melt veins of the Umbarger L6 chondrite: Constraints of shock pressure. Meteoritics & Planetary Science, 3912, 2043–2054.
——— (2007) Host rock solid-state transformation in a shock-induced melt vein of Tenham L6 chondrite. Earth and Planetary Science Letters, 254, 433–445.
Xie, X., Minitti, M.E., Chen, M., Mao, H.-K., Wang, D., Shu, J., and Fei, Y. (2002a) Natural high-pressure polymorph of merrillite in the shock veins of the Suizhou meteorite. Geochimica et Cosmochimica Acta, 66, 2439–2444.
Xie, Z., Tomioka, N., and Sharp, T.G. (2002b) Natural occurrence of Fe_2SiO_4-spinel in the shocked Umbarger L6 chondrite. American Mineralogist, 87, 1257–1260.
Xie, X., Minitti, M.E., Chen, M., Mao, H.-K., Wang, D., Shu, J., and Fei, Y. (2003) Tuite, γ-$Ca_3(PO_4)_2$—A new mineral from the Suizhou L6 chondrite. European Journal of Mineralogy, 15, 1001–1005.
Xie, Z., Sharp, T.G., and DeCarli, P.S. (2006) High-pressure phases in a shock-induced melt vein of the Tenham L6 chondrite: Constraints on shock pressure and duration. Geochimica et Cosmochimica Acta, 70, 504–515.
Xie, Z.D., Sharp, T.G., Leinenweber, K., DeCarli, P.S., and Dera, P. (2011) A new mineral with an olivine structure and pyroxene composition in the shock-induced melt veins of Tenham L6 chondrite. American Mineralogist, 96, 430–436.
Xie, X., Gu, X., Yang, H., Chen, M., and Li, K. (2016) Wangdaodeite, IMA 2016-007. Mineralogical Magazine, 80, 691–697.
——— (2020) Wangdaodoeite, the $LiNbO_3$-structured high-pressure polymorph of ilmenite, a new mineral from the Suizhou L6 chondrite. Meteoritics & Planetary Science, 55, 184–192.
Yagi, T., Suzuki, T., and Akaogi, M. (1994) High pressure transitions in the system $KAlSi_3O_8$-$NaAlSi_3O_8$. Physics and Chemistry of Minerals, 21, 12–17.
Yanai, K. (1994) Angrite Asuka-881371: Preliminary examination of a unique meteorite in the Japanese collection of Antarctic meteorites. Proceedings of the NIPR Symposium on Antarctic Meteorites, 7, 30–41.
Yang, J., and Goldstein, J.I. (2005) The formation of the Widmanstätten structure in iron meteorites. Meteorites & Planetary Science, 40, 239–253.
——— (2006) Metallographic cooling rates of the IIIAB iron meteorites. Geochimica et Cosmochimica Acta, 70, 3197–3215.
Yang, C.-W., Williams, D.B., and Goldstein, J.I. (1996) A revision of the Fe-Ni phase diagram at low temperatures (<400 °C). Journal of Phase Equilibria, 17, 522–531.
——— (1997a) A new empirical cooling rate indicator for meteorites based on the size of the cloudy zone of the metallic phases. Meteoritics & Planetary Science, 32, 423–429.
——— (1997b) Low-temperature phase decomposition in metal from iron, stony-iron and stony meteorites. Geochimica et Cosmochim Acta, 61, 2943–2956.
Yang, J., Goldstein, J.I., and Scott, E.R.D. (2008) Metallographic cooling rates and origin of IVA iron meteorites. Geochimica et Cosmochimica Acta, 72, 3043–3061.
Youdin, A.N., and Goodman, J. (2005) Streaming instabilities in protoplanetary disks. The Astrophysical Journal, 620, 459–469.
Yugami, K., Takeda, H., Kojima, H., and Miyamoto, M. (1997) Modal abundances of primitive achondrites and the end member mineral assemblage of the differentiation trend. Symposium on Antarctic Meteorites, 22, 220–222.
Zhou, Y., Irifune, T., Ohfuji, H., Shinmei, T., and Du, W. (2017) Stability region of $K_{0.2}Na_{0.8}AlSi_3O_8$ hollandite at 22 GPa and 2273 K. Physics and Chemistry of Minerals, 44, 33–42.
Zinner, E.K. (2014) Presolar grains. In A.M. Davis, H.D. Holland, and K.K. Turekian, Eds., Treatise on geochemistry, Vol. 1: Meteorites, comets, and planets, 2nd ed., pp.17–39. Elsevier-Pergamon.
Zolensky, M., Gounelle, M., Mikouchi, T., Ohsumi, K., Le, L., Hagiya, K., and Tachikawa, O. (2008) Andreyivanovite: A second new phosphide from the Kaidun meteorite. American Mineralogist, 93, 1295–1299.

Manuscript received May 21, 2020
Manuscript accepted August 14, 2020
Manuscript handled by Steven Simon